

## Task 1.1

### Task Title

Reservoir exploration, assessment & characterization

### Research Partners

Workers active in the current phase of the task activities belong to the following research groups within Switzerland:

- University of Bern, Institute of Geological Sciences:
  - Rock-Water Interaction Group (Prof. Larryn Diamond)
  - Structural Geology Group (Prof. Marco Herwegh)
- University of Geneva, Section of Earth and Environmental Sciences:
  - Reservoir Geology & Basin Analysis Group (Prof. Andrea Moscariello)
- University of Lausanne, Institute of Earth Sciences:
  - Applied and Environmental Geophysics Group (Prof. Klaus Holliger)
- University of Neuchâtel, Centre for Hydrology and Geothermics:
  - Geothermics Group (Prof. Benoît Valley)
- ETH Zurich, Geological Institute:
  - Rock Deformation Laboratory (Prof. Jean-Pierre Burg)
- University of Fribourg, Unit of Earth Sciences:
  - Tectonics Group (Prof. Jon Mosar)
  - Sedimentology Group (Prof. Anneleen Foubert)

Collaboration is underway with other researchers at:

- Hydrolsotop GmbH, Germany
- University Freiburg Germany
- University of Bochum, Germany
- University of Western Ontario, Canada
- CSIRO, Perth, Australia
- National University of Mexico
- University College London
- Lawrence Berkeley National Laboratory

Collaborations with industry partners include:

- Geo-Energie Suisse
- Axpo | neue Energien (now defunct)
- Corporation for Swiss Petroleum SEAG
- SIG
- Nagra
- Swisstopo

## Current Projects (presented on the following pages)

### Deep saline aquifers as reservoirs for geothermal energy and CO<sub>2</sub>-sequestration

Predicting porosity-permeability relationships in the rock matrix of the Muschelkalk aquifer, NE Swiss Molasse Basin

L. Aschwanden, A. Adams, L.W. Diamond, M. Mazurek

---

Matrix porosity and depth: Contrasting shallow and deep boreholes of the Muschelkalk aquifer, NE Swiss Molasse Basin

A. Adams, L. Aschwanden, L. W. Diamond

---

Identification of deep reservoir targets for geothermal exploration in the Greater Geneva Basin : insights from a multidisciplinary approach

N. Clerc, E. Rusillon, M. Brentini, Y. Makhloufi, A. Moscariello

---

Unconventional petroleum resources in the Geneva basin: myth or reality?

D. Do Couto, A. Moscariello, S. Bou Daher, R. Littke, P. Weniger

---

Geophysical characterisation of Cretaceous formations for underground thermal energy storage in the Geneva Basin

L. Guglielmetti, A. Moscariello, M. Meyer, C. Nawratil de Bono, H. Maurer, D. Dupuy

---

### Fractured crystalline rocks as reservoirs for geothermal energy

Thermal evolution of the Grimsel Pass hydrothermal system: insights from numerical modeling

C. Wanner, P. Alt-Epping, L. W. Diamond

---

Fracture-controlled flow paths in an active hydrothermal system (Grimsel, Swiss Alps)

D. Egli, R. Baumann, S. Küng, A. Berger, L. Baron, M. Herwegh

---

Deep Geothermal Well Optimization Workflow (DG-WOW)

A. Dahrabou, B. Valley, F. Ladner, F. Guinot, P. Meier

---

Structural mapping of a clay fault zone from boreholes data for the FS-experiment in Mont-Terri

M. Kakurina, Y. Guglielmi, C. Nussbaum, B. Valley

---

### Geophysical exploration for deep geo-energy reservoirs

Attenuation estimated from laboratory creep tests on cracked water-saturated glass samples

C. Mallet, B. Quintal, E. Caspari, K. Holliger

---

Effects of incoming seismic waves on a high-enthalpy geothermal field

M. Lupi, F. Fuchs, E.H. Saenger

---

Structural imaging from hydrophone vertical seismic profile data at the Grimsel Borehole

A. Greenwood, T. Zahner, L. Baron, K. Holliger

---

Potential of fracture characterization from hydrophone tube wave data at the Grimsel test site

E. Caspari, A. Greenwood, T. Zahner, L. Baron, J. Hunziker, K. Holliger

---

Fracture connectivity effects on the anisotropy of acoustic waves

J. G. Rubino, E. Caspari, T. M. Müller, K. Holliger

---

## Geophysical characterization of an active hydrothermal shear zone in granitic rocks

T. Zahner, L. Baron, A. Greenwood, E. Toschini, K. Holliger, D. Egli

## Sensitivity of seismic attenuation and phase velocity to intrinsic background anisotropy in fractured formations

N. D. Barbosa, J. G. Rubino, E. Caspari, K. Holliger

### Task Objectives

With respect to geothermal energy production and geological storage of CO<sub>2</sub> in Switzerland, the task has the following general goals:

- Characterize potential reservoirs
- Refine estimates of exploitation potential
- Provide science-based guidelines for exploration companies
- Develop geological models and geophysical exploration techniques to reduce risk of exploration failure

In addition, the task will

- provide Swiss-specific reservoir data to Task 1.2 (Reservoir modelling)
- provide acquired data to Task 4.3 (Swisstopo public archive)

### Interaction Between the Partners – Synthesis

- Numerous workshops have been held between partners in the NRP70 projects and the Geothermie2020 consortium
- Meetings of Task 1.1 members have been held with those of the closely associated Tasks 1.2 and 1.4
- A conference session entitled "Geothermal Energy, CO<sub>2</sub> sequestration and shale gas" has been convened by SCCER-SoE members at the upcoming 13th Swiss Geoscience Meeting in Basel and it has attracted 38 scientific presentations.

### Highlights 2016

- Thermal modelling offers a means to estimate the subsurface heat resource below the NRP70-Swisstopo-BFE-funded research drillhole on Grimsel Pass (Poster Wanner et al.).
- NRP70-funded research has shown that porosities and permeabilities of the regional Muschelkalk aquifer can be predicted from borehole geophysical logs (poster Aschwanden et al.)
- CTI-funded project DG-WOW is developing a workflow to minimize borehole failure and optimize borehole trajectory (Poster Dahrabou et al.)
- The FS-experiment at Mont-Terri provides insight in clay fault stability and new mean of characterizing the stress state in-situ (Poster Kakurina et al.)
- Funded by swisstopo, the project "Stress state, fault criticality and fluids) is investigating the fault anatomy, porosity and pore connectivity of the La Sarraz fault system (Scheidt et al., no poster)
- Part of the EU-funded project image, the relation among stress heterogeneities, fracture network and induced seismicity in deep geothermal reservoirs is analysed (Moein et al., no poster)
- Fracture connectivity has a strong influence on seismic velocity anisotropy thus opening new perspectives for monitoring reservoir stimulation (Poster Rubino et al.).

- Tube wave analysis provides constraints with regard to the S-wave velocity structure and fracture characteristics along the NRP70 borehole (Posters Caspari et al. and Greenwood et al.).
- Laboratory-based creep tests allow for estimating frequency-dependent attenuation due to wave-induced fluid flow between connected fractures in saturated fractured materials (Poster Mallet et al.)

## Predicting porosity-permeability relationships in the rock matrix of the Muschelkalk aquifer, NE Swiss Molasse Basin

L. Aschwanden<sup>1</sup>, A. Adams<sup>1</sup>, L.W. Diamond<sup>1</sup>, M. Mazurek<sup>1</sup>

<sup>1</sup>) Rock-Water Interaction Group, Institute of Geological Sciences, University of Bern, Baltzerstrasse 1+3, CH-3012 Bern, Switzerland

### 1. Introduction

In the Swiss Molasse Basin, the Middle Triassic carbonate rocks of the Middle- and Upper Muschelkalk are one of the options under investigation for geothermal energy production and for storage of gas. The mixed results obtained in geothermal exploration wells at Riehen, Schlattingen and Triemli show that the distribution of porous and permeable zones are spatially heterogeneous and that site selection for future projects requires serious exploration. Generally, exploration campaigns rely on borehole log data from which the porosity of the rock can be deduced. However, this data can be biased by borehole and environmental effects and has to be processed and interpreted with great care. In this context the present study offers the opportunity to support exploration by integrating data from laboratory analysis of drill cores and thus to test the reliability of the borehole log data. Furthermore, a correlation has been sought between plug porosity and plug permeability, which could provide a basis for determining the rock's matrix permeability from porosity logs.

### 2. Methods

Petrophysical borehole logs are being processed by following the principles by Schlumberger (1989, 1997) and accordingly porosity was deduced from neutron-, density- and sonic logs.

The drill cores are being investigated by a variety of laboratory methods, including:

- Density, porosity and permeability analyses of plug samples
- Petrographic characterization
- GEOTEK Multi-Sensor Core logger (MSCL) for measurements of bulk density along entire drill cores (at a resolution of 5 mm)
- Visual logging of the geometry and frequency of macroscopic structures in the drill core (e.g. fractures)

### 3. Results

Figure 1a shows the MSCL-density log of the Bözberg drill core (TD: Trigonodus Dolomit; HMK: Hauptmuschelkalk; DAG: Dolomit der Anhydritgruppe). Robust correlation between MSCL-density and plug porosity (Fig. 1b) allows reliable calculation of the porosity, its distribution and average value for the entire drill core (Fig. 2c).

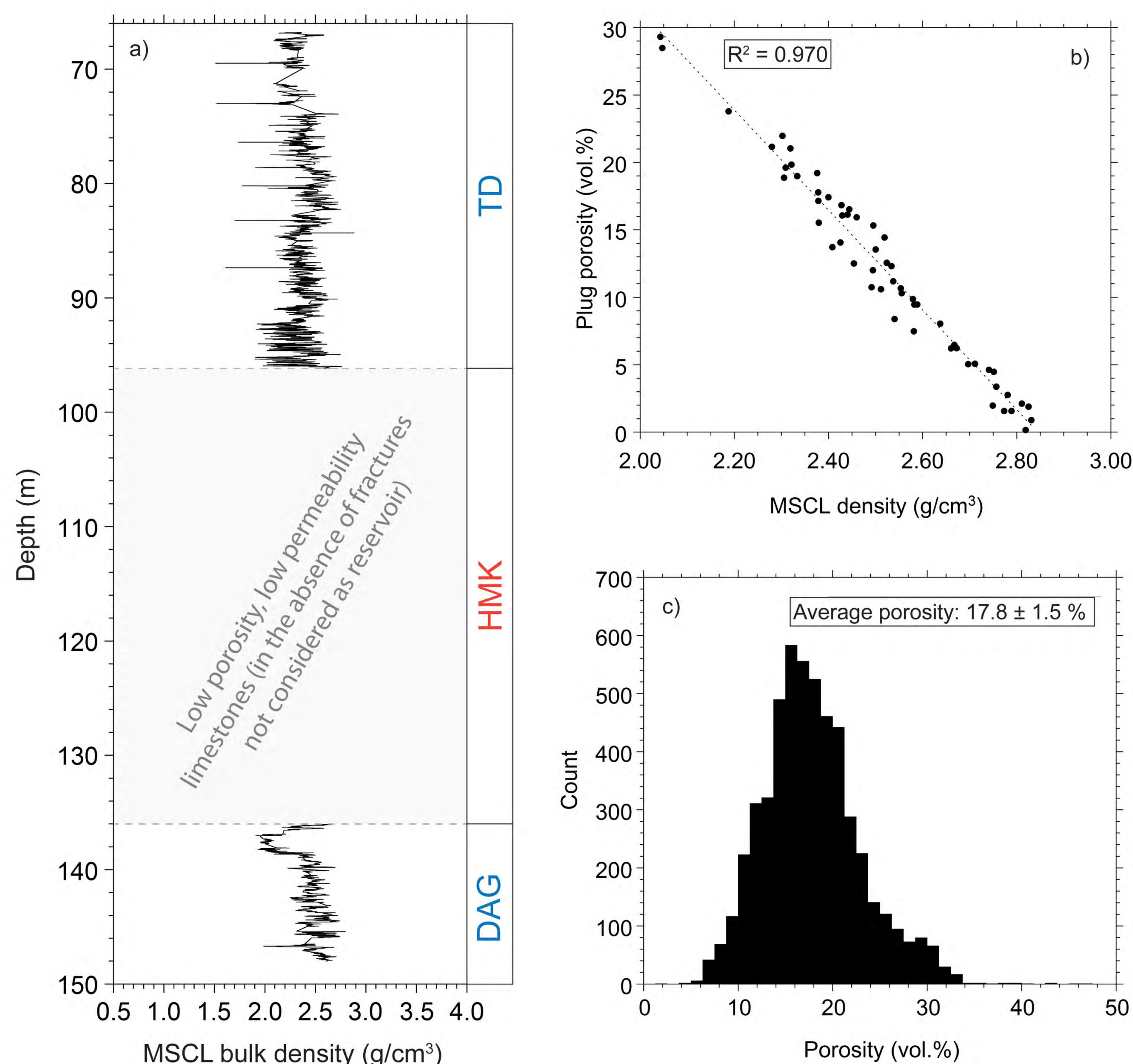


Fig. 1a: MSCL-density log of the Bözberg drill core (TD: Trigonodus Dolomit; HMK: Hauptmuschelkalk; DAG: Dolomit der Anhydritgruppe). b) Robust correlation between MSCL-density and plug porosity allows c) calculating the porosity, its distribution and average value for entire drill cores

Figure 2 shows the downhole correlation between the porosity calculated from borehole logs and from MSCL-density logs at the Schafisheim well.

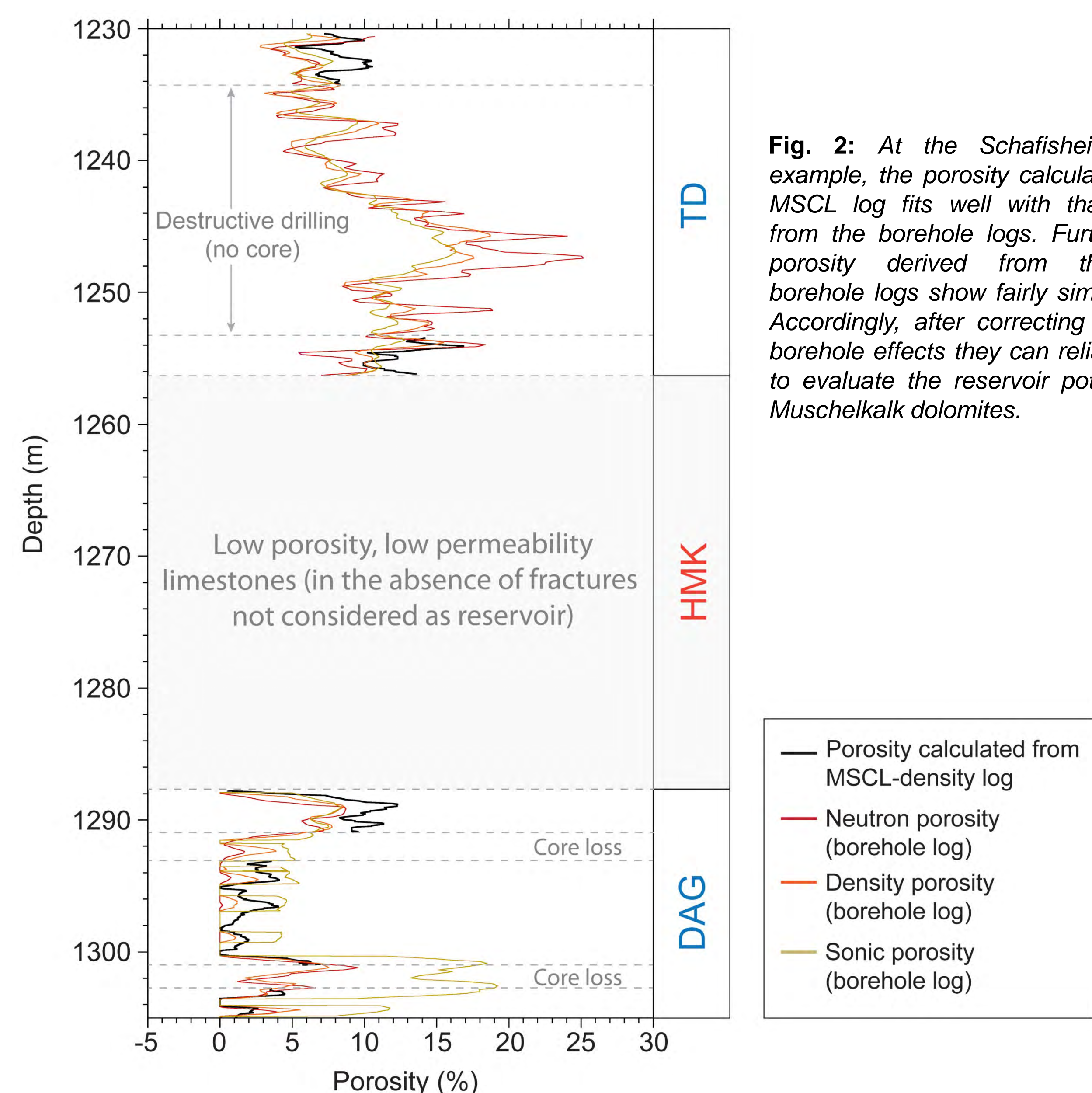


Fig. 2: At the Schafisheim well, for example, the porosity calculated from the MSCL log fits well with that calculated from the borehole logs. Furthermore the porosity derived from the different borehole logs show fairly similar patterns. Accordingly, after correcting the logs for borehole effects they can reliably be used to evaluate the reservoir potential of the Muschelkalk dolomites.

Figure 3 shows a robust correlation between plug porosity and plug permeability and between the predominant pore type and the porosity-permeability trend.

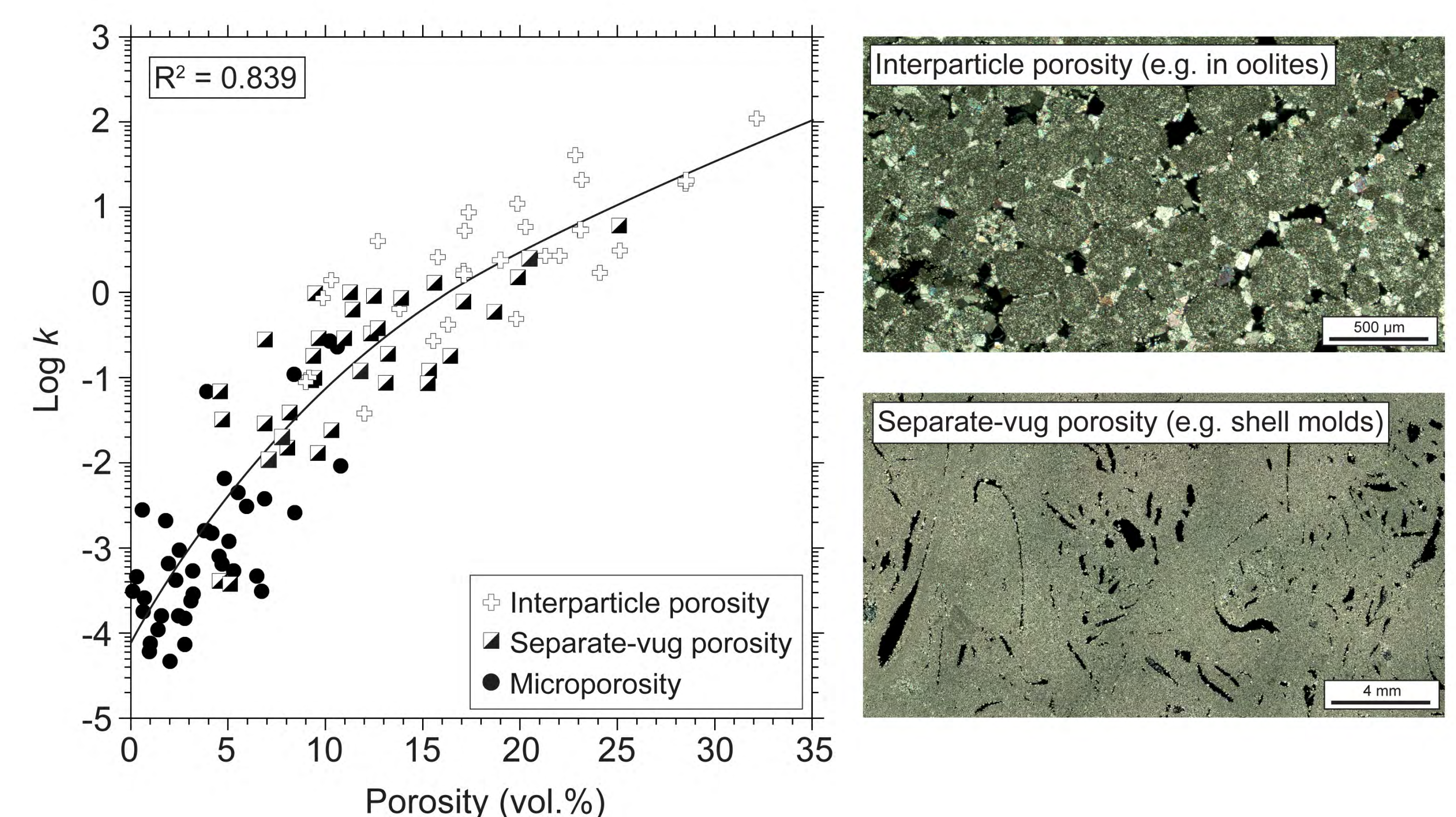


Fig. 3: Correlation between plug porosity and plug permeability in the Upper- and Middle Muschelkalk dolomites. A strong correlation exists between pore types and the porosity-permeability trend. Best reservoir properties are associated with interparticle pore space (in oolites and sucrosic dolomite), whereas separate-vug porosity (shell- and anhydrite molds) yields lower values. Samples of macroscopically tight appearance are summarized as samples with microporosity, which show the lowest reservoir potential.

### 4. Conclusions

Robust correlations between MSCL-density and plug porosity, and between plug porosity and plug permeability allow the distribution and average of these properties to be calculated along entire drill cores. Moreover, the porosity calculated from the MSCL-density logs fits well with that calculated from the corresponding borehole logs. In the Muschelkalk dolomites all these correlations allow reliable prediction of matrix porosity and matrix permeability from geophysical borehole logs, which is particularly important for existing and future wells where no drill core is available.

### References

- Schlumberger (1989). Log Interpretation Principles/Applications. Schlumberger Educational Services, Houston.  
Schlumberger (1997). Log interpretation charts. Schlumberger Wireline & Testing, Houston.

# Matrix porosity and depth: Contrasting shallow and deep boreholes of the Muschelkalk aquifer, NE Swiss Molasse Basin

A. Adams<sup>1</sup>, L. Aschwanden<sup>1</sup>, L. W. Diamond<sup>1</sup>

1) Rock-Water Interaction Group, Institute of Geological Sciences, University of Bern, Baltzerstrasse 1+3, CH-3012 Bern, Switzerland

## 1. Introduction

The Upper Muschelkalk (now Schinznach Formation) of the Swiss Molasse Basin is under study as a potential gas storage reservoir and for geothermal energy production. The dolomitized fraction of the unit displays promising aquifer properties, however any exploration potential is encumbered by significant vertical and spatial porosity and permeability heterogeneities. Spatial variations may be due to differences in depositional facies (Adams et al. 2015), while vertical porosity heterogeneities are likely a function of the lithology and burial depth. The aim of this study is to observe and quantify the differences in porosity from two boreholes; a shallow borehole (Bözberg), and a deep borehole (Lindau) to help characterize reservoir differences using digital image analysis as a quick, reliable and non-destructive method to analyse individual pores.

## 2. Methods

- Core plug analysis (porosity, permeability and density)
- Digital image analysis (DIA) based on the method of Anselmetti et al. 1998; images taken with a JEOL-JXA 810 electron probe microanalyzer.
  - Microporosity (<500µm<sup>2</sup>) 24 images at 1000x.
  - Macroporosity (>500 µm<sup>2</sup>) 12 images at 70x.
- Porosity characterization with ImageJ software
- DIA obtained porosity was compared with helium pycnometry porosity and Multi-Sensor Core Logger (MSCL) derived porosities.

## 3. Results

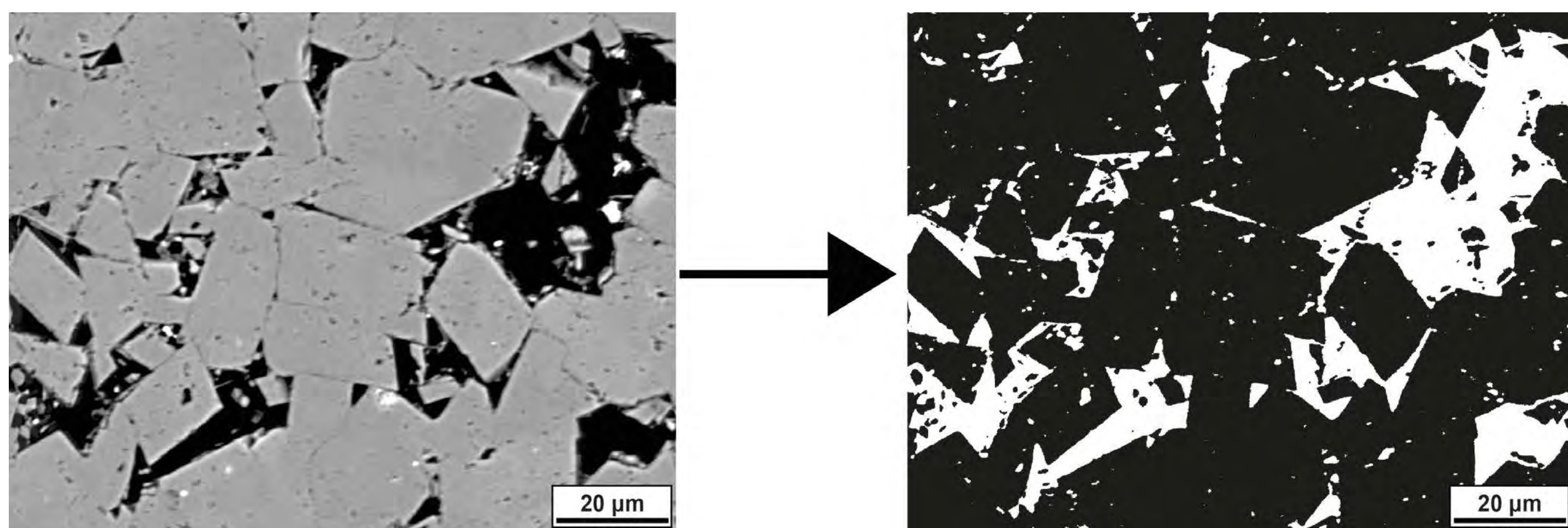


**Figure 1) Bözberg** from a depth 94.66 ( $\Phi = 11.68\%$ )  
Each image is manually thresholded, whereby white space is rendered as porosity in ImageJ. Then the micro/macroporosity is calculated from the average of the stack of images and combined where:  
 $\Phi_{total} = \Phi_{macro} + \Phi_{micro}(1 - \Phi_{macro})$

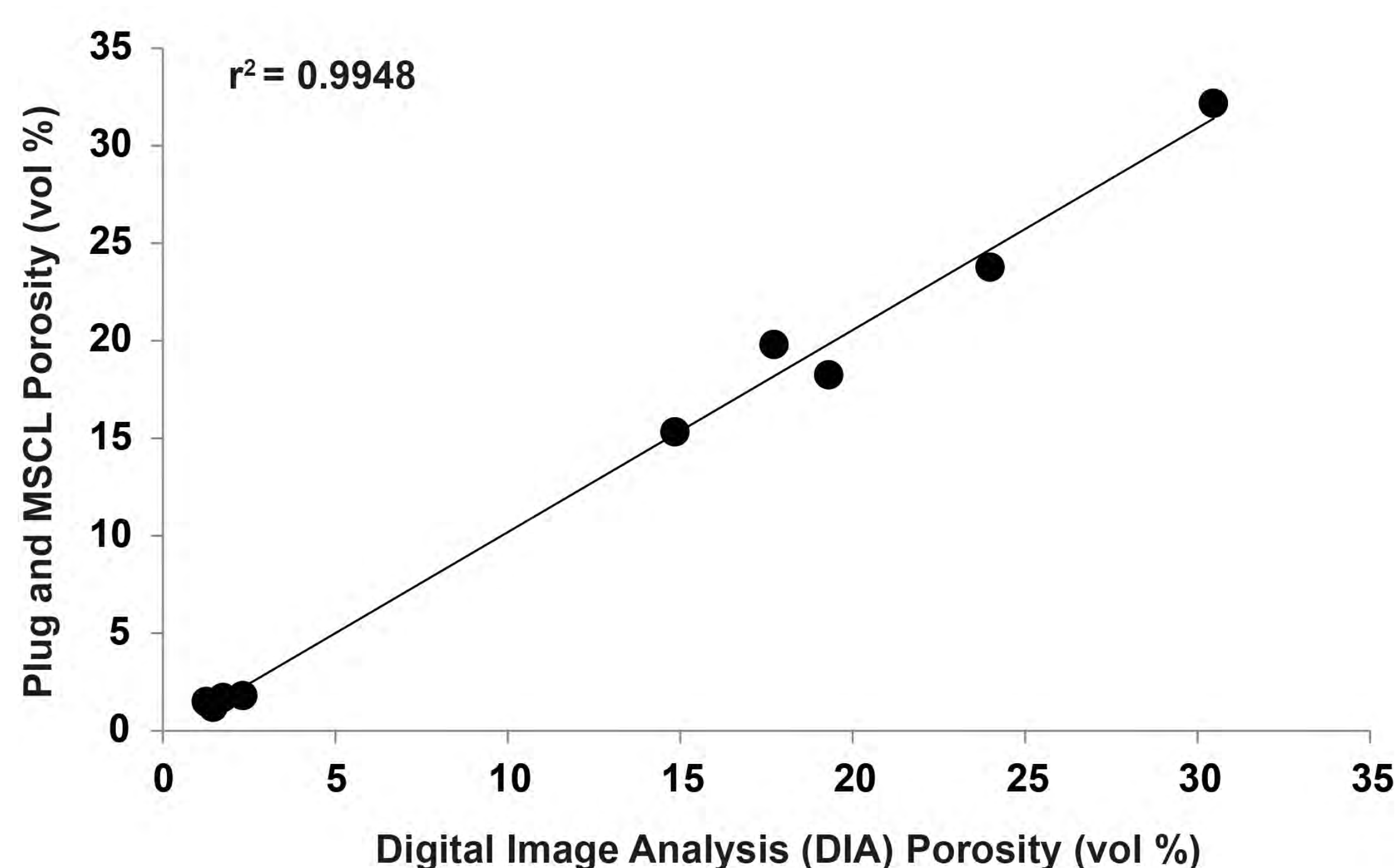


**Figure 2) Correlation plot** of DIA derived porosity and plug/MSCL derived porosity. DIA derived porosity shows an excellent correlation with measured porosity values, and that pores are adequately accounted for by image analysis

## 4. Porosity Characteristics of Shallow and Deep Boreholes

Bözberg (58.44 – 96.00 m)

Lindau (2225 - 2265 m)

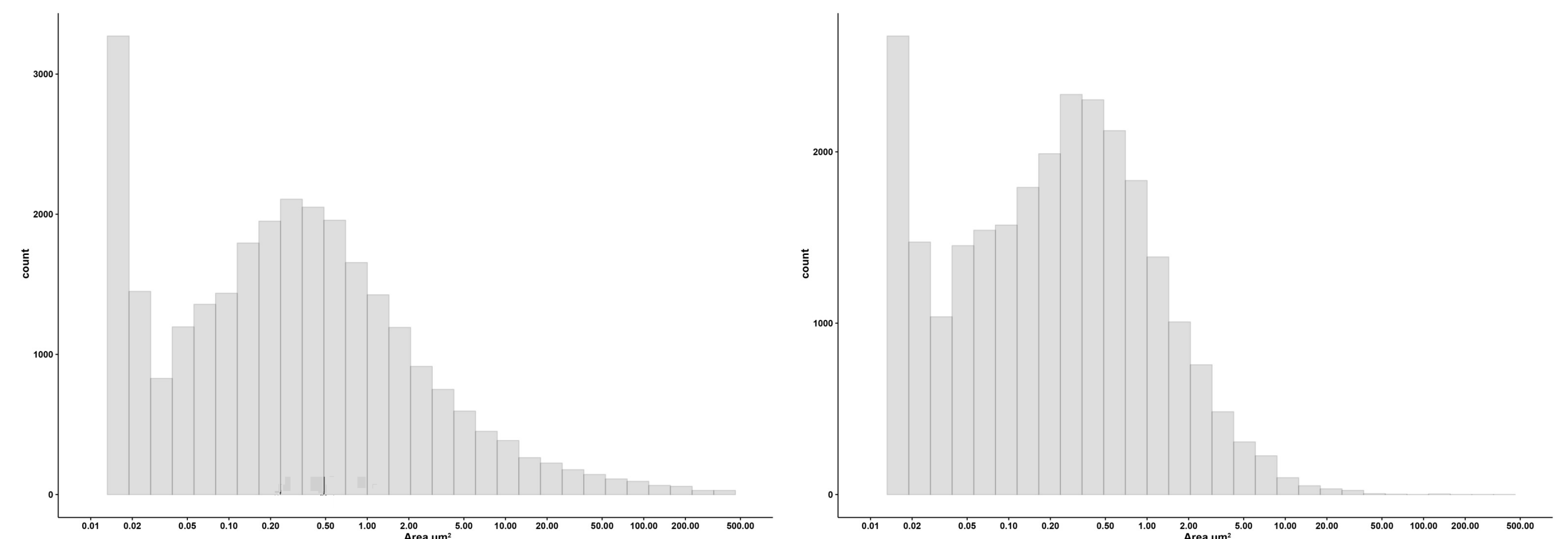


**Figure 3) Micropore size distributions.** Despite over 1500 meters of additional burial in Lindau each borehole shows similar pore size distributions, modes and average.

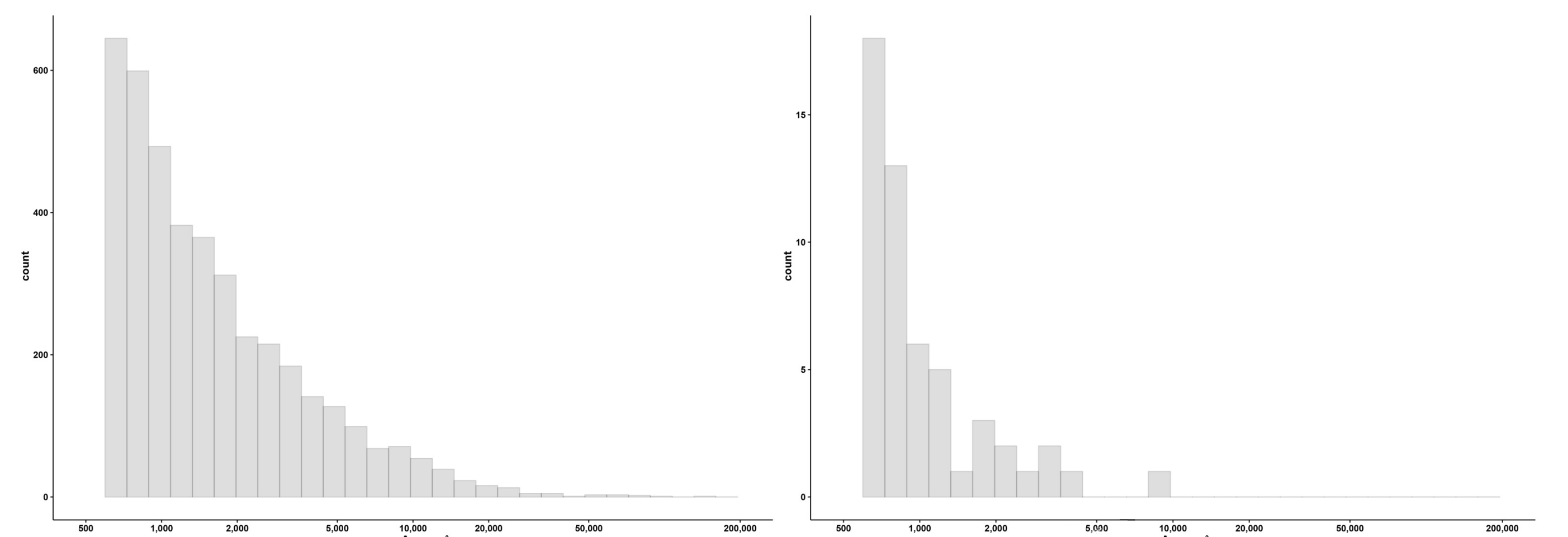


**Figure 4) Macropore size distributions.** Lindau shows a substantial decrease in macropores. In the case of Bözberg; over 10 % of its porosity is derived from pores greater than 500 µm<sup>2</sup>.

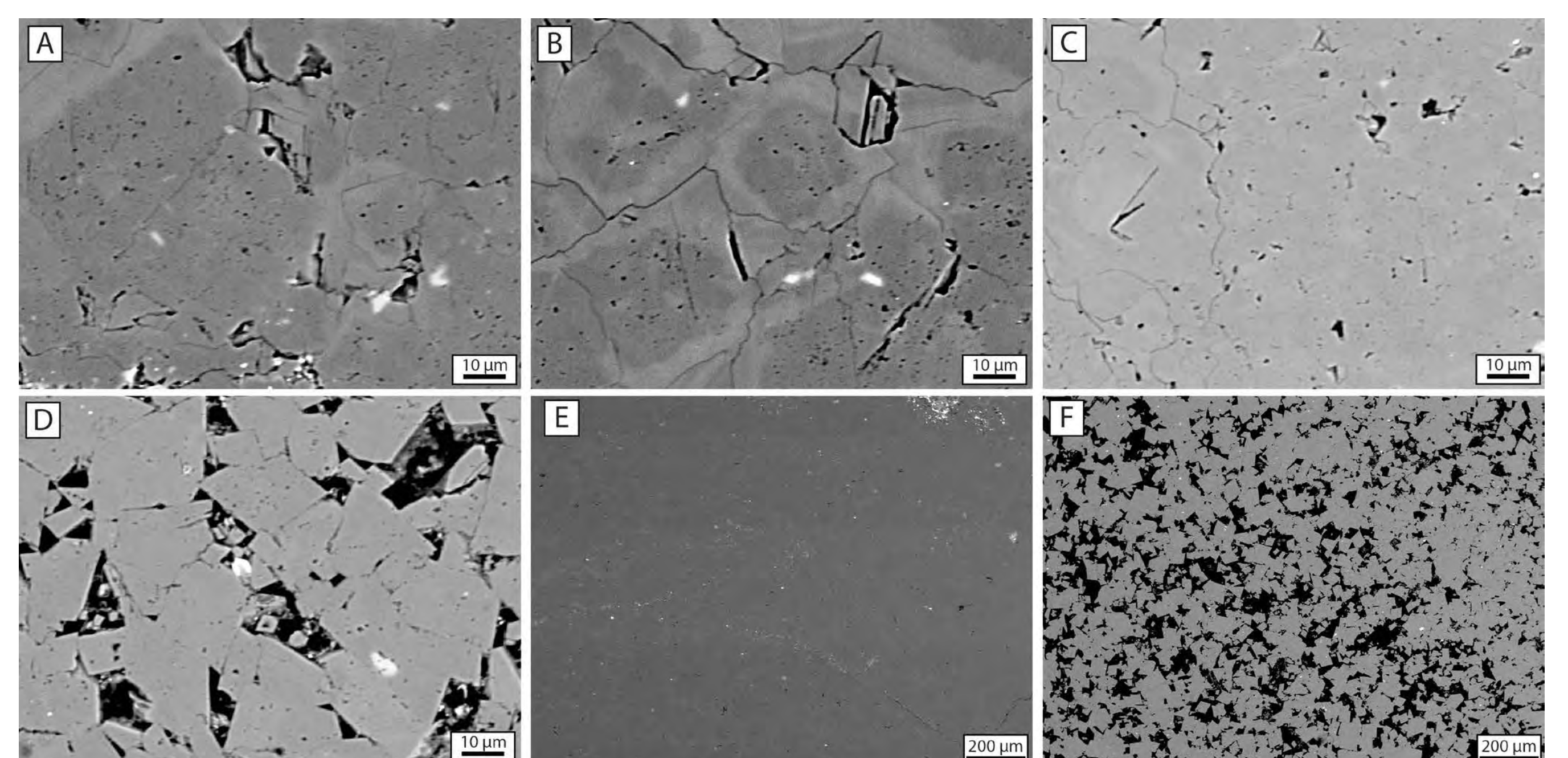


**Figure 5) Backscattered Electron Images of Lindau (A, B, C, E) and Bözberg (D, F).** Zonations in Lindau matrix dolomites reveal intracrystalline dissolution seams along anhedral crystal boundaries, similar to miniaturized stylolites. Bözberg and shallower boreholes on the contrary, show euhedral crystals with brittle contacts. Micropores in Lindau appear to be constrained to fractures along crystal boundaries and the likely remains of fluid inclusions at the center of crystals (A & B).

## 5. Conclusions

Digital image analysis is a viable method to estimate and characterize porosity in matrix dolomites. We have revealed that macropores, which can make up over 30% of a bed's porosity, are completely obliterated at depth leading to micropores being the only source of dolomite matrix porosity in deep boreholes. Intercrystalline porosity is impeded by chemical compaction at crystal boundaries. The sink for the dolomite released during chemical compaction is not yet known, and may constitute another porosity decreasing phase of cementation. Future work will focus on finding the dolomite sink and quantifying the amount of carbonate dissolved by chemical compaction.

## References

- Adams A., Aschwanden L., Diamond L.W. (2015) Facies architecture and its controls on porosity distribution on a Triassic Swiss carbonate ramp. 15<sup>th</sup> Bathurst Meeting of Carbonate Sedimentologists.
- Anselmetti F.S., Luthi S., Eberli, G.P. (1998) Quantitative Characterization of Carbonate Pore Systems by Digital Image Analysis. AAPG Bulletin, 82, 1815 – 1836.

# Identification of deep reservoir targets for geothermal exploration in the Greater Geneva Basin : insights from a multidisciplinary approach

Nicolas Clerc\*, Elme Rusillon\*, Maud Brentini\*, Yasin Makhoulfi\*, Andrea Moscardiello\*

## Introduction

During the last decades, interest for the development of deep geothermal energy has raised in Switzerland, not only for electricity, but also for heat/cold production to serve heating/cooling of greenhouses and buildings.

A multi-phased program aiming at assessing and developing medium and deep geothermal energy resources in Geneva is being developed since 2012. In this framework, a detailed subsurface study focused on both structural and reservoir rock typing is being carried out across the trans-border (Swiss-French) Greater Geneva Basin (GGB) to identify and characterize potential geothermal reservoirs.

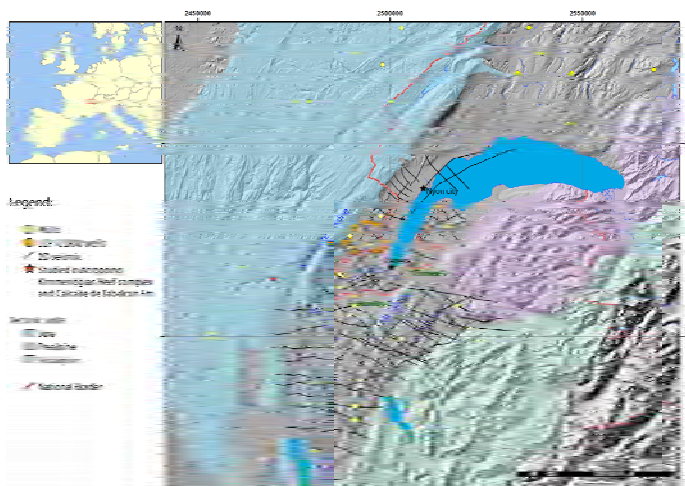


Figure 1: The Greater Geneva Basin (GGB) showing tectonic units, 2D seismic profiles and key locations.

## Stratigraphic framework

### Main challenges

- Create composite logs for each surrounding regions
- From outcrops to boreholes
- Harmonization of regional stratigraphy
- Establishment of a regional stratigraphic catalog

### Main issues

- Heterogeneities and discrepancies of data
- Important lateral variabilities
- Differences between local stratigraphic nomenclature and HARMOS.

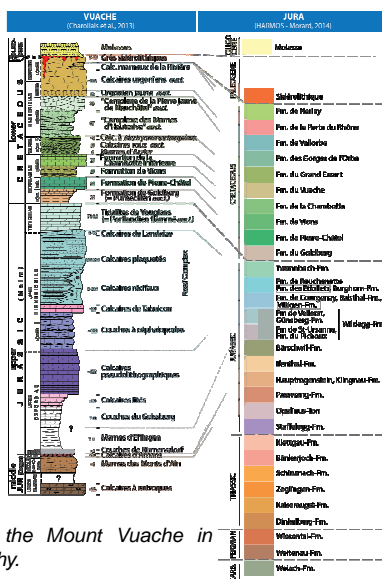


Figure 2: Stratigraphic column of the Mount Vuache in comparison with HARMOS stratigraphy.

- **Objectives:** assessment of geothermal reservoir potential in the Greater Geneva basin.
- **Concept:** structural interpretation, stratigraphic homogenization, rock typing and reservoir geometry.
- **Main partners involved:** Services Industriels Genevois (SIG), Etat de Genève (GESDEC), University of Geneva.

## Basin and rock properties

- In addition to the Vuache fault, well-known from its surface expression, other NW-SE striking left-lateral wrench fault systems or corridors affect the Geneva basin.
- They are known from SW to NE as the Cruseilles, Le Coin and the Arve fault zones (Fig. 3).
- Detail subsurface mapping from 2D seismic data reveals more complex structural scheme.

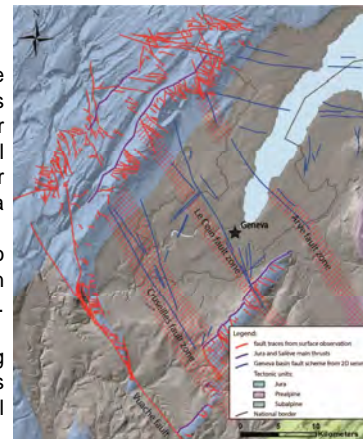


Figure 3: Schematic map of the Geneva basin with location of four main strike-slip fault zones (red, blue lines and dashed areas).

- Porosity and permeability measurements from core and outcrop samples identify the Kimmeridgian Reef Complex (RC) unit and underlying Calcaires de Tabalcon (Ctab) formation (Fig. 2,4) as most promising geothermal reservoirs.

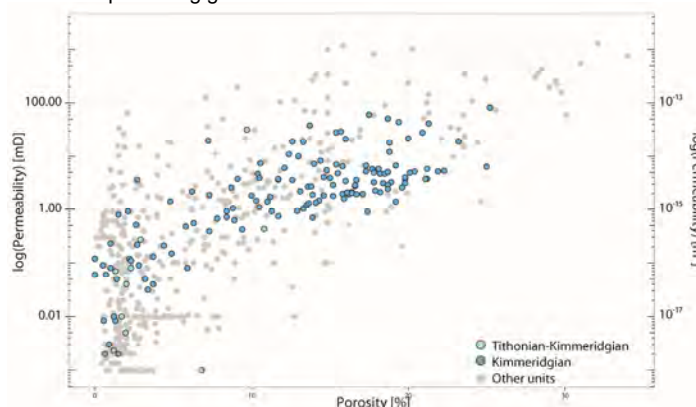


Figure 4: Porosity-permeability measurements in reservoir units of the Geneva Basin. RC and Ctab samples are highlighted in blue.

- Characterization of the diagenetic cementation (calcite) and recognition of a late diagenetic dolomitization process (Fig. 5).

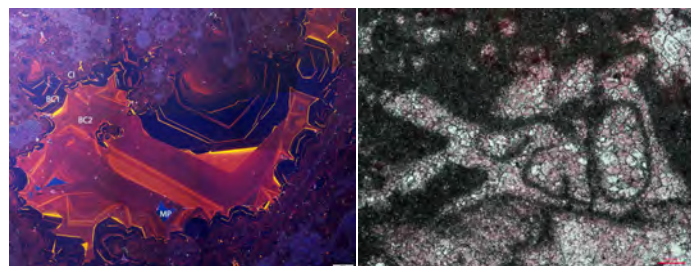


Figure 5: Cathodoluminescence picture of the top RC showing calcitic cementation and revealing late dolomitization (uncolored).

## Conclusions and outlooks

- ✓ New insights on the detail structural characterization, the reservoir assessment and the stratigraphic framework of the GGB.
- ✓ Implementation of reservoir rock types integrating petrophysical properties, depositional facies, pore types, diagenesis imprint and log signature
- ✓ Elaboration of a harmonized stratigraphic catalogue helping both field work and core facies recognition.
- ✓ Understanding and integrating reservoir rock types distribution with detailed fault mapping (and associated fracture-related enhanced permeability zones) leads to the identification of most productive geothermal reservoirs targets for future drilling location.

# Unconventional petroleum resources in the Geneva basin: myth or reality?

Damien Do Couto\*, Andrea Moscariello\*, Samer Bou Daher\*\*, Ralf Littke\*\* & Philipp Weniger\*\*\*

\*Université de Genève, \*\* EMR-RWTH Aachen University, \*\*\*BGR Hannover

## Introduction

While the future provision of energy is challenging the scientific community, the interpretation of the Swiss subsurface geology and the assessment of the potential energetic resources (both fossil and renewable) appear essentials to avoid any conflict of use in the next future. The conventional petroleum exploration that took place in Switzerland and neighbouring France in the past century did not reveal the occurrence of major petroleum accumulation below the Molasse basin, despite numerous oil and gas shows at the surface and in the subsurface.

However, and as long as unconventional resources represent a major new source of energy in countries around the globe, the potential discovery of unconventional oil and gas at depth sharpened many concerns in the past few years, in particular after the discovery of a tight gas accumulation in Paleozoic rocks near the Geneva Lake (Noville-1 well).

In this contribution, we investigate the unconventional petroleum potential below the Geneva Basin (Fig. 1).

## Methods

- Cuttings, core fragments, gas and bitumen seeps have been sampled.
- Focus on two major source-rocks : the Posidonia shale (Lower Jurassic) and the Permo-Carboniferous *sensu lato*.
- Evaluation of the organic geochemistry: TOC, maturity, biomarker analysis, gas chromatography and isotopic analysis.

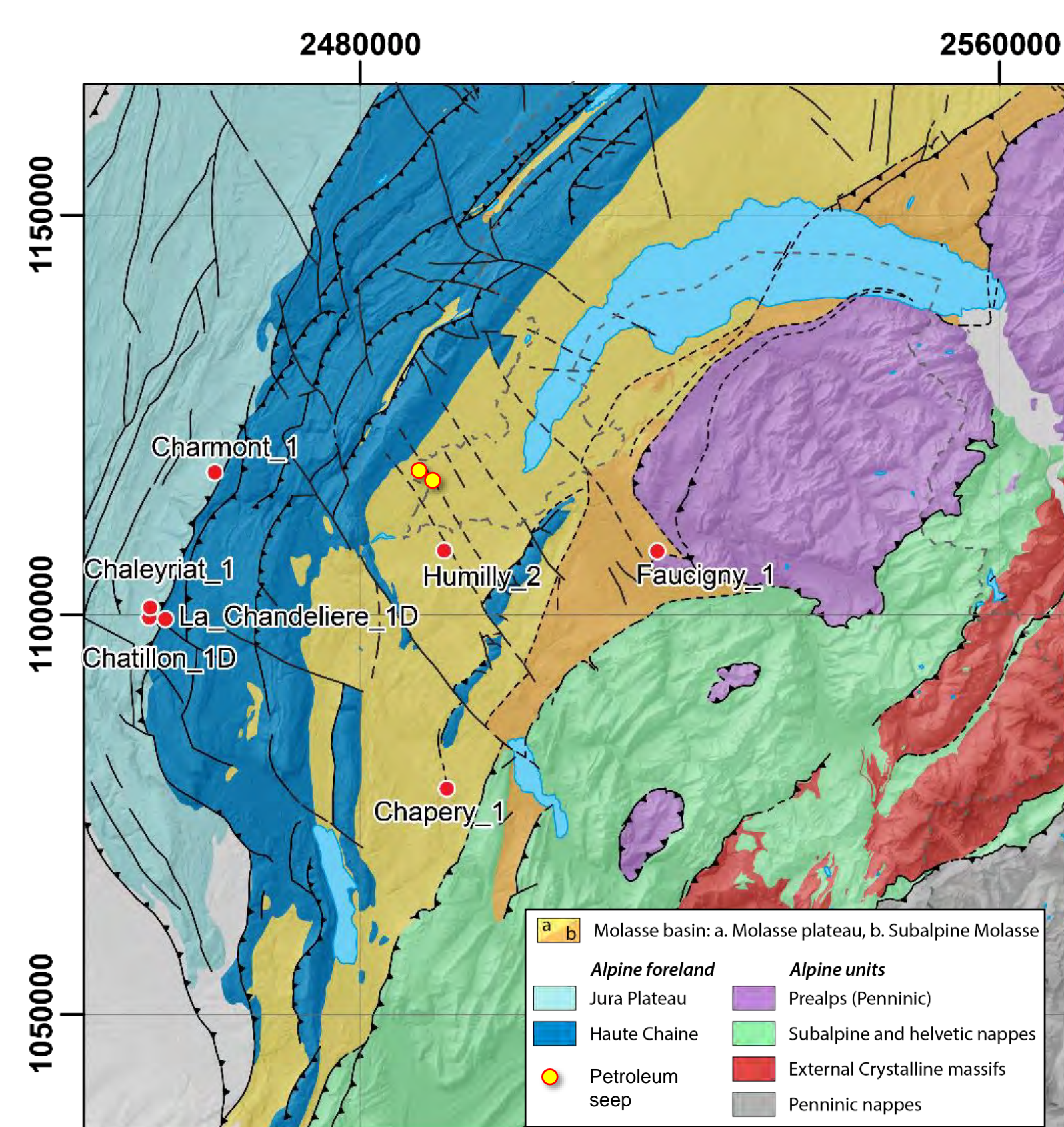


Figure 1: Geological map of the studied area with the location of wells and seeps.

## Organic geochemistry

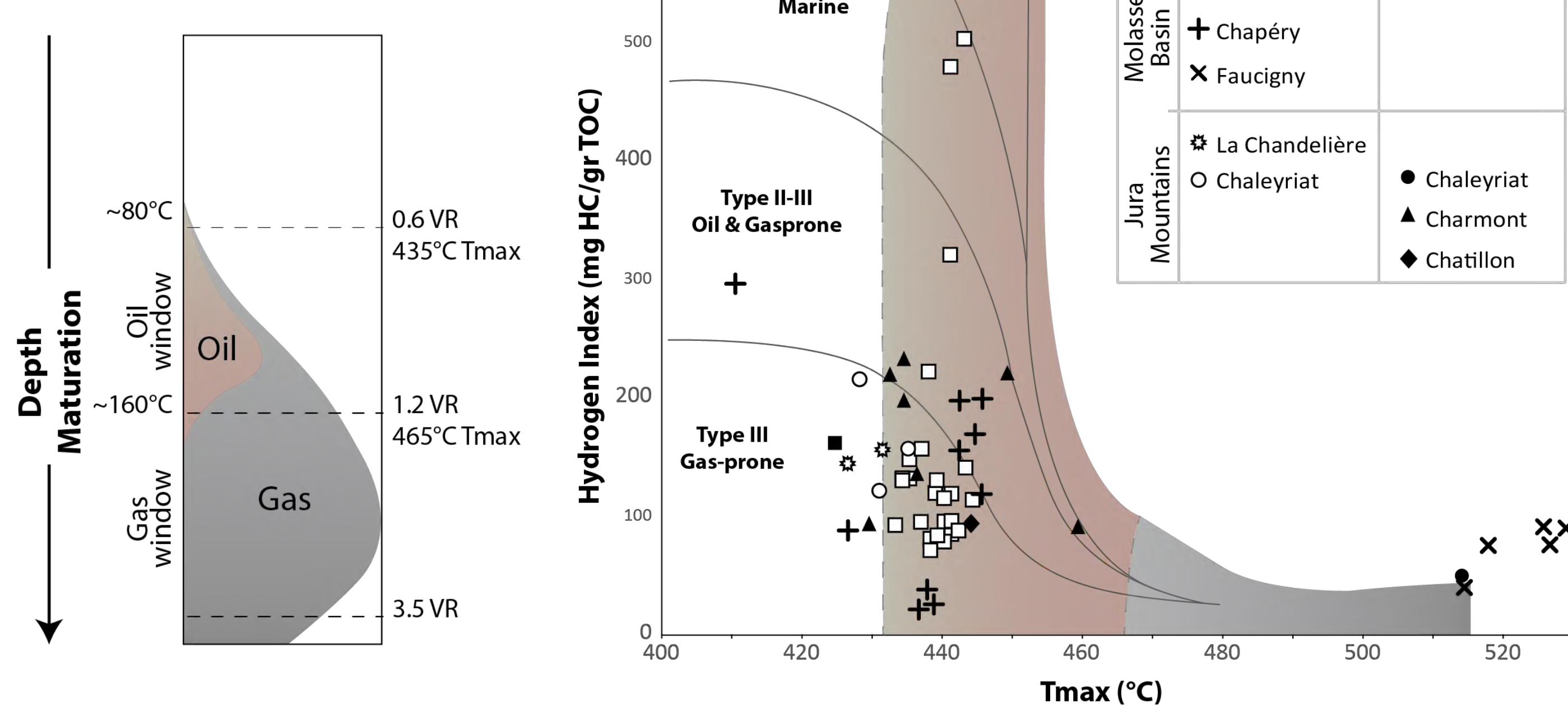


Figure 2: Plot of HI vs. Tmax outlining kerogen types and source-rock maturity

- Posidonia shales (Toarcian) are in the oil window (early mature) or immature → one may expect a good to very-good source-rock quality in the centre of the basin
- Permo-Carb coal beds are in the oil window in the Jura but no direct information in the centre of the basin due to the lack of penetration

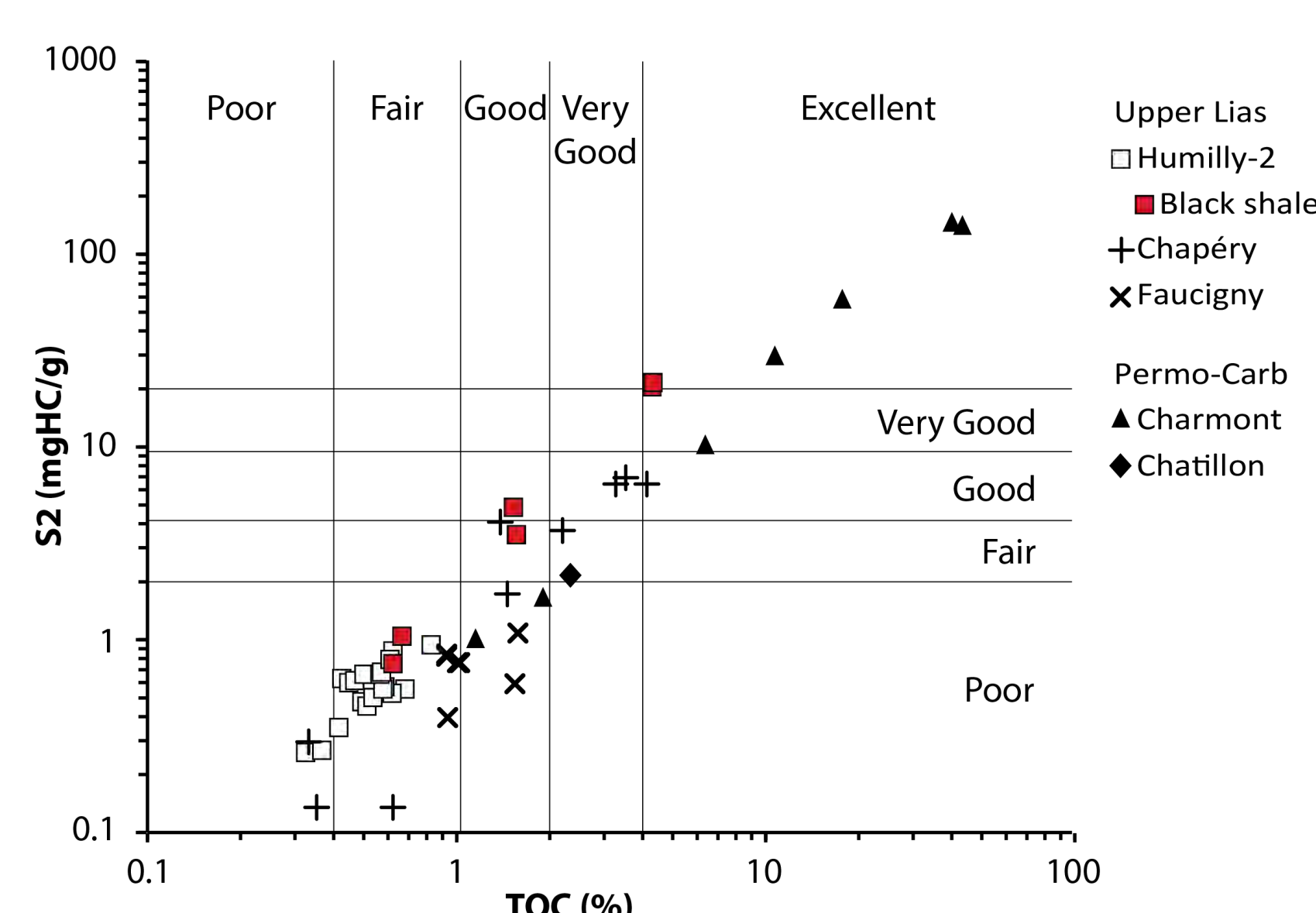


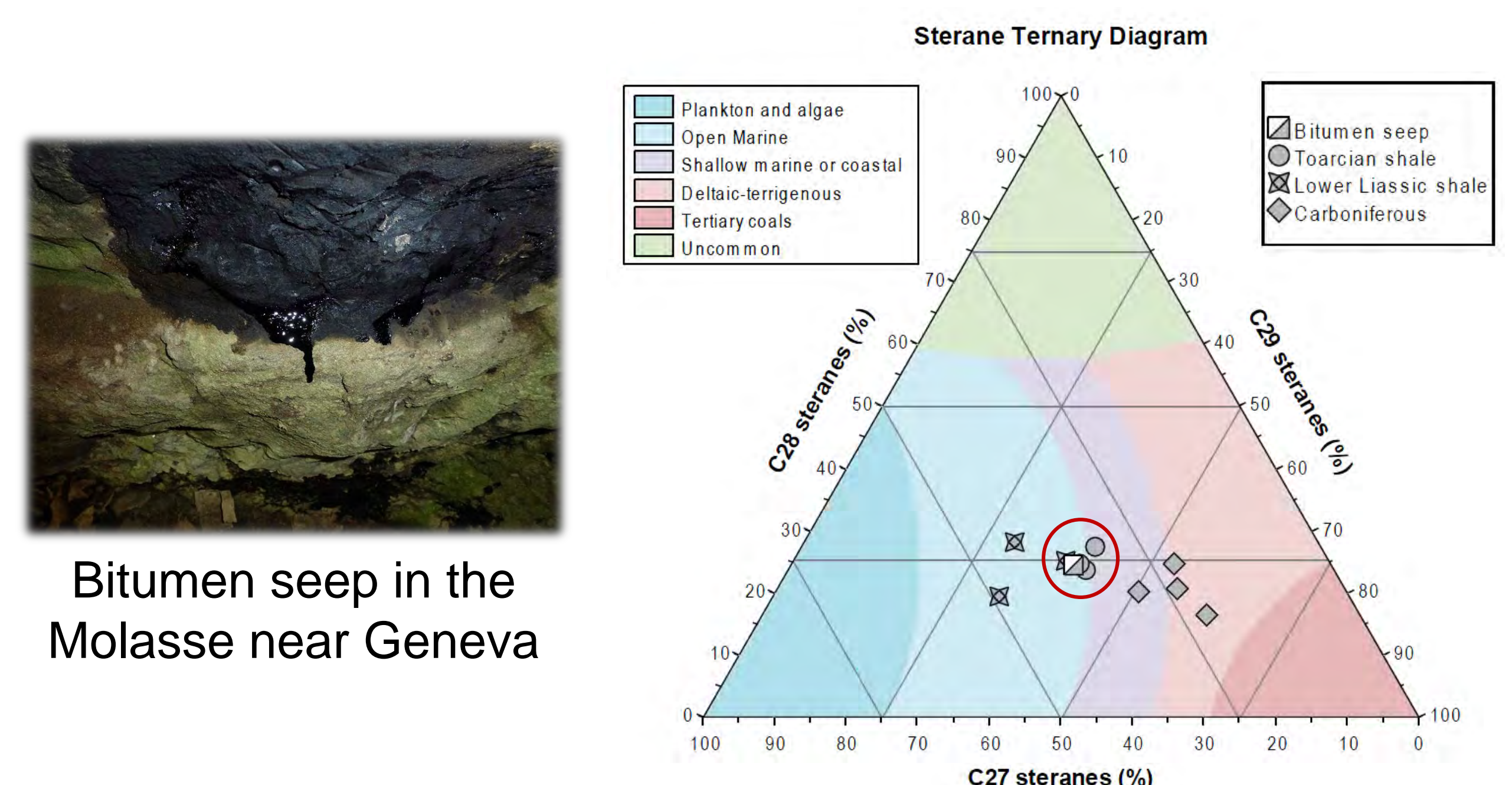
Figure 3: Plot of S2 vs. TOC showing source rock potential

Data are kindly provided by



## Source-rocks maturity and HC sources

- The Posidonia shales (oil window) are currently expelling hydrocarbons
- The bitumen sampled at the surface shows a similar carbon isotopic composition than the Posidonia shale (Fig. 4).



Bitumen seep in the Molasse near Geneva

Figure 4: Ternary diagram of regular steranes (C27 - C29)

- Geochemistry of gas (retrieved from a shallow borehole) evidenced the participation of both biogenic and thermogenic sources.
- Gas geochemistry most probably indicate an early mature type III kerogen as precursor.

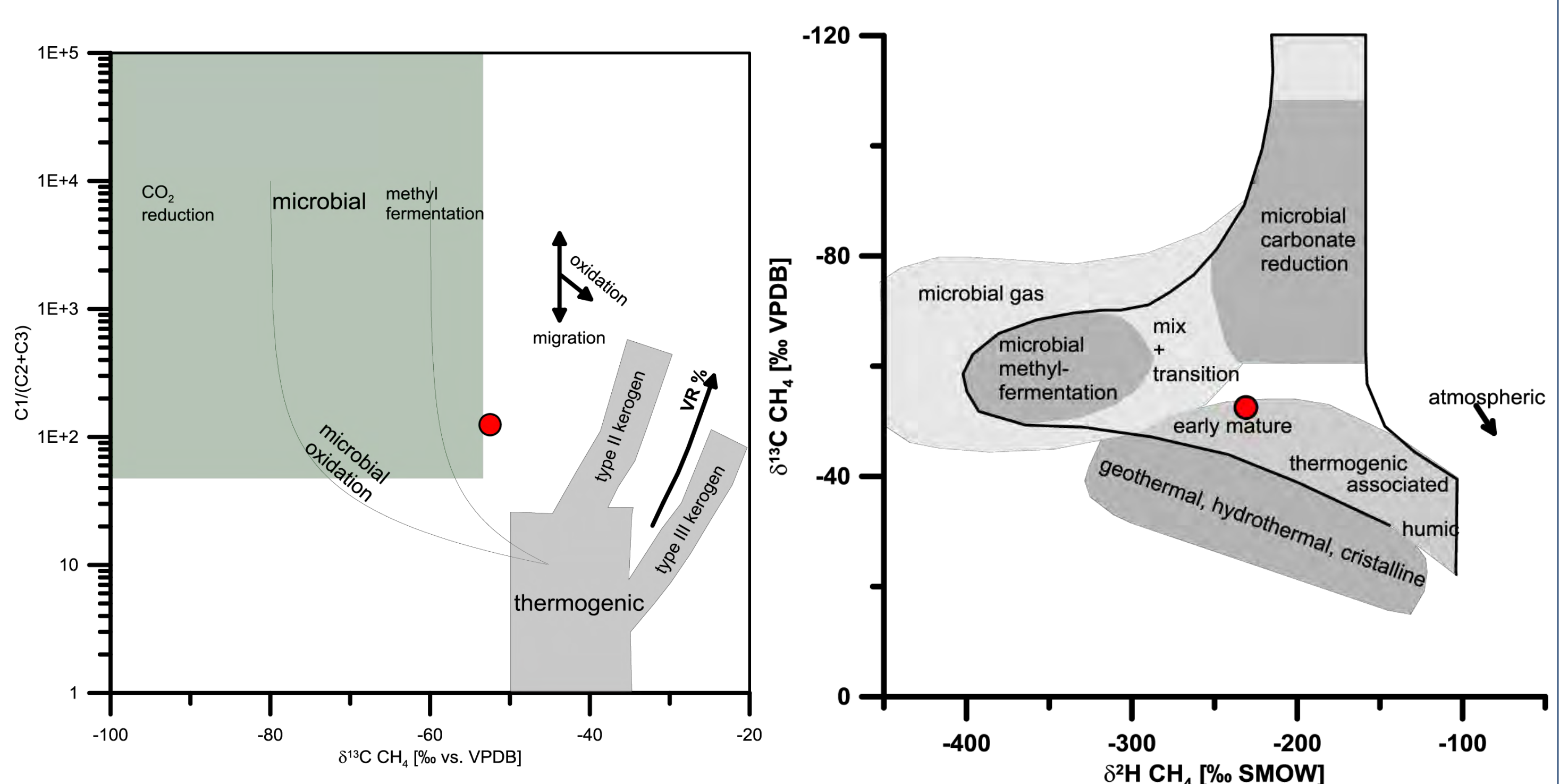


Figure 5: Carbon isotope composition of the gas sampled showing a biogenic and thermogenic (early mature) mixing sources

## Conclusions and outlooks

- Posidonia shale have reached the oil window in the centre of the basin (Humilly-2 and Chapéry) and generate bitumen currently flowing at the surface
- the Permo-Carboniferous coal beds encountered in the Jura Mountains have reached the oil (Charmont and Chatillon) and sometimes the gas windows (Chaleyriat)
- recent HC analysis have confirmed the presence of a deep Type III kerogen source rock (most likely Permo-Carboniferous)

- ✓ Oil shale potential rather than shale gas potential for the Posidonia shale in the Geneva Basin
- ✓ The potential of the Permo-Carboniferous needs to be developed
- ✓ Limitations: the large amount of fracturation of the Molasse basin leading to the leakage of hydrocarbons

# Geophysical characterisation of Cretaceous formations for underground thermal energy storage in the Geneva Basin

Luca Guglielmetti\*, Andrea Moscariello\*, Michel Meyer\*\*, Carole Nawratil de Bono\*\*, Hansruedi Maurer\*\*\* & David Dupuy\*\*\*\*

## Abstract

In the framework of the Swiss Competence Centers for Energy Research (SCCER) one of the action fields in energy research is Heat and Electricity Storage (HaE). The University of Geneva is an active member of SCCER and the Earth Sciences Department has been developing a geothermal exploration strategy (Moscariello, 2016) of the Geneva Canton in the framework of the Geothermie 2020 program, in collaboration with Services Industriels de Geneve (SIG), and the Geneva State Geological Survey. The main goal at this stage is to characterise the subsurface in support of geothermal energy exploration and development at different depth for both heat production, storage, and power generation.

The first main step in geothermal development is the understanding of the geothermal conditions at depth in order to provide feasibility scenarios to decision makers. Therefore the understanding of porosity, permeability and saturation of fluids is crucial to plan correctly a sustainable approach to the geothermal resource exploitation.

Within this large exploration effort, a specific 'geophysical acquisition and processing optimisation' project will aim at:

1. Developing an optimised exploration strategy in terms of geophysical data acquisition,
2. Producing a software tool able to manage the several geophysical datasets under a unique workflow in order to make it as a standard for future projects aiming at characterizing geothermal reservoirs in Switzerland and abroad.

The Project partners are: \*\*Services Industriels de Geneve SIG, \*University of Geneva, \*\*\*ETHZ, \*\*\*\*Geo2X, Geneva GeoEnergy

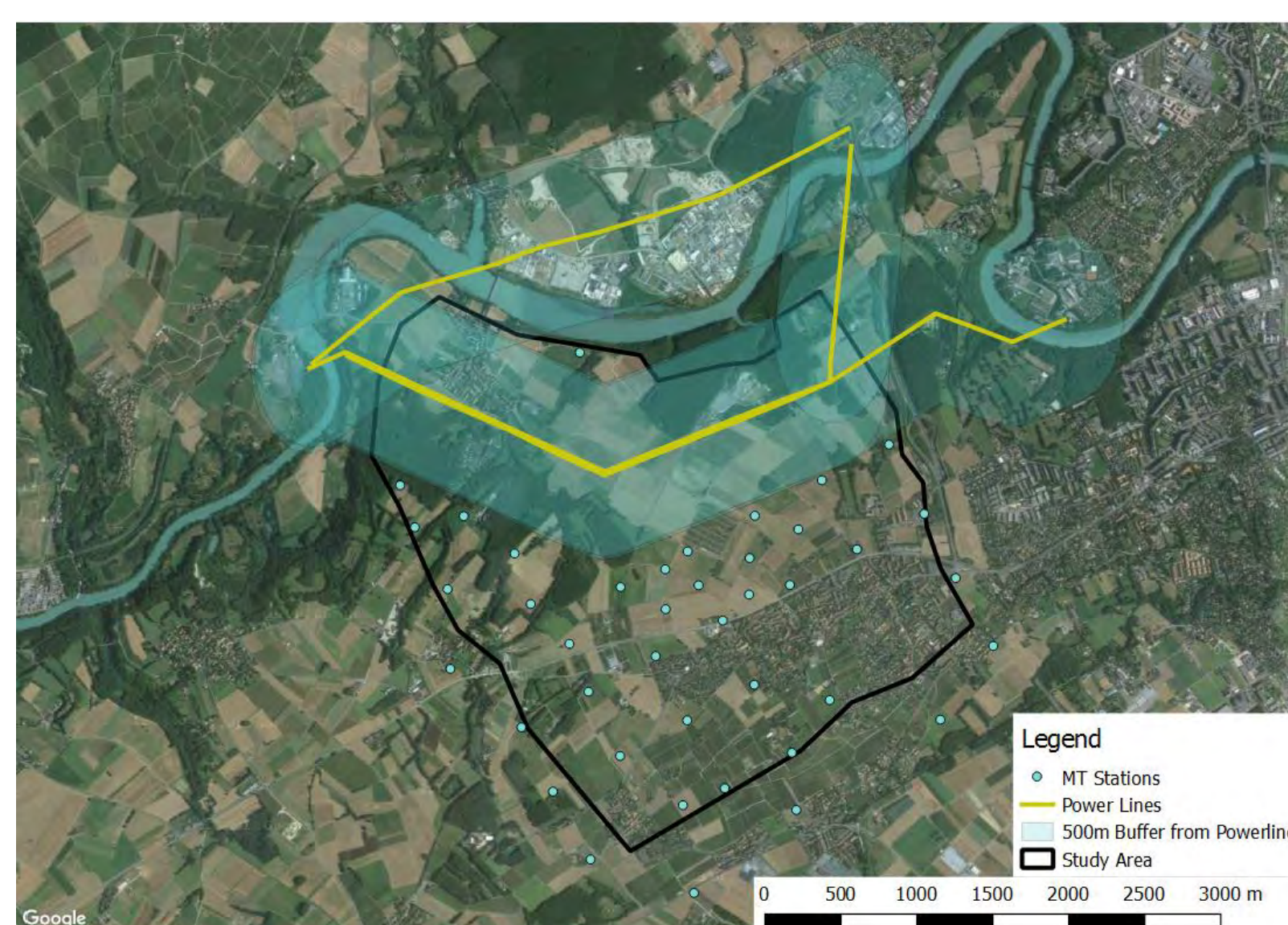
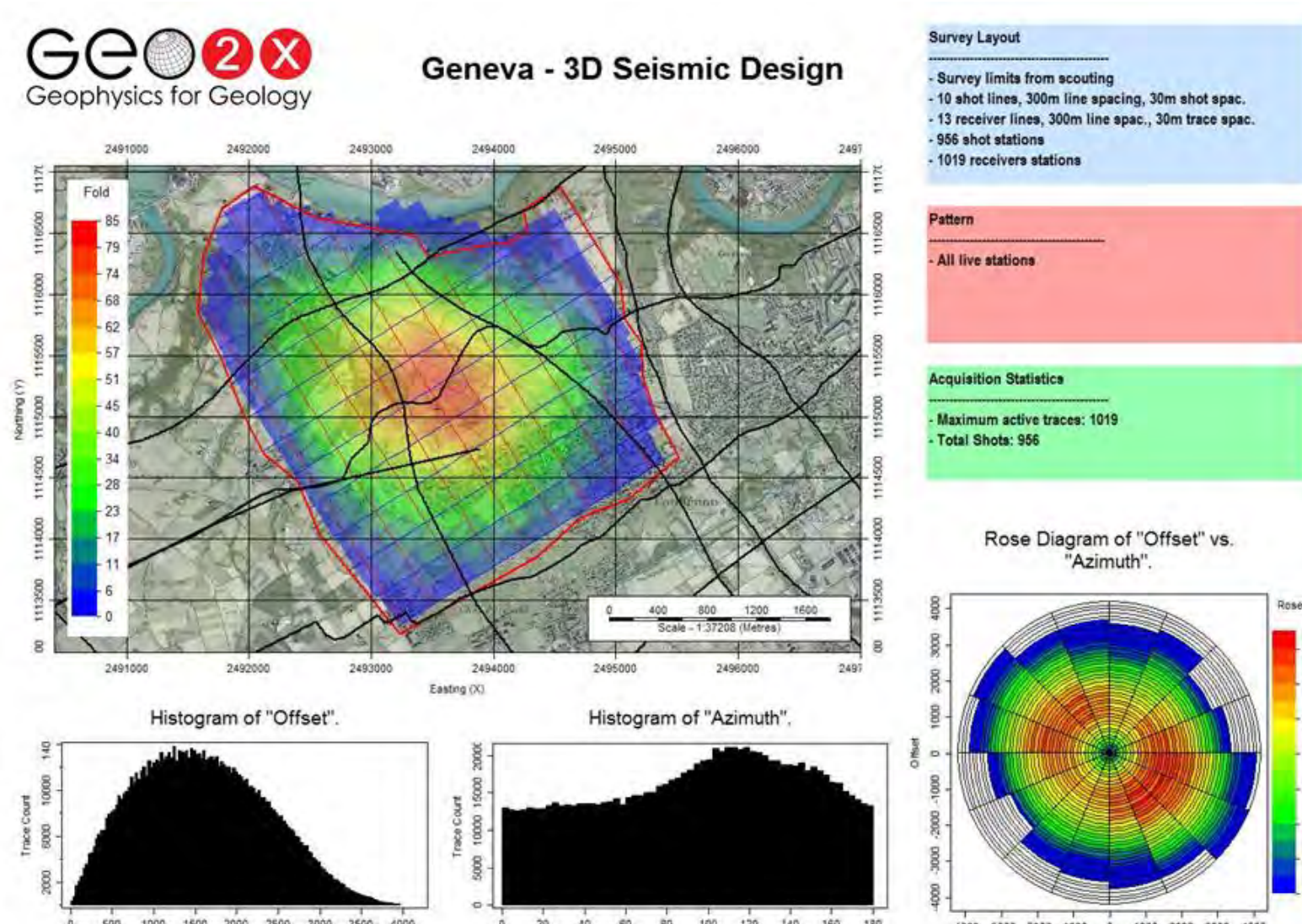
**Objectives:** The main goal of this project is to assess geophysical signatures of properties such as porosity, permeability, water saturation and reservoir connectivity which controls the reservoir compartmentalisation and fluid circulation at depth. In this project new seismic, gravity and MT data will be acquired and the data will be integrated to the 3D geological model available already (Figure 1). We estimate that our development will be applicable on the "Swiss Plateau", where 80% of the geothermal projects are planned. Specifically, this project will include 2 main phases:

### 1. Acquisition of geophysical data:

**3D reflection seismic.** The survey will cover an area of approximately 3x3km to ensure a 1km<sup>2</sup> full fold illumination of the geological target at about 1000m in depth. The acquisition method relies on the utilization of two Vibroseis, one for P-Waves and one for S-Waves. The acquisition layout for P-waves counts for 10 vibration lines, 13 receiver lines. The acquisition layout of S-waves will be set on 4 lines.

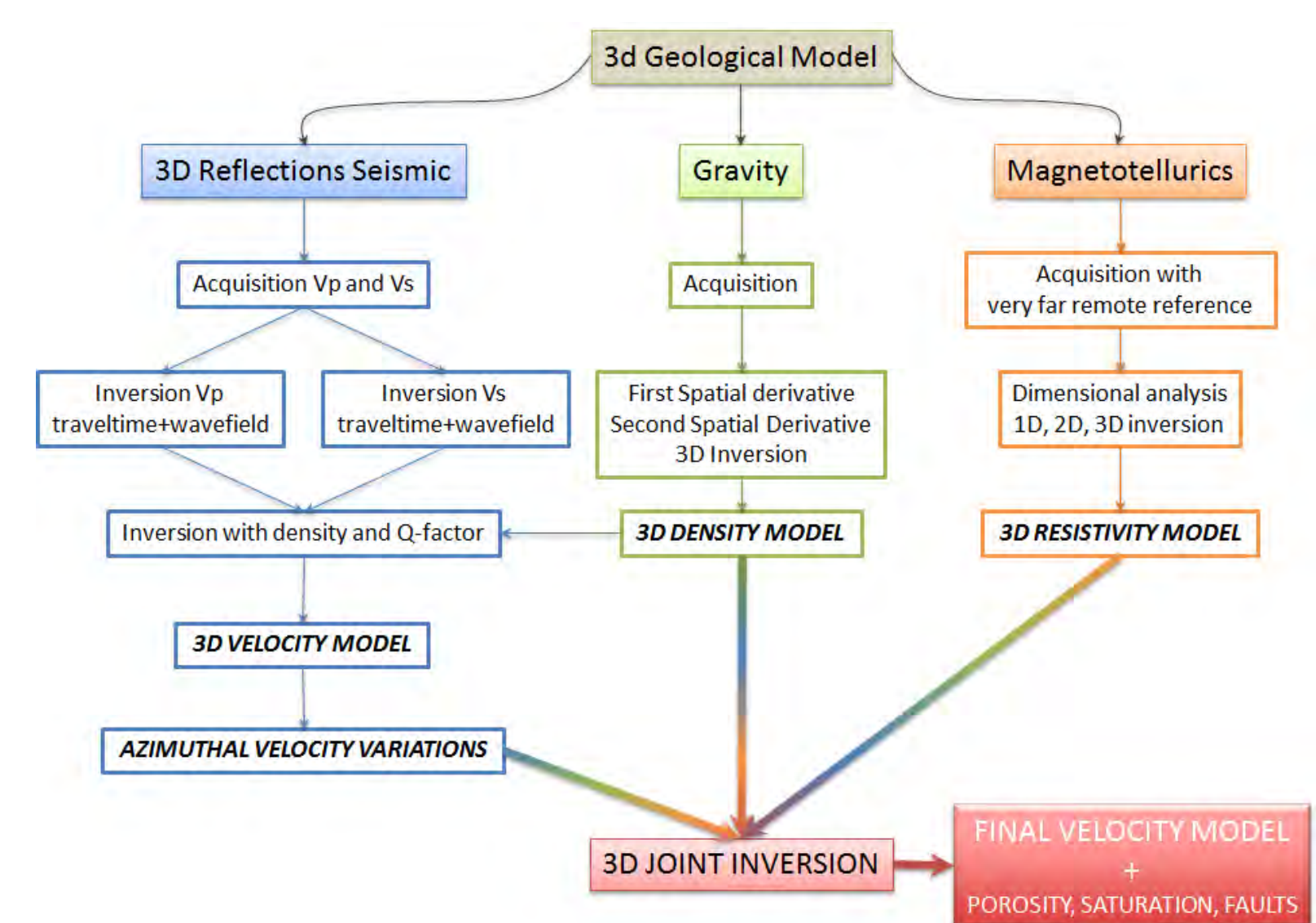
**Gravity** data acquisition with station spacing of 100 m. During the survey, at least 5 gravity readings will be taken at each base or station, checking the accuracy of the measurement will be. Data will be collected using a Scintrex CG-5 gravity meter and their geographical position will be recorded using a RTK GPS.

**Magnetotelluric** data will be collected in this project using the very far remote reference method using data provided by Ecole et Observatoire des Sciences de la Terre EOST in Strasbourg will contribute to remove man-made noise in the 0.1-100 Hz frequency range which strongly affects the quality of the electromagnetic signal. The acquisition will be carried out using two MT instrumentation Metronix ADU-07 with MFS-06/07 coils. Data will be acquired overnight providing normally 12-14 hours of data



### 2. Data Integration via Joint Inversion processing:

- Azimuthal Velocity Variations will be the main goal to achieve by means of the 3D seismic survey. The main advantage of acquiring Vp and Vs separately is that P-wave and S-wave velocities will be initially inverted separately, than simultaneous Vp and VS inversion will be run including also density and Q-factor (anelastic seismic attenuation) as a third inversion step to finally highlight azimuthal velocity variations.
- The processing of gravity data in this project envisages to consider the so-called full gravity tensor (FTG) which will help constraining lateral density variations. The inversion process employed will be based on a 3D compact constrained gravimetric inversion, developed from the original approach by Last and Kubik (1983).
- MT field data (Time Series) processing workflow in this project will follow some standard procedures using the Larsen and Chave codes. Dimensional analysis, 1D, 2D and 3D inversions will be run to result in a 3D resistivity model



The Joint Inversion approach which will be developed in this project will be based on the initial computation of individual inversion models from seismic, gravity and MT data.

It is expected that the inverted models will not completely respond to the field observations therefore a misfit will be measured running several forward model of each inverted result and by comparing these results to the field observations until an acceptable misfit will be achieved. To further minimize the misfit and improve the resolution of the individual models joint inversion will be run on the three datasets in order to and retrieve the porosity and saturation distributions with particular focus on the location of faults in the shallow subsurface

The rationale of this approach is that the minimization process is driven simultaneously by independent observations belonging to different geophysical domains (seismic, gravity, electromagnetic) and, at the same time, it takes in account for the physical link between the different model parameters.

## Expected Results.

The expected results are the following:

- Characterization of the 3D variations of velocity, density and resistivity
- Definition of the geometry of the brittle structures with seismic and gravity data
- Identification of the saturation conditions in the subsurface with seismic and MT data
  - Definition of the permeability conditions in the subsurface
- Development of a replicable and site-specific exploration, processing and interpretation approach
  - Testing the approach with real data
- Provide a geophysical exploration strategy to be applied also for 4D time-laps reservoir monitoring

# Thermal evolution of the Grimsel Pass hydrothermal system: insights from numerical modeling

Christoph Wanner, Peter Alt-Epping, Larry W. Diamond  
Institute of Geological Sciences, University of Bern

## 1. Introduction

Hydrothermal springs with discharge temperatures of up to 28 °C are found beneath the Grimsel Pass in the Transitgas AG tunnel crosscutting through crystalline units of the Aar massif (Pfeifer et al., 1992). The springs are of meteoric origin, occur over a narrow tunnel section of <100 m and are associated with a major E-W fault-zone, the Grimsel Fault Breccia (GFB). In the framework of the SCCER-SoE Task 1.1 we are conducting a numerical modeling study aiming at (i) unraveling the thermal and hydrodynamic evolution of the Grimsel Pass hydrothermal system and (ii) evaluating the general geothermal potential of fracture-flow hydrothermal systems. The latter is particularly important with respect to Switzerland's efforts to access and/or engineer such systems for geothermal power production. Numerical simulations were performed using two different approaches, a continuum approach using TOUGHREACT and a discrete fracture network approach using ConnectFlow coupled to PFLOTRAN.

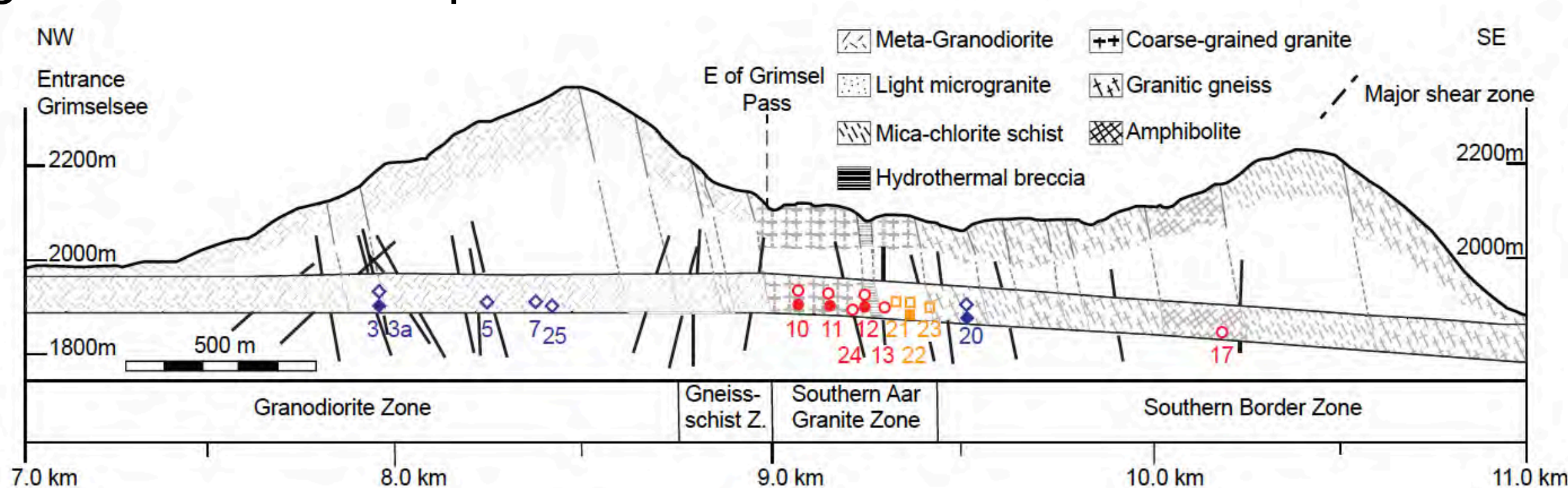


Fig. 1: Geological cross section of the Transitgas AG tunnel showing thermal (red), subthermal (orange) and cold springs (blue). Adapted from Waber et al. (2016).

## 2. Continuum model (TOUGHREACT)

### Model setup:

- 3D with variable depth (20 x 20 x 5.25-5.75 km)
- Constant width of the GFB along the tunnel (100 m)
- Variable extent of the upflow zone parallel to the GFB (25-100 m)
- Maximum GFB permeability of  $10^{-13} \text{ m}^2$
- Initial and boundary conditions:
  - Hydrostatic pressure distribution
  - $P > P_{\text{hydrostatic}}$  and  $T = 160 \text{ °C}$  below upflow zone; overpressure corresponds to the hydraulic head driving the system and depends on the simulated infiltration altitude (500-1000 m above tunnel)
  - Conductive temperature distribution (4 °C at the surface; 25 °C/km)

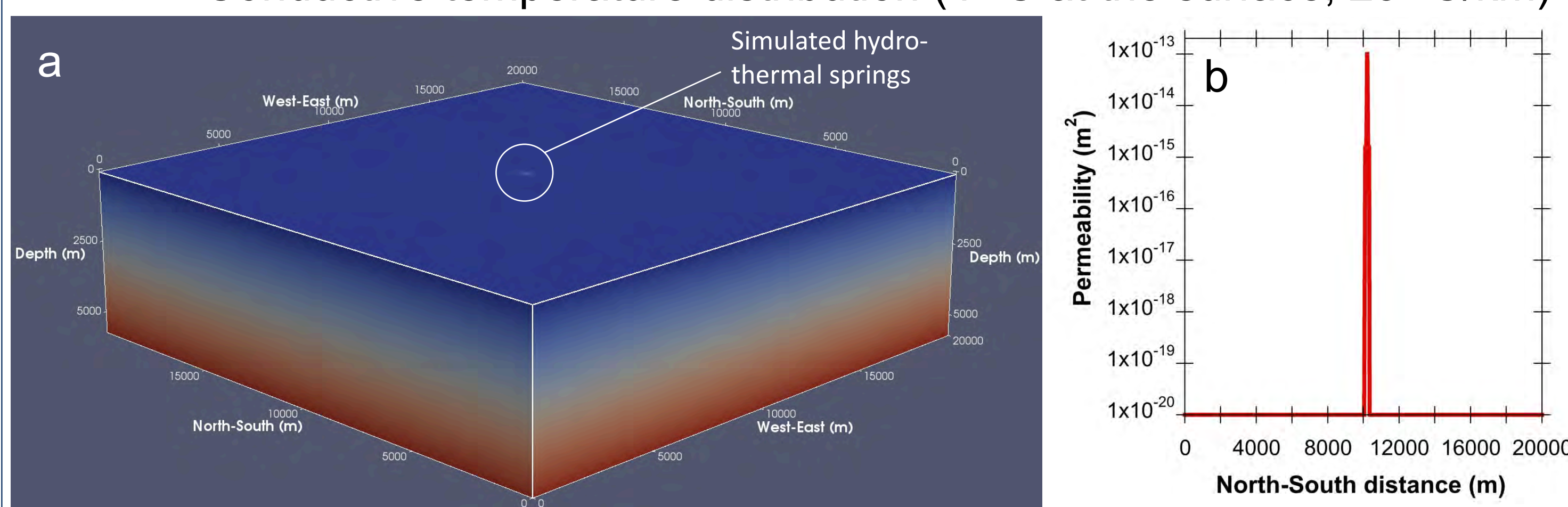


Fig. 2: Model setup (a) and permeability distribution specified within the upflow zone along the Transitgas AG tunnel (b).

### Model results

- Steady-state temperature distribution is approached in less than 2000 a
- The extent of temperature anomalies induced by fracture-flow hydrothermal systems are mainly controlled by
  - the 3D extent of the fault system
  - the upflow velocity, i.e., by the fault zone permeability as well as the hydraulic head driving hydrothermal circulation

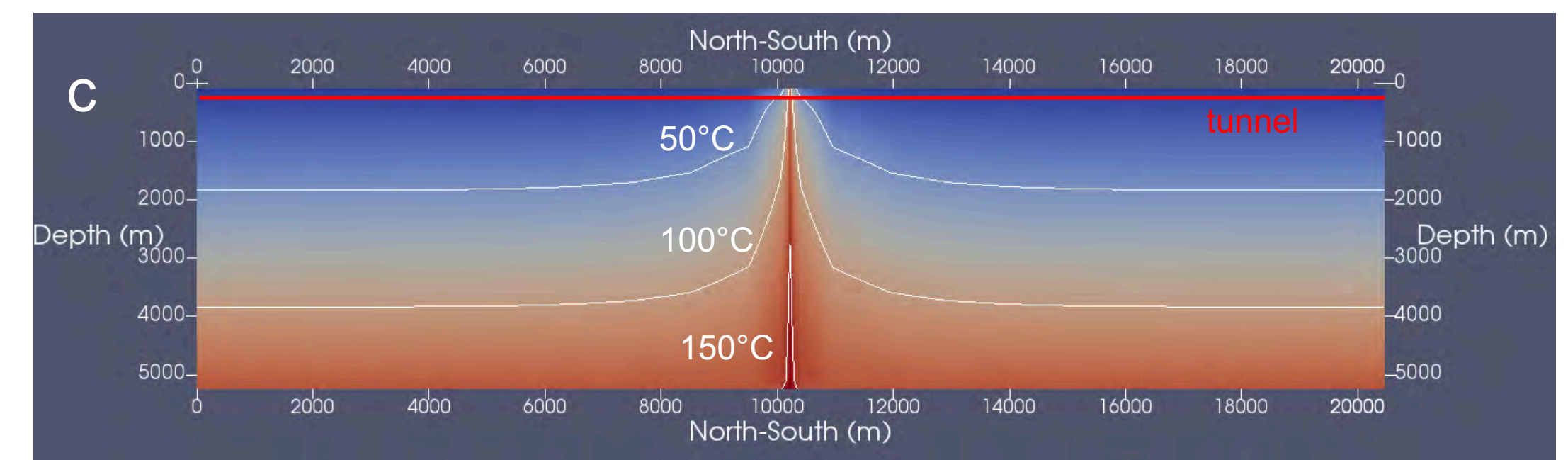
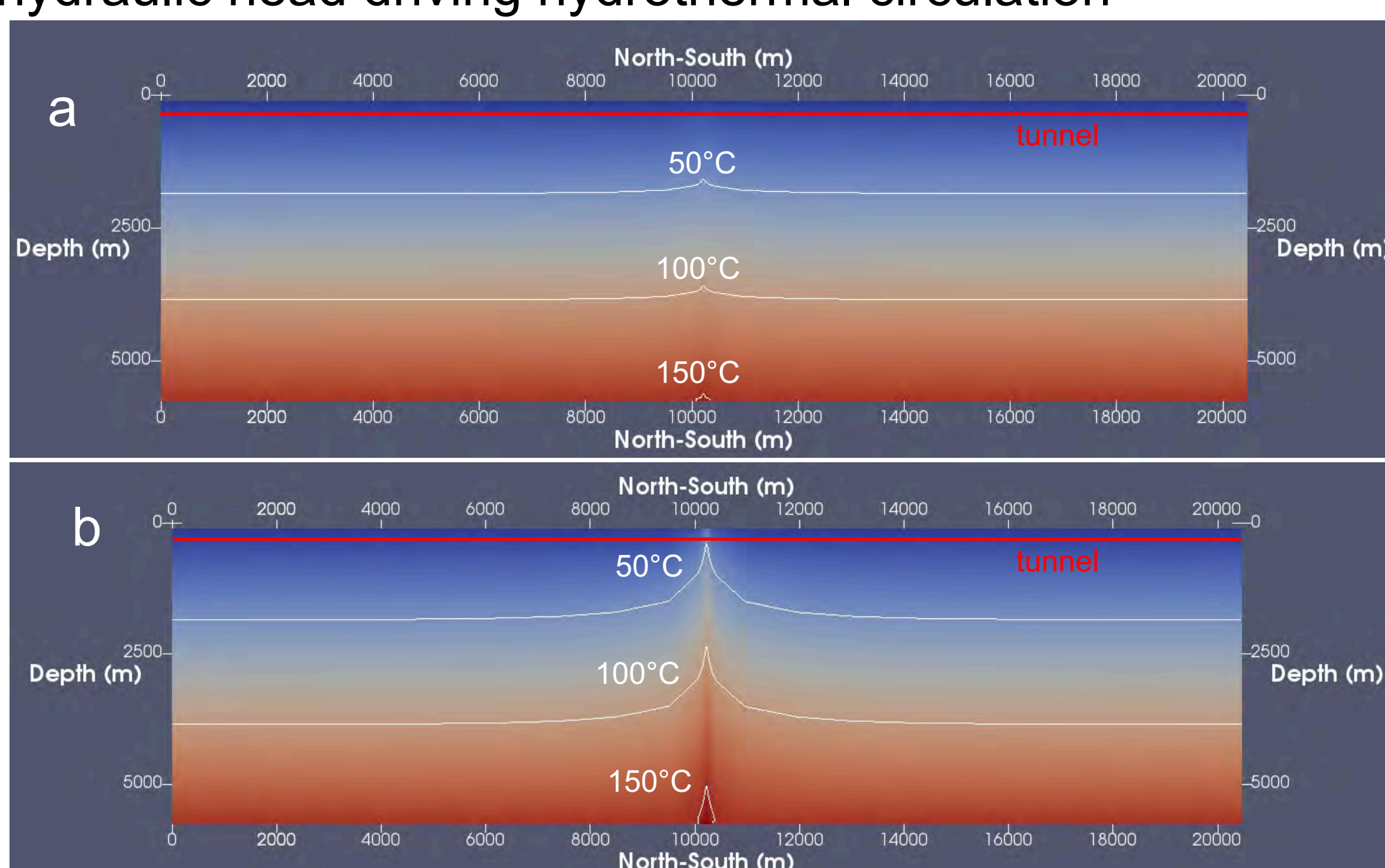


Fig. 3: 2D Steady state temperature distributions shown for the plain intersecting the GFB at an angle of 90° and including the tunnel. (a) and (b) correspond to a hydraulic head of 500 m and an East-West (along strike) extent of the upflow zone of 25 (a) and 100 m (b), respectively. (c) illustrates the temperature distribution for a hydraulic head of 1000 m and an East-West extent of 50 m.

## 3. Discrete fracture network model

We use ConnectFlow (AMEC, 2012) to generate discrete fracture networks and convert them into equivalent permeability and porosity fields. The GFB is represented as a dense network of subvertical, subparallel (yet intersecting) fracture planes yielding an equivalent bulk permeability of about  $10^{-13} \text{ m}^2$ . The upscaled permeability and porosity fields are read into PFLOTRAN (www.pflotran.org). Here we present preliminary results of this type of loose coupling.

### Model setup:

- 3D (300 x 100 x 4000 m)
- Length (along strike) and width of GFB: 100 m and 9 m, respectively
- Initial and boundary conditions:
  - Hydrostatic pressure distribution
  - Below upflow zone:  $P > P_{\text{hydrostatic}}$  (10 MPa overpressure),  $T = 105 \text{ °C}$
  - Conductive temperature distribution (4 °C at the surface; 25 °C/km)

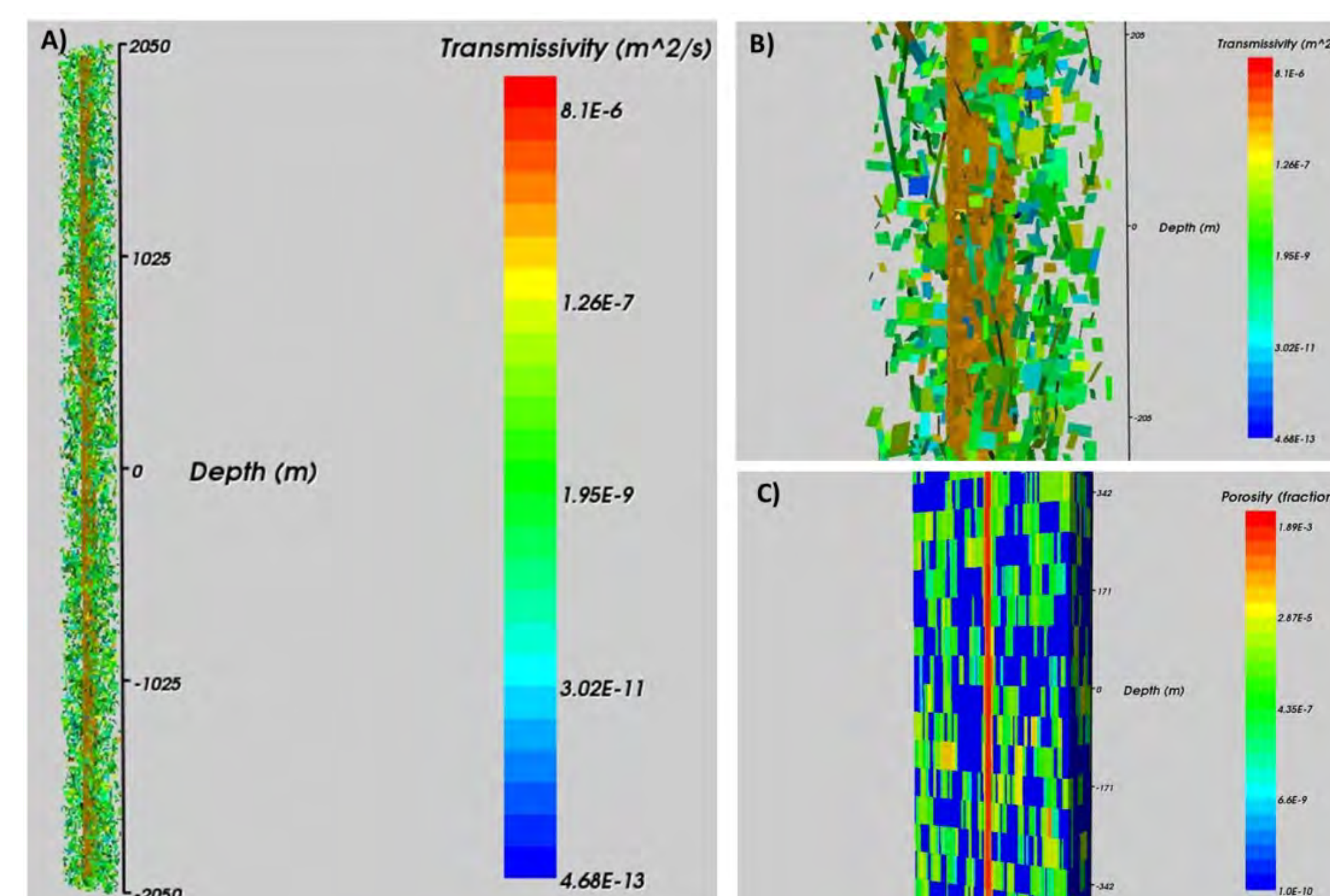
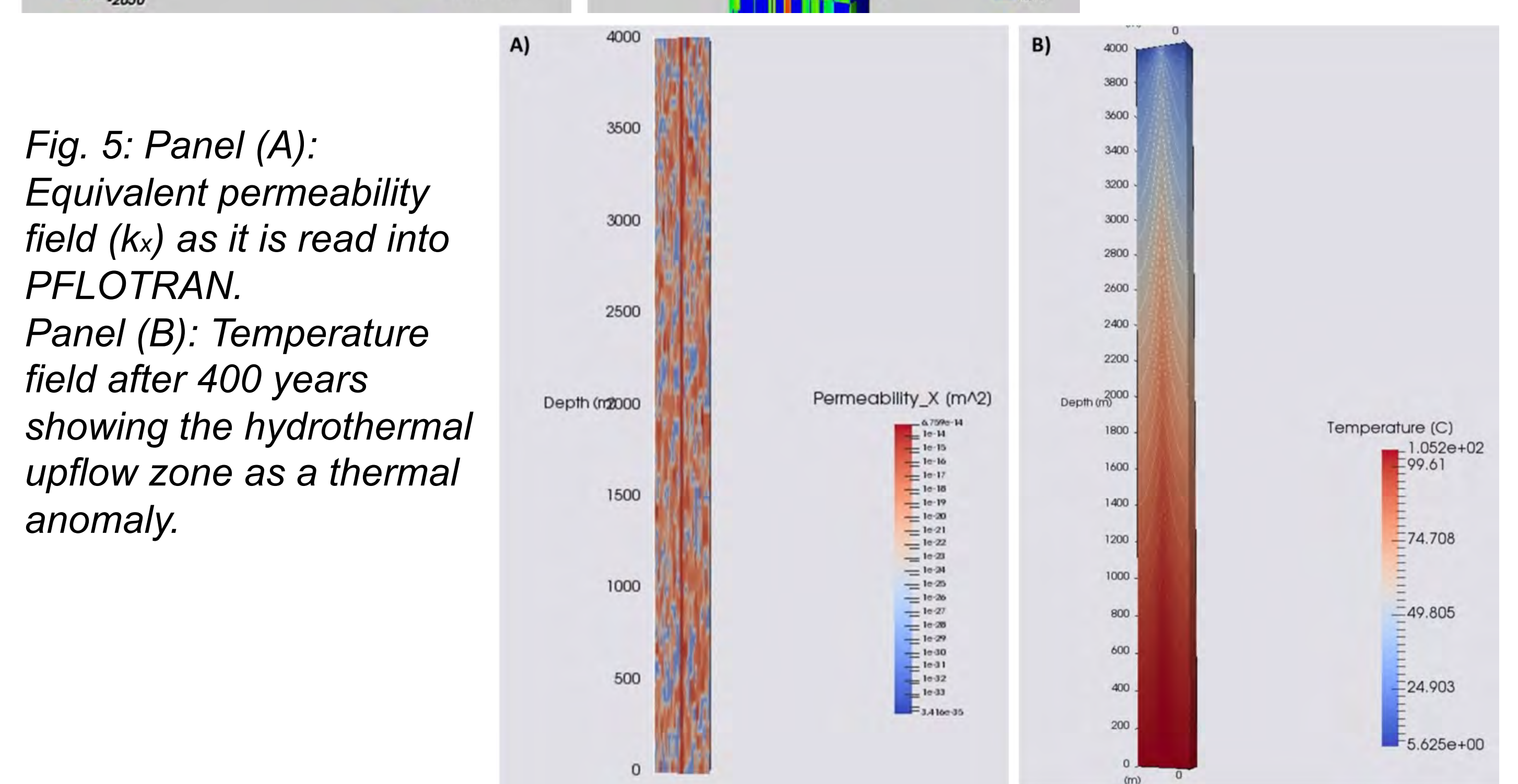


Fig. 4: The GFB is represented as a network of dense, subparallel fractures. The rock exhibits a relatively low fracture density (panel A). Panels (B) and (C) are a detailed view of the fracture network and the upscaled equivalent permeability field, respectively.



## Conclusions & outlook

- Our simulations suggest that the small thermal anomaly observed in the Transitgas AG tunnel results from low discharge rates (<50 L/min) induced by the relatively low fault-zone permeability of about  $10^{-13} \text{ m}^2$
- Future work will particularly focus on evaluating the geothermal potential of fracture-flow hydrothermal systems (e.g., quantification of enthalpy accessible at specific depths).

### References

AMEC, 2012. CONNECTFLOW, Release 10.4, Technical summary document. AMEC/ENV/CONNECTFLOW/15, AMEC, UK  
Pfeifer, HR; Sanchez A.; Degueldre, C. Thermal springs in granitic rocks from the Grimsel Pass (Swiss Alps): The late stage of a hydrothermal system related to Alpine Orogeny. In: Kharaka YK & Maest AS, editors, Proceedings of Water-Rock Interaction WRI-7, Park City, Utah, A.A. Balkema, Rotterdam, The Netherlands; 1992. p. 1327-1330. Waber H.N, Schneeberger, R.; Mäder, U.K.; Wanner, C. 2016. Constraints on evolution and residence time of geothermal water in granitic rocks at Grimsel (Switzerland). Procedia Earth and Planetary Science. Proceedings of the 15th Water-Rock Interaction Symposium WRI-15, Evora, Portugal.

# Fracture-controlled flow paths in an active hydrothermal system (Grimsel, Swiss Alps)

Daniel Egli<sup>1</sup>, Rahel Baumann<sup>1</sup>, Sulamith Küng<sup>1</sup>, Alfons Berger<sup>1</sup>, Ludovic Baron<sup>2</sup> & Marco Herwegh<sup>1</sup>

<sup>1</sup>Institute of Geological Sciences, University of Bern, Baltzerstrasse 3, CH-3012 Bern, daniel.egli@geo.unibe.ch, <sup>2</sup>Institut des sciences de la Terre, Université de Lausanne, Bâtiment Géopolis, CH-1015 Lausanne

## 1. Introduction

Flow paths in fault-bound hydrothermal systems are strongly controlled by the spatial distribution and continuity of ductile and brittle structures (shear zones, fractures, joints) that can provide the main fluid pathways and enhance permeability of the rock mass by joining existing pores and creating new pore space but can also act as seals to fluid flow. Better understanding of the occurrence and behaviour of such naturally porous and permeable rock masses at suitable depths could provide an

alternative to enhanced geothermal systems for future geothermal exploration and eventually energy production. This study focuses on an active fault-bound hydrothermal system in the crystalline basement of the Aar Massif (Fig. 1) that has been exhumed from few km depth and which documents at least 3 Ma of hydrothermal activity (Hoffmann et al., 2004; Belgrano et al., 2016).

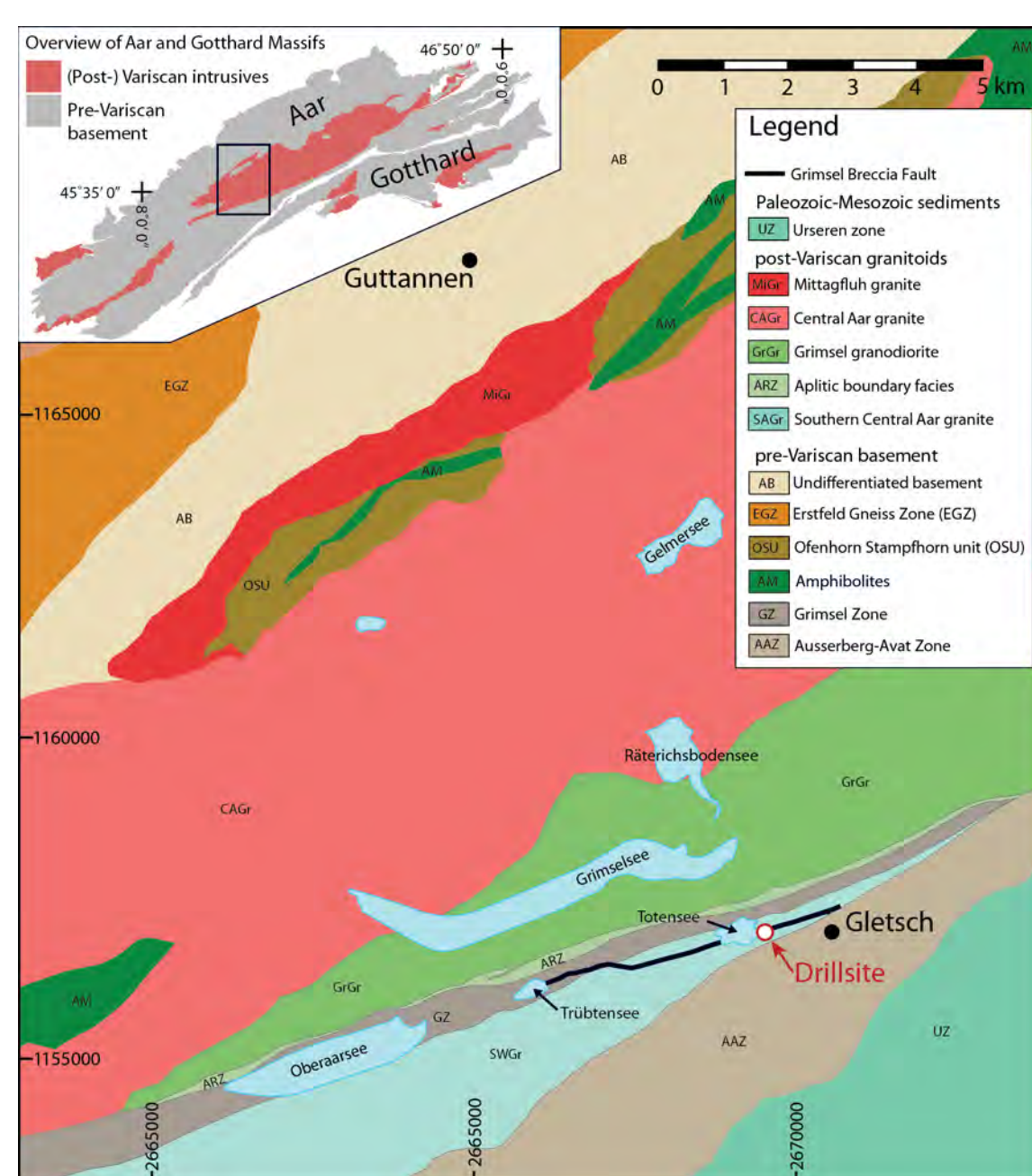


Fig. 1 Geological map of the SW Aar Massif. Modified after Belgrano (2016)

## 2. Approach and objectives

On the basis of structural data collected from a 125 m long drillhole, the corresponding drill core and surface mapping, we evaluate the porosity, permeability and fracture distribution around a central water-bearing breccia zone from the micrometre to decametre scale. Analyses of deformation of the granitic host rock, its degree of alteration as well as the type and amount of pore space give important insight on past and present fluid circulation. To that end, classic structural analysis is combined with drill core mapping, borehole log interpretation, photogrammetry and UV-microscopy.

## 3.1 Borehole and core mapping

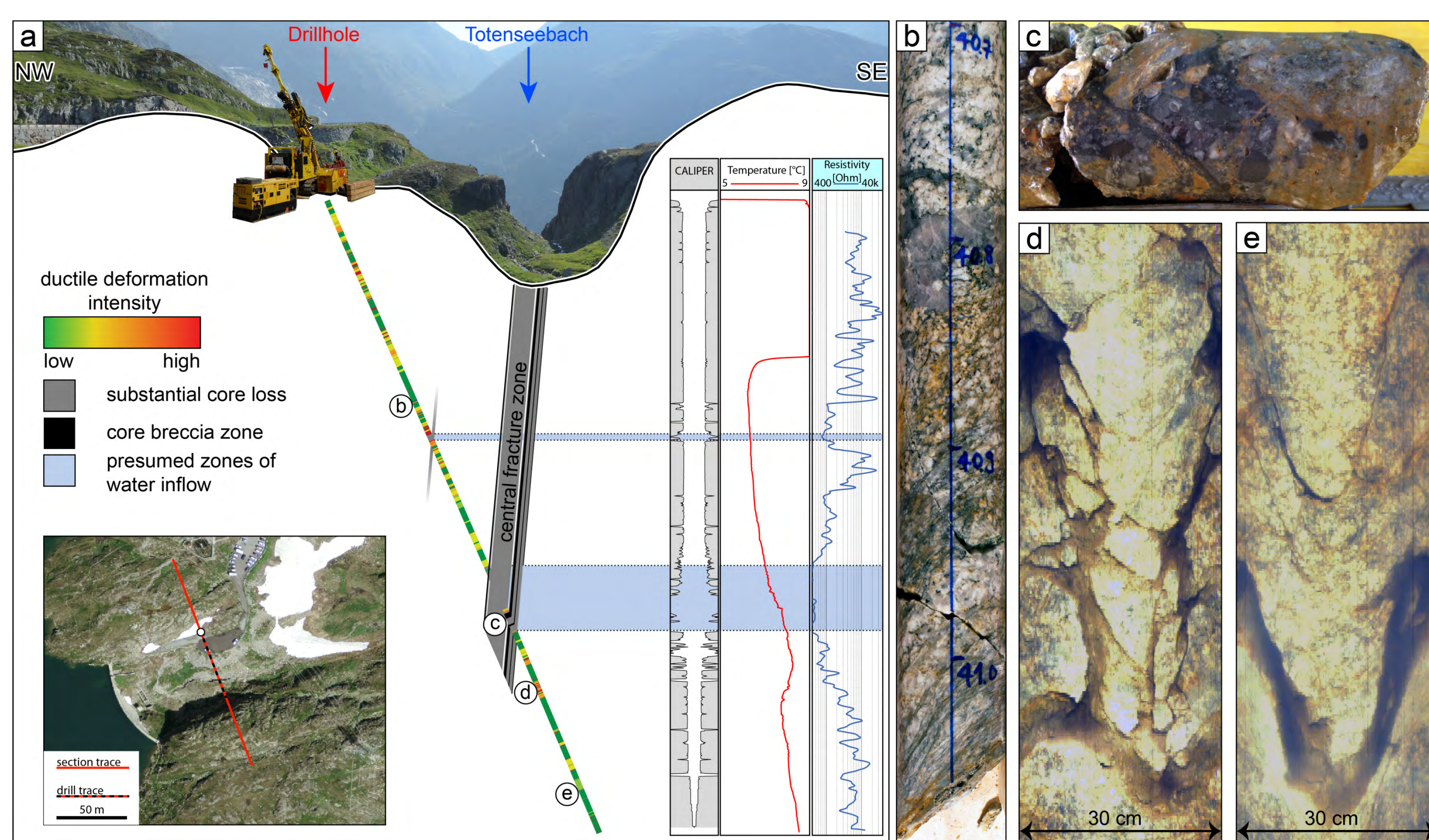


Fig. 2 shows an overview of the borehole including intensity of ductile deformation, the central breccia zone as well as temperature and resistivity logs (a), and examples from the core (b-c) and televiewer imaging (d-e). We could identify at least two potential inflow zones of thermal waters in the central brecciated part as well as in adjacent fracture zones. Although the host rock is very heterogeneous with alternations of intact rock, shear zones and fractures, it is comparatively dense (b), which is also true for the main breccia zone (c). Fluid flow appears to be controlled by a network of large open fractures (d-e) emphasizing the importance of fracture porosity.

## Acknowledgments

This project is part of the NRP70 program and is funded by the Swiss National Science Foundation. We thank Swisstopo, the Swiss Federal Office of Energy, NAGRA and the Kraftwerke Oberhasli AG for additional financial and practical support.

## 3.2 Correlation of surface structures

Correlation of the surface fracture network and structures detected by drill core mapping or drillhole televiewer imaging allows assigning a kinematic and chronologic context to the drillhole structure dataset. Both datasets show a similar fracture distribution dominated by regional SW-NE striking main deformation zones (Group 1) connected by 2 differently oriented fracture sets (Groups 2 & 3). We are currently evaluating orientation consistency, aperture, spacing and indicators for fluid flow of both datasets to quantify fracture porosity and related permeability of the rock mass surrounding the hydrothermal zone.

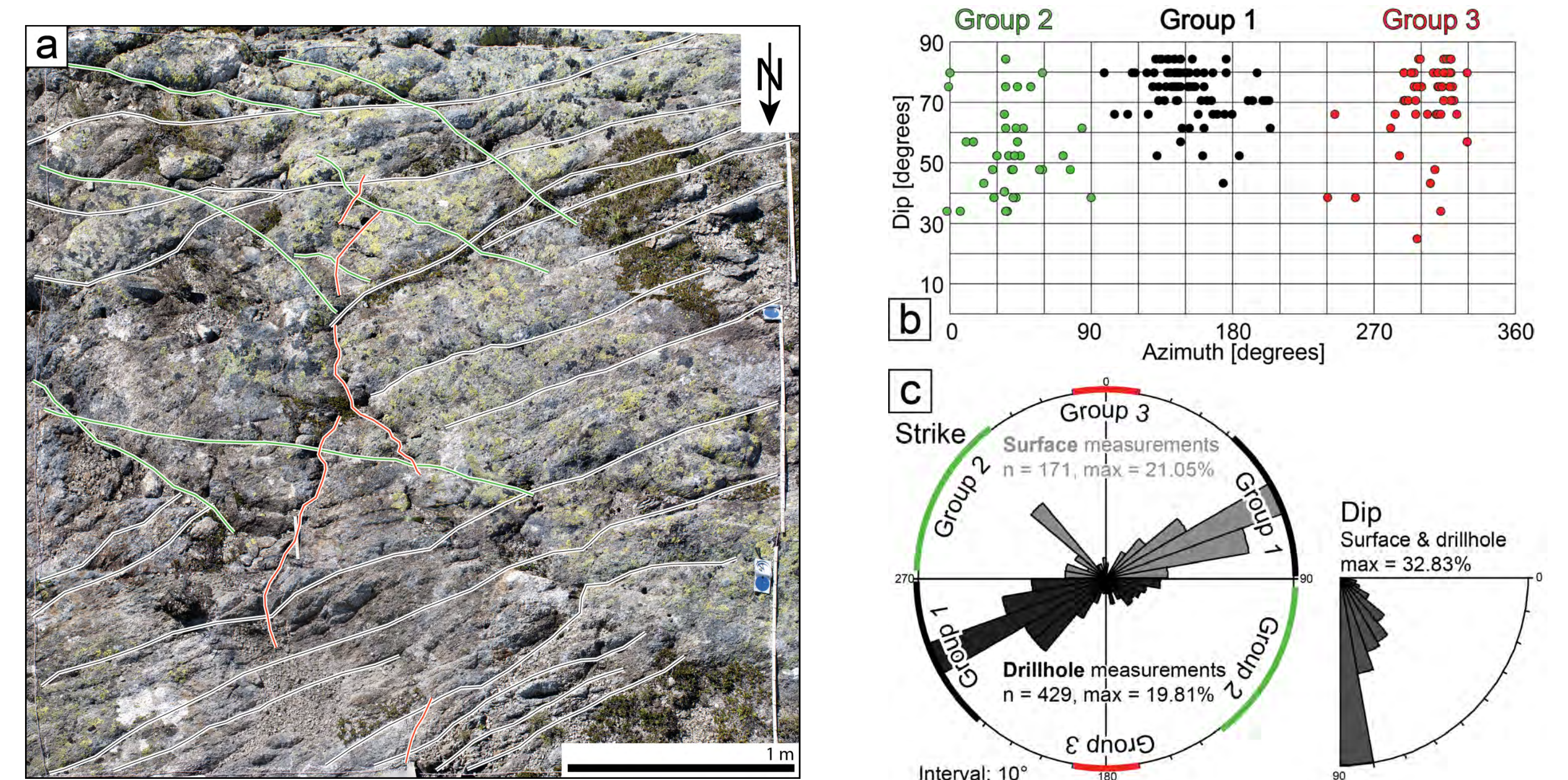
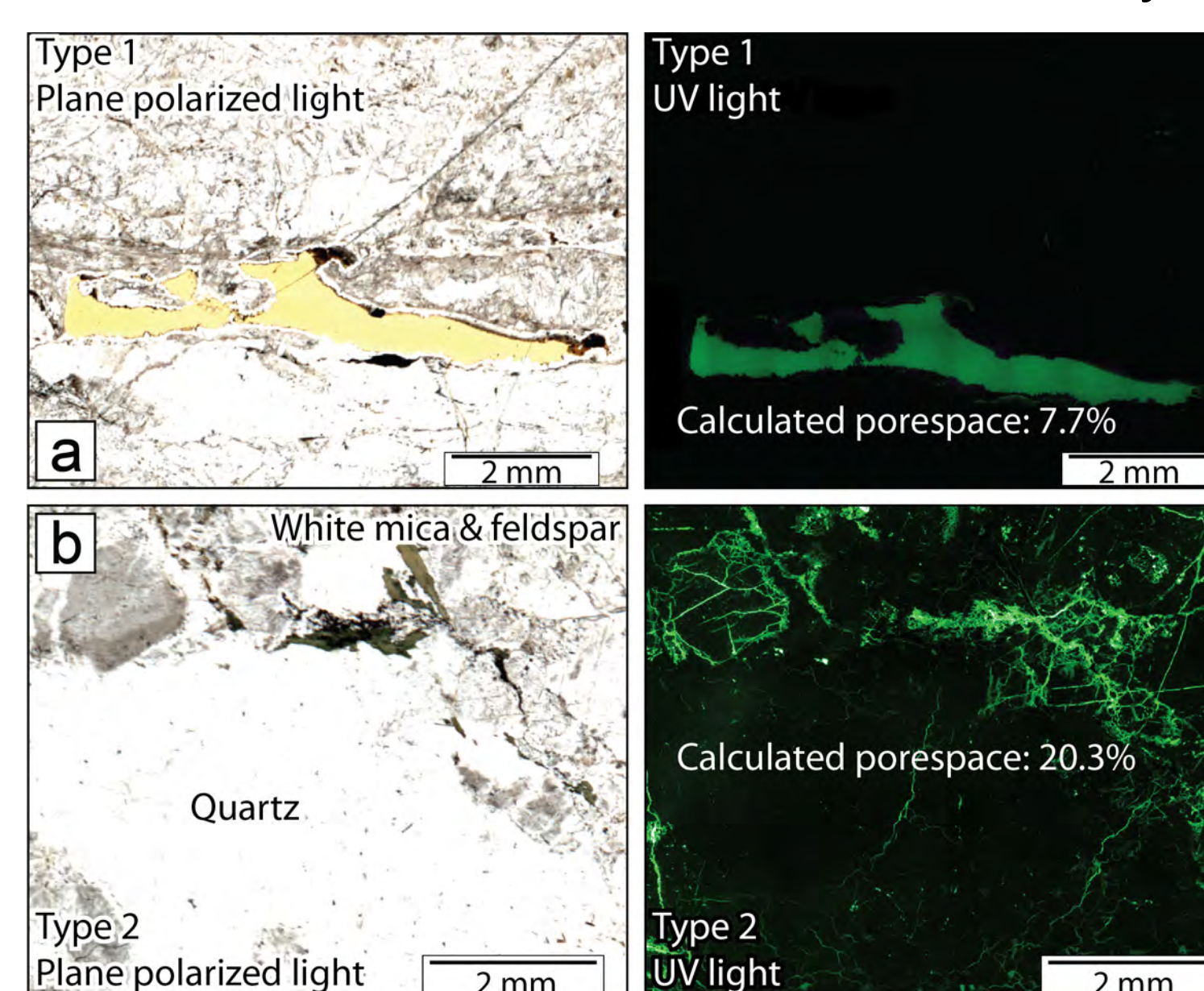


Fig. 3 Main fracture pattern in outcrop (a), surface measurements in dip-vs-azimuth diagram (b), and comparison of surface and borehole data in rose diagram (c)

## 3.3 Quantitative porosity analysis

Total 2D porosity as calculated from UV microscopy is extremely variable throughout the drillcore and ranges from < 1% in undeformed granite to > 30% in fractured zones and comprises two main types: Type 1 builds up to several mm large open pores, which are often connected and are expected to largely contribute to fluid flow (Fig. 4a). Type 2 shows mainly intergranular porosity and forms an extensive network of microcracks (Fig. 4b). Pore space is closely linked to brittle deformation and is thus controlled by the above mentioned fracture



pattern. Its effect on permeability is strongly related to the size distribution and the spatial arrangement of the pores, which are currently being analysed.

Fig. 4 Plane polarized and UV light microphotographs of Type 1 (a) and Type 2 (b) porosity

## 4. Discussion and outlook

On the basis of structural and geophysical observations on an active hydrothermal system we were able to identify discrete zones of enhanced fluid flow related to a complex regional 3D fracture pattern. We are currently working on quantifying effective porosity present as large fractures, significant open pore space as well as minor fissures and its connectivity to calculate values for permeability and evaluate potential for fluid circulation. These values can then be used as input for numerical modelling and reservoir characterisation at 3-5 km depth.

## References

- Belgrano, T.M., Herwegh, M. & Berger, A. 2016: Inherited structural controls on fault geometry, architecture and hydrothermal activity: an example from Grimsel Pass, Switzerland. Swiss J. Geosci.  
Hoffmann, B.A., Helfer, M., Diamond, L.W., Villa, I.M., Frei, R. & Eikenberg, J. 2004: Topography-driven hydrothermal breccia mineralization of Pliocene age at Grimsel Pass, Aar massif, Central Swiss Alps. Schweiz. Mineral. Petrogr. Mitt., 84, 271–302.

# Deep Geothermal Well Optimization Workflow (DG-WOW)

Asmae Dahrabou<sup>(1)</sup>, Benoît Valley<sup>(1)</sup>, Florentin Ladner<sup>(2)</sup>, Frédéric Guinot<sup>(2)</sup>, Peter Meier<sup>(2)</sup>

(1) Centre for Hydrogeology and Geothermics, University of Neuchâtel, Emile-Argand 11, 2000-Neuchâtel, Switzerland.

(2) Geo-Energie Suisse AG, Reitergasse 11, 8004 Zürich, Switzerland.

## I- Context

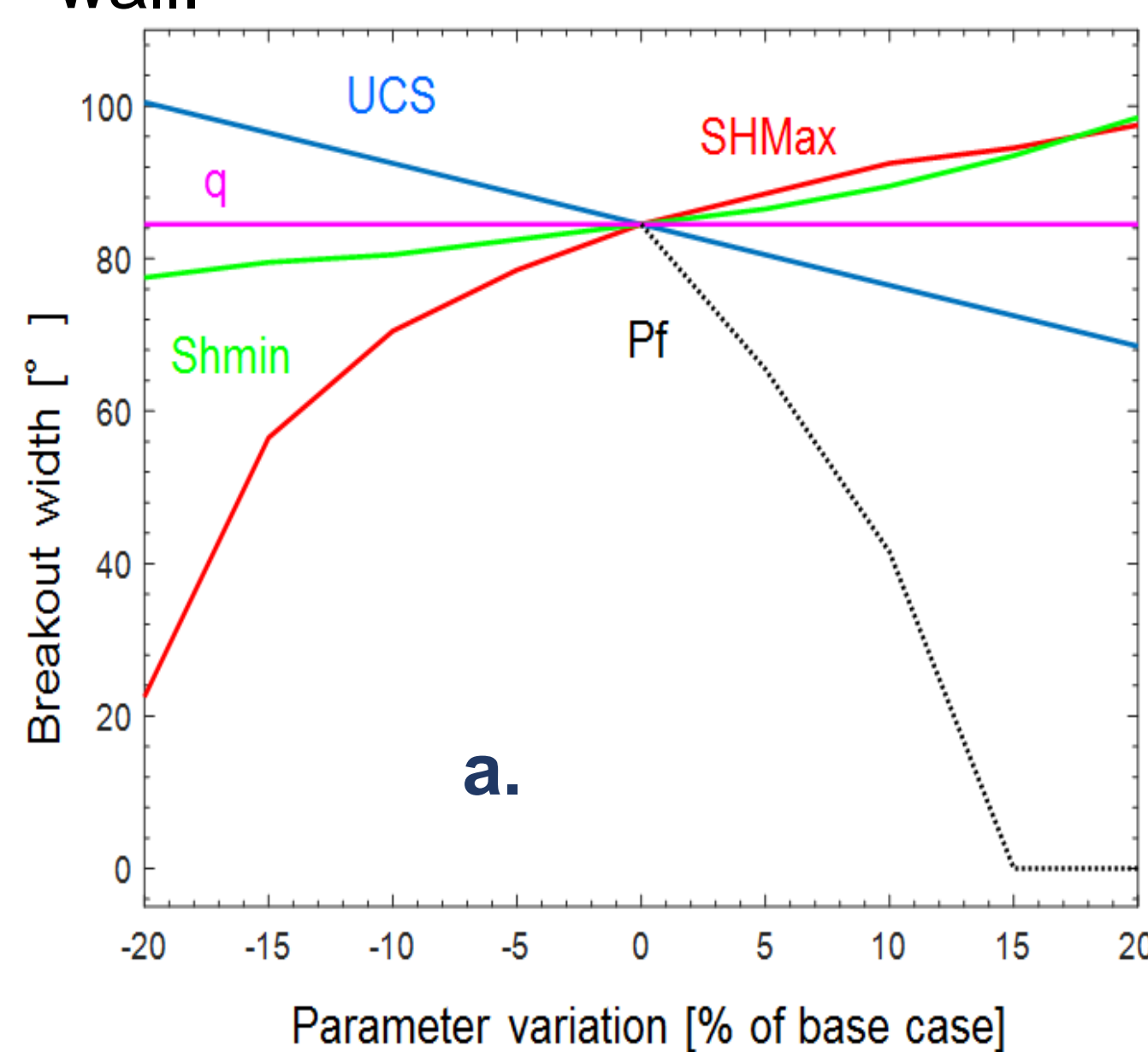
In the frame of a CTI-project the CHYN and Geo-Energie Suisse AG are developing a workflow and associated software tools that enable a fast decision process for selecting an optimal well trajectory while drilling deep inclined wells for EGS-projects. Optimal well trajectory is needed to minimize borehole instabilities and maximize the intersection with natural fractures. Minimizing borehole instabilities will on one hand improve drilling performance and on the other hand will allow to deploy innovative reservoir creation technology ("multi-stage stimulation concept" by Geo-Energie Suisse) that requires an almost in-gauge borehole for proper packer sealing. Both aspects will bring down risks and costs associated with drilling, completion and reservoir stimulation.

## II- Initial linear elastic analyses

In an initial set of analyses, a linear-elastic solution for stress concentration around a borehole was implemented in MATLAB and a graphical user interface (GUI) was created to facilitate borehole stability evaluation. At the moment, the angular opening of the borehole breakouts (referred as breakout width) was used as a borehole stability indicator.

## III- Sensitivity analyses

Sensitivity analyses were performed by using MATLAB software and the framework Uqlab in order to identify the key parameters that influence wellbore failure specifically the stress state at the borehole wall.



The depth is fixed (5000m in figure 1.a) then the UCS, SHmax, Shmin, Pf and q were varied from -20% to 20% of the base case in order to see how the breakouts width vary with respect to these inputs.

- Pearson product-moment correlation were calculated by using the framework Uqlab. It measures the strength of the linear association between variables. (blue bars fig.1-b)

- Linear correlation, however, is known to be inaccurate in the presence of strongly non-linear dependence between variables. A more stable estimator is then used. It relies on monotonicity instead of the linearity of the dependence of two variables. It is called the Spearman's rank correlation index ps. (orange bars)

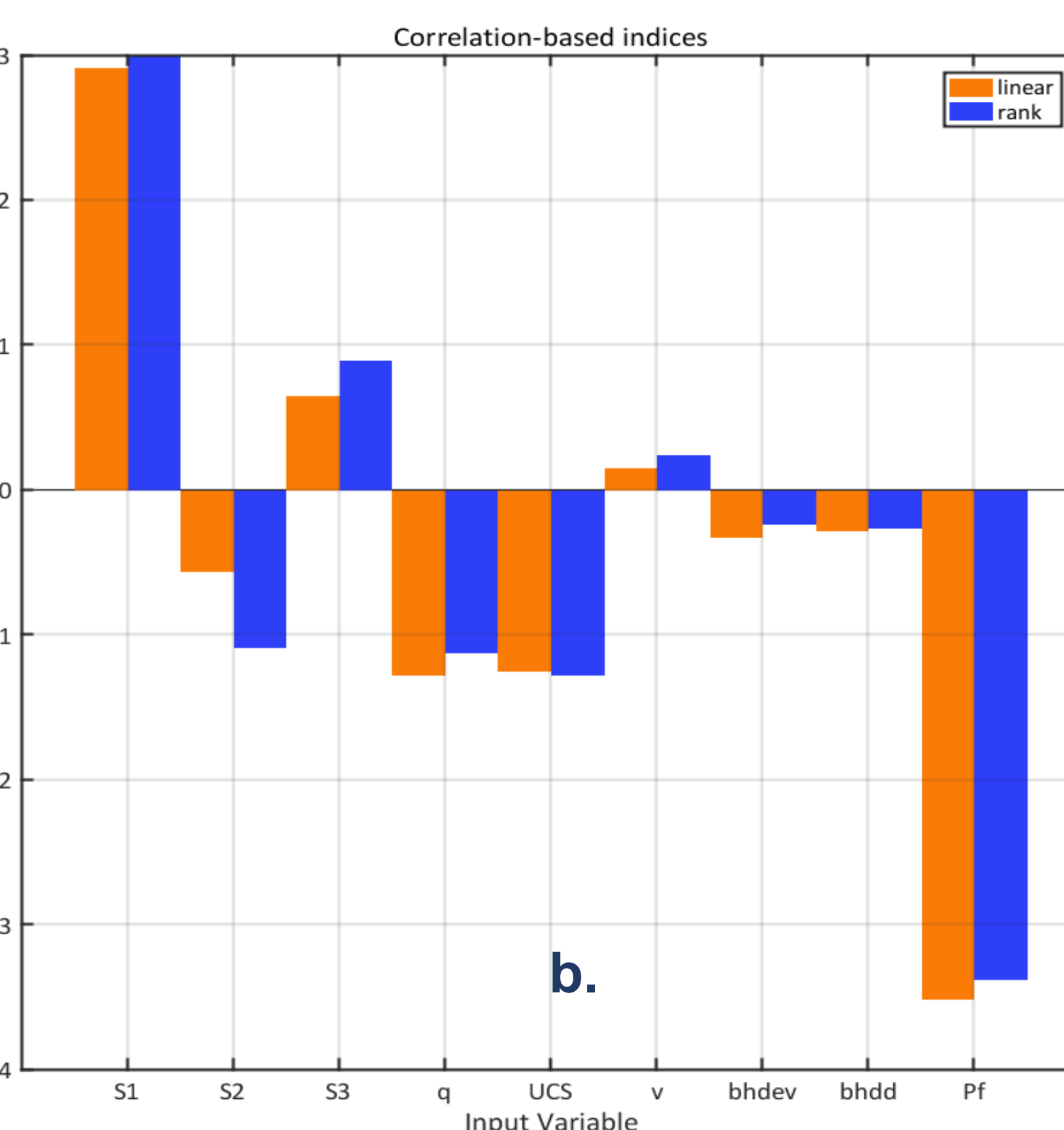


Figure 1: Results of basic sensitivity analysis using Matlab (a), and Uqlab (b) for a depth of 5000m. The orange bars show the Linear coefficient of Pearson and the blue ones show the rank coefficient of Spearman.

## References

Bell, J. S., and D. I. Gough, The use of borehole breakouts in the study of crustal stress, U.S. Geol.  
Mark D. Zoback, 2010, Reservoir Geomechanics.  
Valley, B. & Evans, K.F., 2015. Estimation of the Stress Magnitudes in Basel Enhanced Geothermal System. World Geothermal Congress 2015, (April), p.12.

## IV- Sensitivity of borehole stability to borehole deviation

Figure 2 shows the impact that the drilling direction decision can have on the borehole stability. It shows that depending on the stress regime (normal or strike-slip faulting) and the drilling direction, inclining the borehole can either promote or prevent breakouts formation.

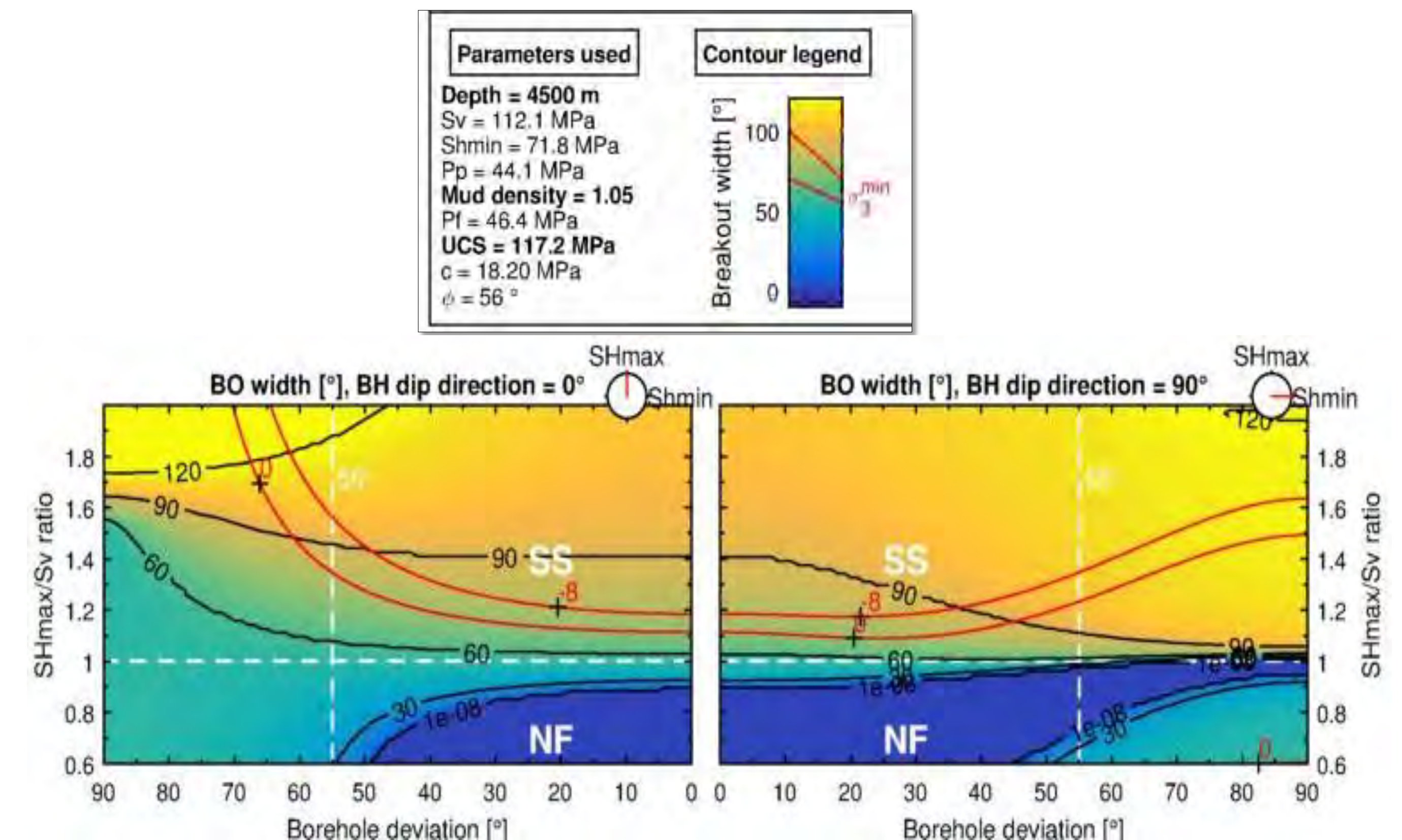


Figure 2: Contour plots of breakout width for increasing borehole deviation and a range of SHmax/Sv ratio for 2 drilling directions (0° and 90°). All other parameters are considered constant and are listed in the figure legend box.

## V- BS-1 Borehole shape analyses

To differentiate breakout geometries, which give similar minimum radius of curvature but will have different implications for the packers and their ability to seal a borehole section, the minimum radius of curvature must be combined with other parameters, like breakout width or depth. Data of the deep Heat Mining Project Basel BS-1 where more than 80% of the crystalline hole section presents breakouts were used in order to describe breakout shape in such a way that it will be helpful in decision making.

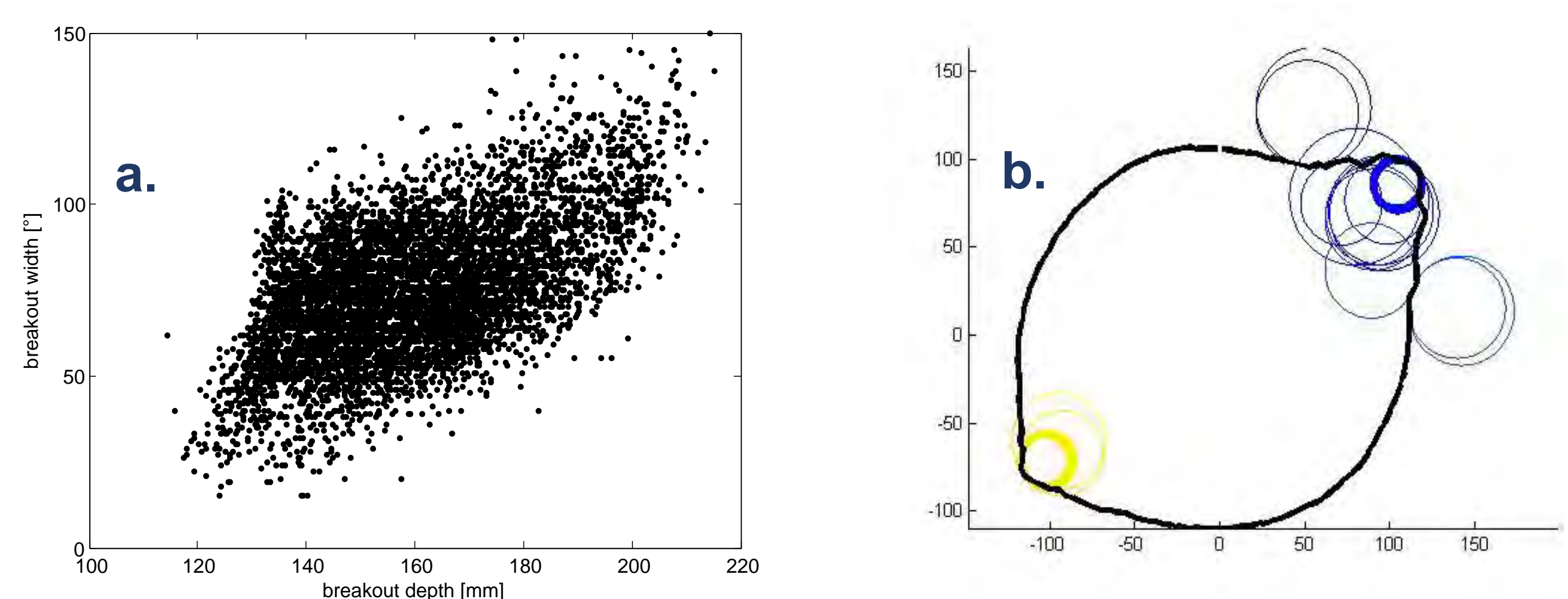


Figure 3: (a) Correlation between breakout width and breakout depth, (b) Example of different breakout geometries for a same minimum radius of curvature

## VI- Conclusions

- By using both approaches for sensitivity analysis, it can be concluded that the most influential parameters are the maximum horizontal stress SHmax, the uniaxial compressive strength UCS, and the mud pressure Pmud.
- Horizontal wells are less subject to tensile failure which gives more space for well control with dense drilling mud.
- Depending on the stress regime and drilling direction, deviating the well can either promote or prevent breakouts formation. Additional information on the stress conditions are thus required to take a decision on the optimal borehole deviation angle.
- Relatively low correlation between breakout width and breakout depth suggests that a combination of these parameters in addition to borehole cross sectional area, ellipticity and minimum radius of curvature will be required to assess the suitability of the borehole wall geometry for setting packers.

## VII- Perspectives

- Develop a borehole stability analyses framework in order to simulate not only breakout width but also other key breakout shape parameters
- Integrate these results in a complete workflow and a required production tool to execute it.
- Test and calibrate the tools on Basel (BS-1) breakout data set and other deep borehole datasets.
- Get the framework ready for a real-life application of the approach at the Haute-Sorne project.

# Structural mapping of a clay fault zone from boreholes data for the FS-experiment in Mont-Terri

Maria Kakurina<sup>1</sup>, Yves Guglielmi<sup>2</sup>, Christophe Nussbaum<sup>1</sup> and Benoit Valley<sup>1</sup>

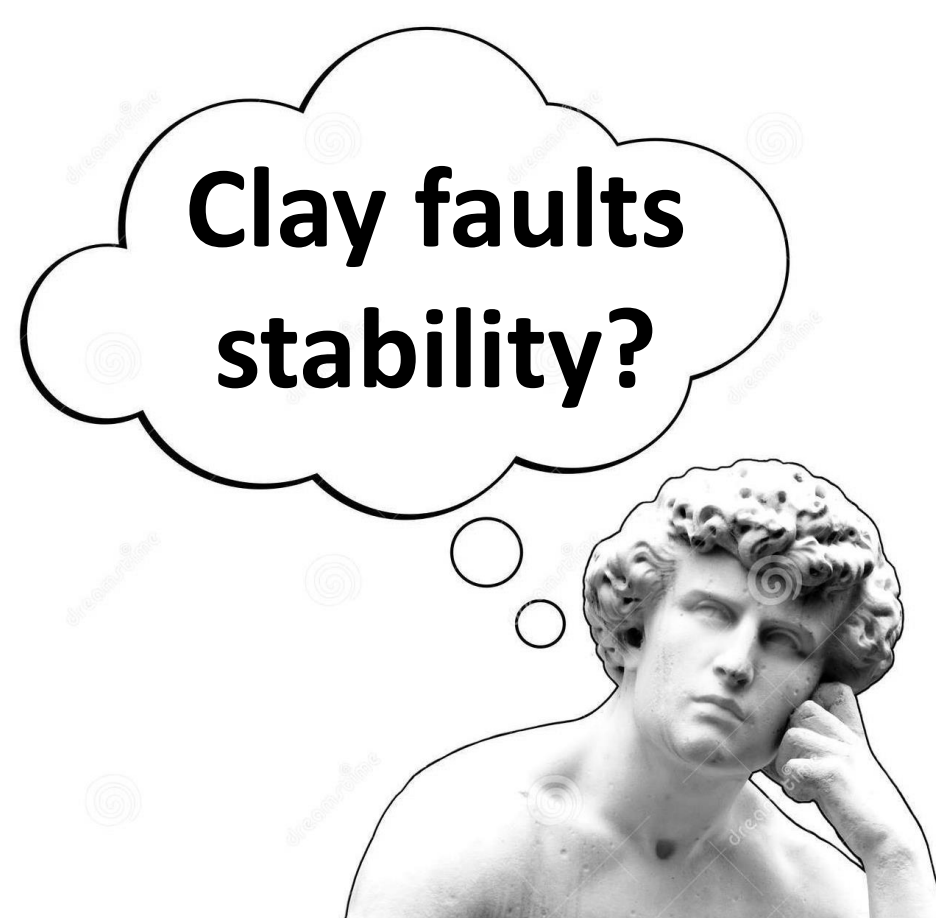
(1)University of Neuchâtel, CHYN, Neuchâtel, Switzerland, (2)University of California Berkeley, Berkeley, CA, United States, (3)Swisstopo, Wabern, Switzerland

## Why are we doing this/ Introduction?

This work contributes to a highly-detailed structural analysis of three boreholes, which cross-cut a clay fault zone called the "Main Fault" in the Mont Terri underground rock laboratory, Switzerland. The data is required for interpretation the results of the Fault Slip (FS) experiment, that aims at understanding the conditions for slip activation and stability of clay faults (Guglielmi, 2016). The experiment consisted in hydraulic injection below, above and across the Main Fault by using the SIMFIP probe (Guglielmi et al, 2013).

Stages of the FS project:

- Structural mapping of the fault zone
- Analysing the FS experiment data
- Numerical simulation of the mass respond to hydraulic injection



## Methodology

- Core mapping and optical televiewer data analyses
- Interpretation and classification of the data in structural facies
- Fracturing measurements and analyses
- Faults measurements including slickensides description
- Kinematic analyses
- Crosshole correlation

## Results:

- The observed tectonic faults can be compiled into three fault systems that differ by the orientation and kinematic characteristics of the fault planes (Figure 1)
- The faults systems of the Main Fault observed in the investigated boreholes correspond to the main fault systems of the Mont Terri Region (Nussbaum et al, 2011) (Figure 2)
- Both the fault planes and the structural facies are non-planar and discontinuous which makes crosshole correlation challenging (Figure 3)

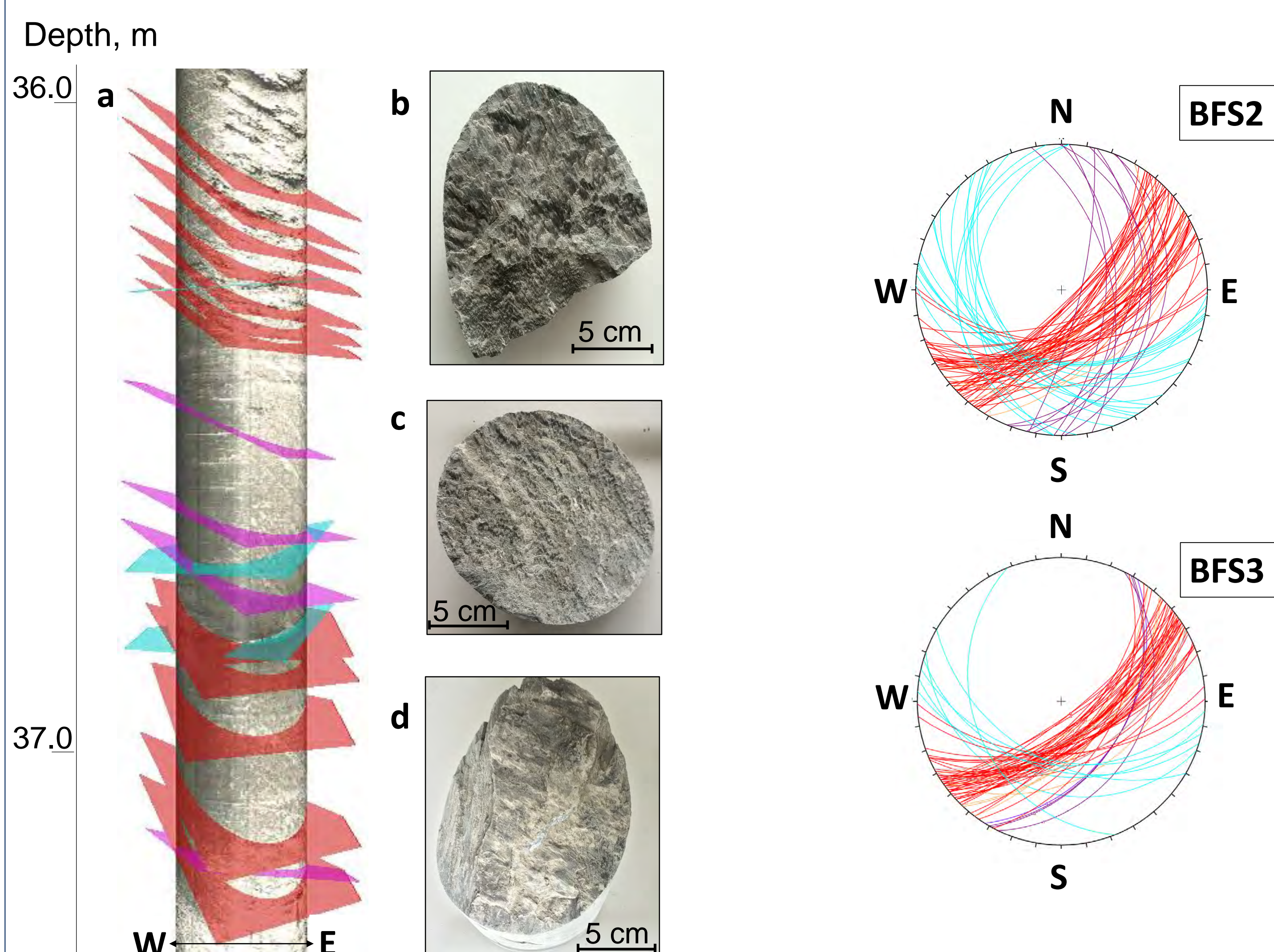


Figure 1: a – Structural map of BFS3; b – Slickenside of the SSE dipping fault system (red), c - Slickenside of the N trending faults (violet), d – Slickenside of the SW dipping fault system

Figure 2: Stereoplots of the fault structures in BFS2 and BFS3 representing three main systems in the Main fault (see the legend in Figure 3)

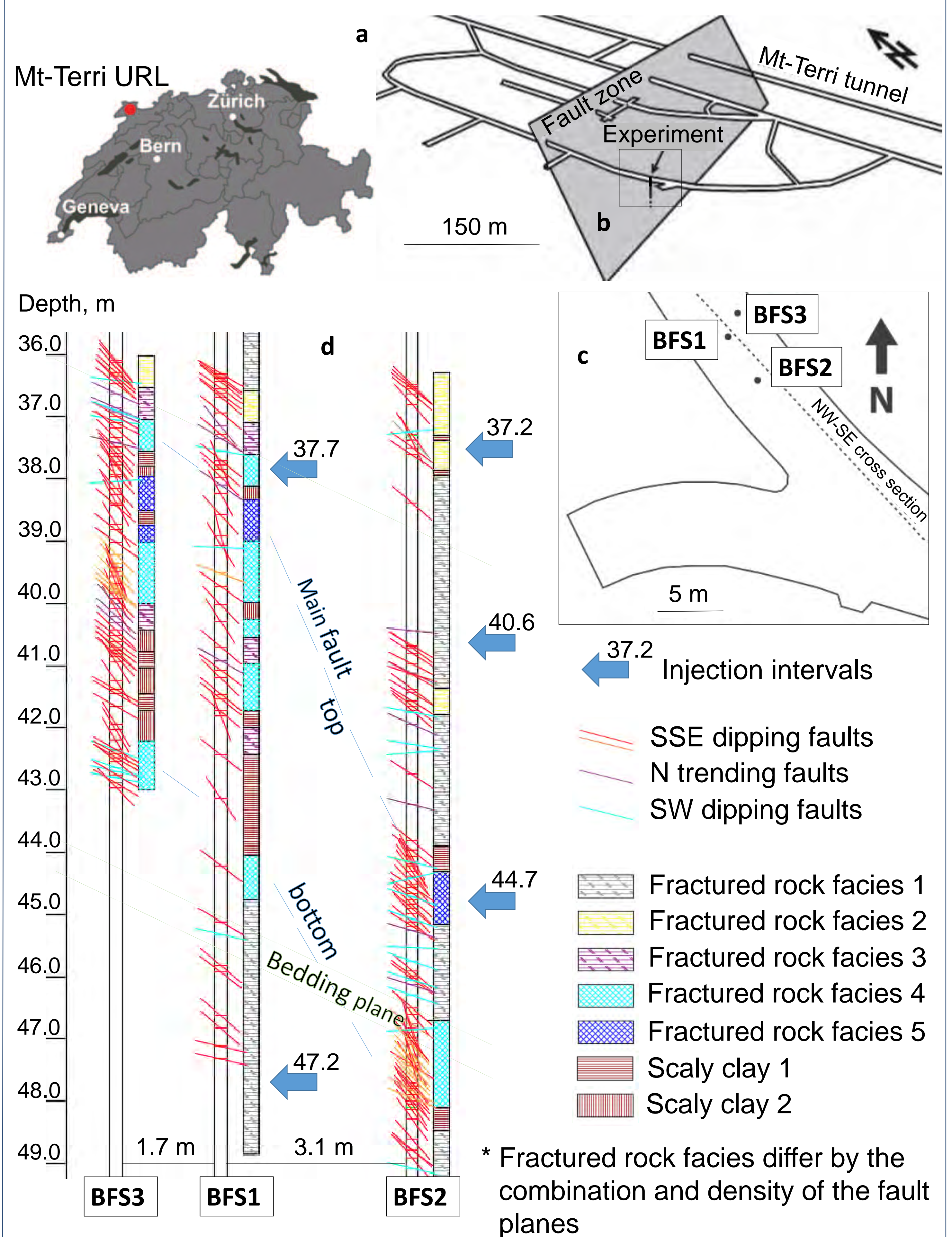


Figure 3: a,b - Experimental location in Mt-Terri URL; c – Map of the boreholes geometry in the FS experiment zone, d – Cross section of the Main Fault geometry

## Conclusions

- The Main fault core consists of a thrust zone of about 4.0-5.0 m wide, that includes scaly clay and non-scaly fabrics intersected by various density of secondary fault planes.
- The fault rocks are classified in 7 different fault facies: 2 scaly clay facies and 5 fractured rock facies.
- Complex variability of the fractured zones as well as the continuity of the borders of the Main Fault are hard to correlate even with highly detailed geological data within the relatively small volume of the experiment.
- This high heterogeneity within the fault zone is likely to impact the fault rock response to fluid injection and its reactivation.

## References

- Guglielmi, Y. (2016). In-situ clay faults slip hydro-mechanical characterization (FS experiment), Mont Terri underground rock laboratory. Technical Note 2015-60, p. 1-63
- Guglielmi, Y., Cappa, F., Lançon, H., Janowczyk, J. B., Rutqvist, J., Tsang, C. F., & Wang, J. S. Y. (2013). ISRM suggested method for step-rate injection method for fracture in-situ properties (SIMFIP): Using a 3-components borehole deformation sensor. In The ISRM Suggested Methods for Rock Characterization, Testing and Monitoring: 2007-2014 (pp. 179-186). Springer International Publishing.
- Nussbaum, C., Bossart, P., Amann, F., & Aubourg, C. (2011). Analysis of tectonic structures and excavation induced fractures in the Opalinus Clay, Mont Terri underground rock laboratory (Switzerland). Swiss Journal of Geosciences, 104(2), 187-210.

# Attenuation estimated from laboratory creep tests on cracked water-saturated glass samples

Céline Mallet, Beatriz Quintal, Eva Caspari, Klaus Holliger

## Introduction

The geophysical and hydraulic characterization of fractured rocks is widely regarded as an ultimate objective for the optimized production of geothermal energy. There is increasing evidence to suggest that a number of seismic attributes are not only sensitive to the presence of fractures *per se*, but also to their interconnectivity. For hydraulically connected fractures, a propagating seismic wave causes fluid flow from fractures into the other ones. This “s squirt-type” dissipation mechanism in the mesoscopic scale range may open new avenues for the hydraulic characterization of fractured formations based on seismic observations. The corresponding evidence is, however, entirely based on numerical simulations and hence the practical importance of this energy dissipation mechanism remains uncertain.

We estimate attenuation at sub-seismic frequencies from experimental creep test performed on a thermally cracked water-saturated glass sample. The time-dependent axial stress and strain rates are used to infer frequency-dependent attenuation and Young's modulus. The Young's modulus presents a dispersion between 60 and 70 GPa. The corresponding attenuation is highest between  $3 \times 10^{-4}$  and  $7 \times 10^{-3}$  Hz. Based on a “s squirt-type flow” mechanism at the mesoscopic scale an analytical characteristic frequency is estimated at  $5 \times 10^{-3}$  Hz. We then compare the experimentally observed attenuation with results of numerical simulations based on Biot's poroelastic equations and using a digitized thin section of the cylindrical cracked glass sample.

## Energy dissipation extracted from creep test

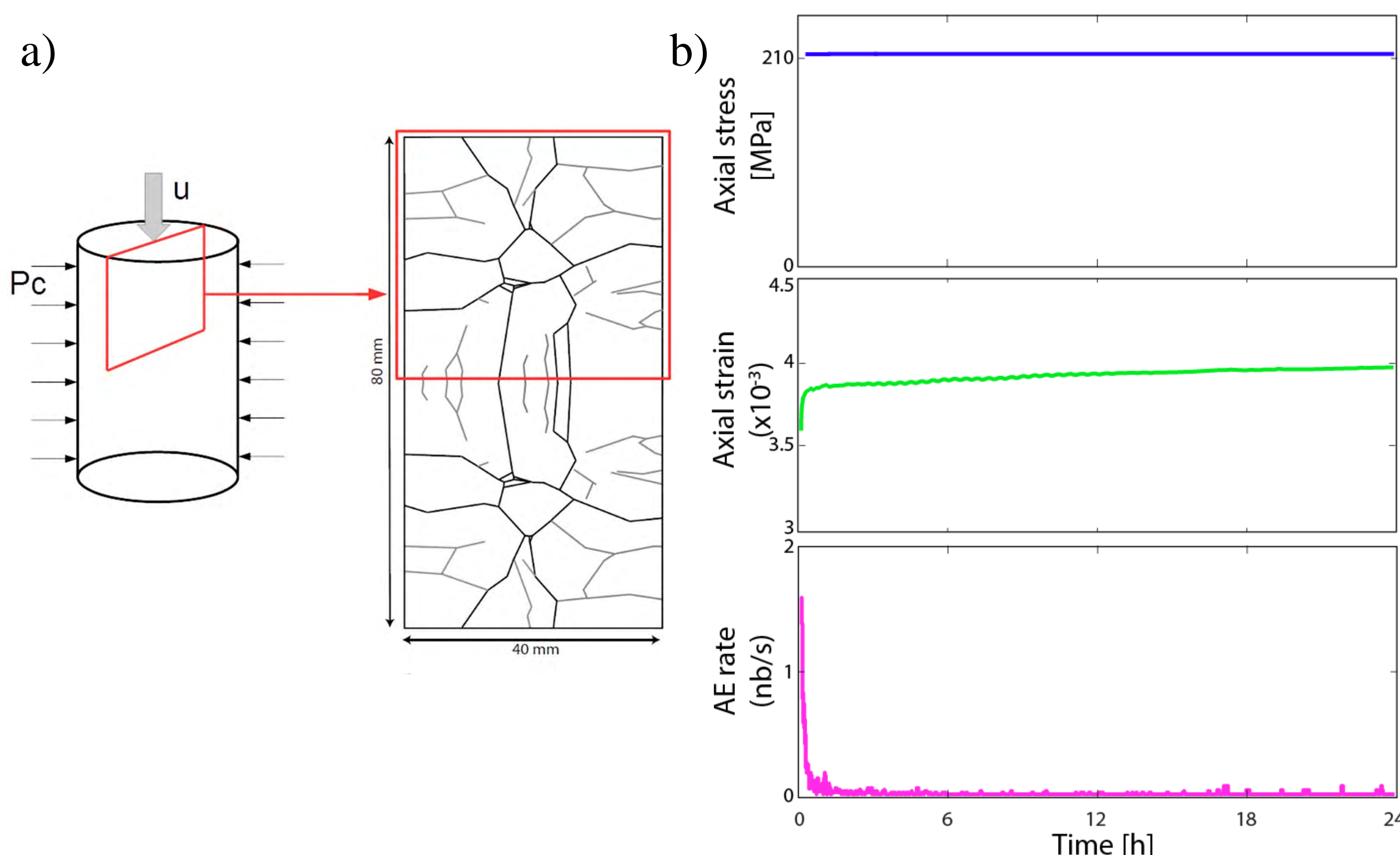


Figure 1: a) Schematic illustration of the applied creep experimental conditions (left) and digitized crack network along a vertical cross section. b) Applied stress, measured strain and recorded acoustic emission rate during a creep step.

➤ The creep stress and strain rates are transformed into the frequency domain using a Fourier transformation:

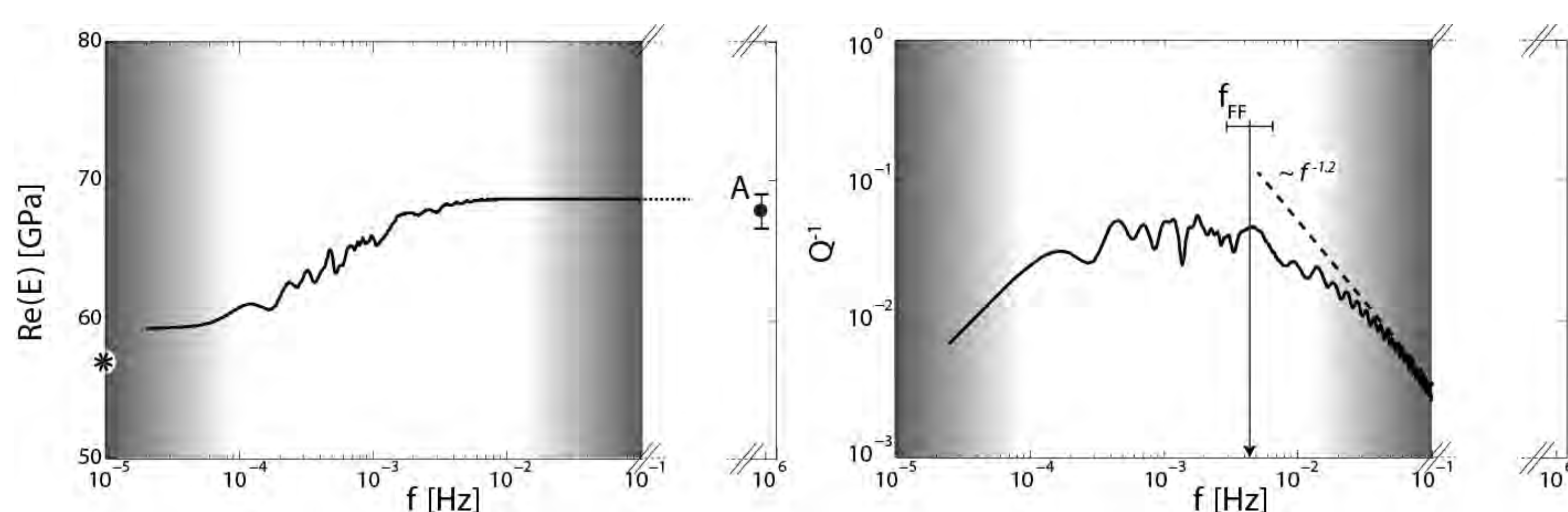


Figure 2: Dispersion of the real part of the Young's modulus (left), where the A point represents the Young's modulus inferred from the ultrasonic measurements while the asterisk results from the static measurement; and attenuation (right), where  $f_{FF}$  denotes the analytically estimated characteristic frequency. Grey zones represents uncertainties due to the experimental setup: too short total time probably leading to overestimation at low-frequencies and not instantaneously applied stress leading to some artifact at high-frequencies.

## Interpretation

### • Fracture-to-Fracture flow

We interpret the frequency dependence of the Young's modulus and its attenuation as a mechanism of fluid flow at a mesoscopic scale within the connected cracks. It is characterized by the frequency  $f_{FF}$ :

$$f_{FF} \approx \frac{k^{eff}}{b^2} \frac{\xi E^{eff}}{2\eta_f}$$

where  $k^{eff}$  and  $E^{eff}$  are the effective permeability and Young's modulus,  $b$  is the average crack length,  $\xi$  is the aspect ratio and  $\eta_f$  is the fluid viscosity.

### • Numerical comparison

Numerical simulations are performed based on Biot's quasi-static poroelastic equations (e.g., Quintal et al. 2011, JGR) for a 2D model based on the image of the cracked sample (Figure 1a), using the following equations and material properties

#### • Stress equilibrium:

$$\nabla \cdot \sigma = 0$$

#### • Darcy's flow :

$$i\omega \frac{\eta}{k} w = -\nabla P_f$$

	Glass matrix	Cracks
Permeability	$10^{-5}$ mD	$\sim 1$ D
Porosity	0.1%	99%
Bulk Modulus	56.2 GPa	[0.06-0.15] GPa
Shear modulus	32.8 GPa	[0.06-0.15] GPa

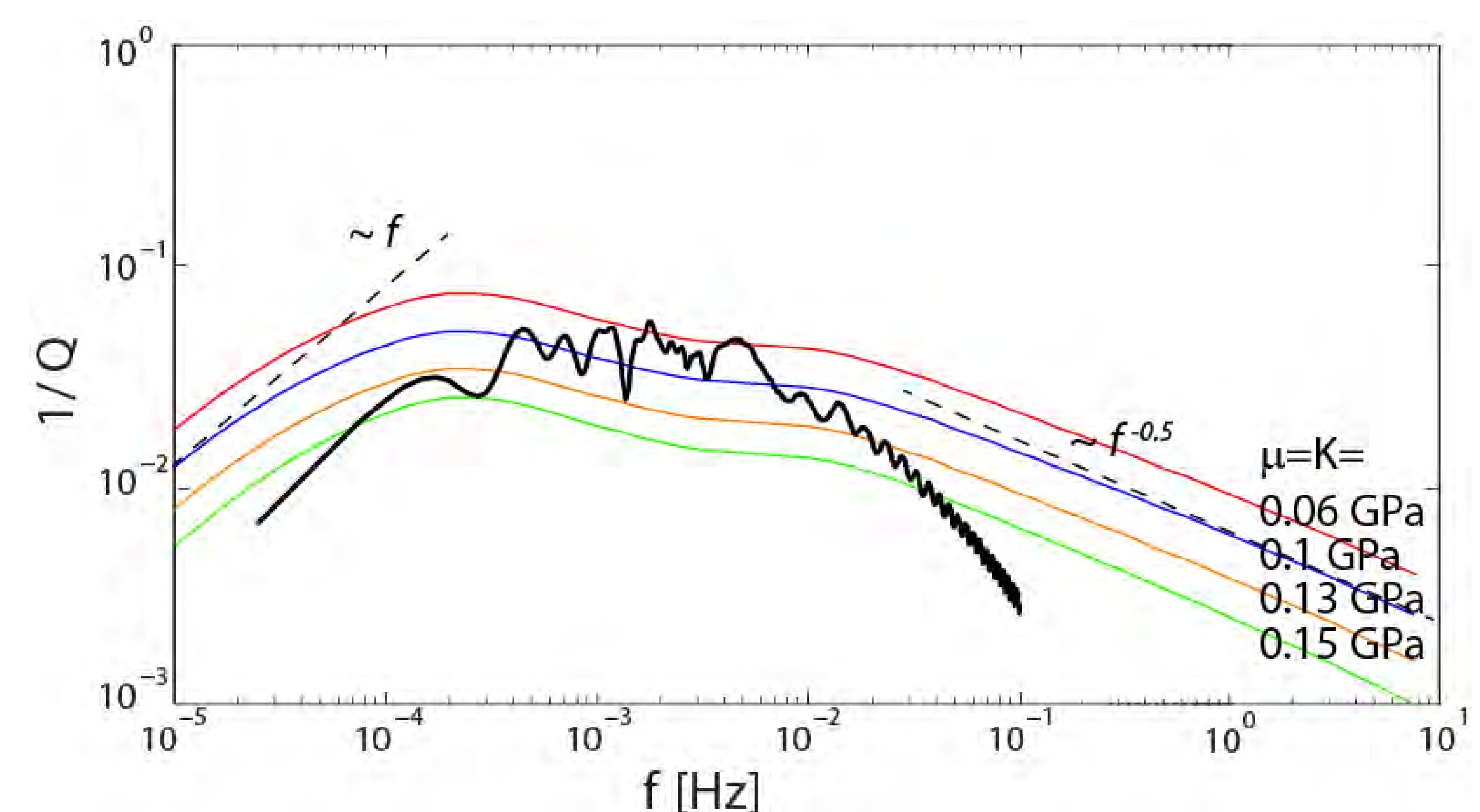


Figure 3: Comparison of energy dissipation of the experimental data (black curve) with corresponding numerical simulations for crack compressibilities ranging from 0.06 to 0.15 GPa. Only the effect of the fluid flow can be compared (thus the attenuation) and not the sample compressibility due to some variations in the boundary conditions between the experimental test and the numerical simulations.

## Conclusions and Outlooks

- Frequency dependent attenuation and Young's modulus dispersion can be extracted from creep tests performed on thermally fractured water-saturated samples.
- Analytical and numerical descriptions indicates that the fluid flow between interconnected cracks is the predominant mechanism responsible for the observed frequency-dependent behavior.
- The results of this study may open the perspective of obtaining wave attenuation information from a vast reservoir of corresponding laboratory measurements on a wide variety of materials, in particular, on cracked water-saturated rocks.

This work has been completed within the Swiss Competence Center on Energy Research – Supply of Electricity, with the support of the Swiss Commission for Technology and Innovation. The author would like to thank Yves Guéguen and Joël Sarout for their inspiring discussion and constructive comments.

# Effects of incoming seismic waves on a high-enthalpy geothermal field

Matteo Lupi<sup>a)</sup>, Florian Fuchs<sup>b)</sup>, Erik H. Saenger<sup>c)</sup>

a) Department of Earth Sciences, University of Geneva, Rue des Maraichers 13, CH-1205, Geneva, CH; b) Department of Meteorology and Geophysics, University of Vienna, Vienna, Austria; c) International Geothermal Centre, 44801, Bochum, Germany.

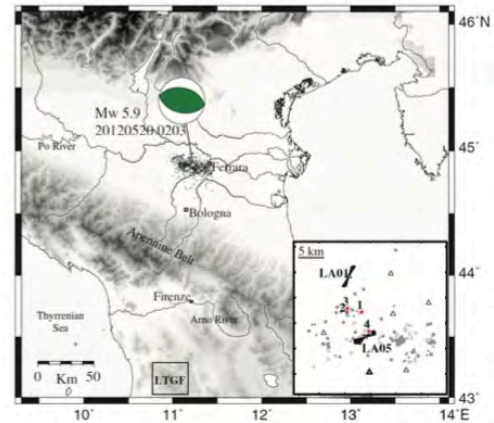
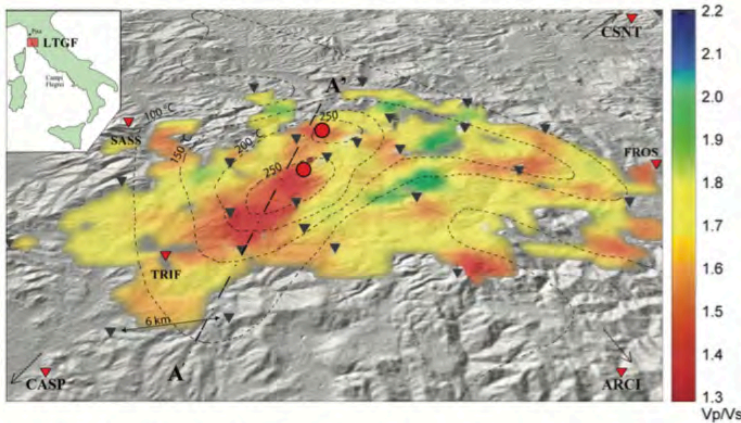


Figure 1. Map of the Larderello-Travale Geothermal Field and p/vs ratio distribution between 2 km and 3 km depth - map adapted from [De Matteis et al., 2008]. The dashed isolines mark the estimated temperature at 1 km depth. The dashed bold black line shows the position of the cross section used for the numerical simulation shown below. It should be noticed that the triggered seismic events (red circles) fall in areas of low vp/vs ratios. The inverted triangles point out the location of the seismic stations used by De Matteis et al. [2008] to

invert for the velocity model. The red inverted triangles show the location of the seismic stations used to locate the seismic events triggered by the passing seismic waves generated by the M9.0 Tohoku earthquake. ARCI, CASP and CSNT seismic station used to is not on the map as it is too far.

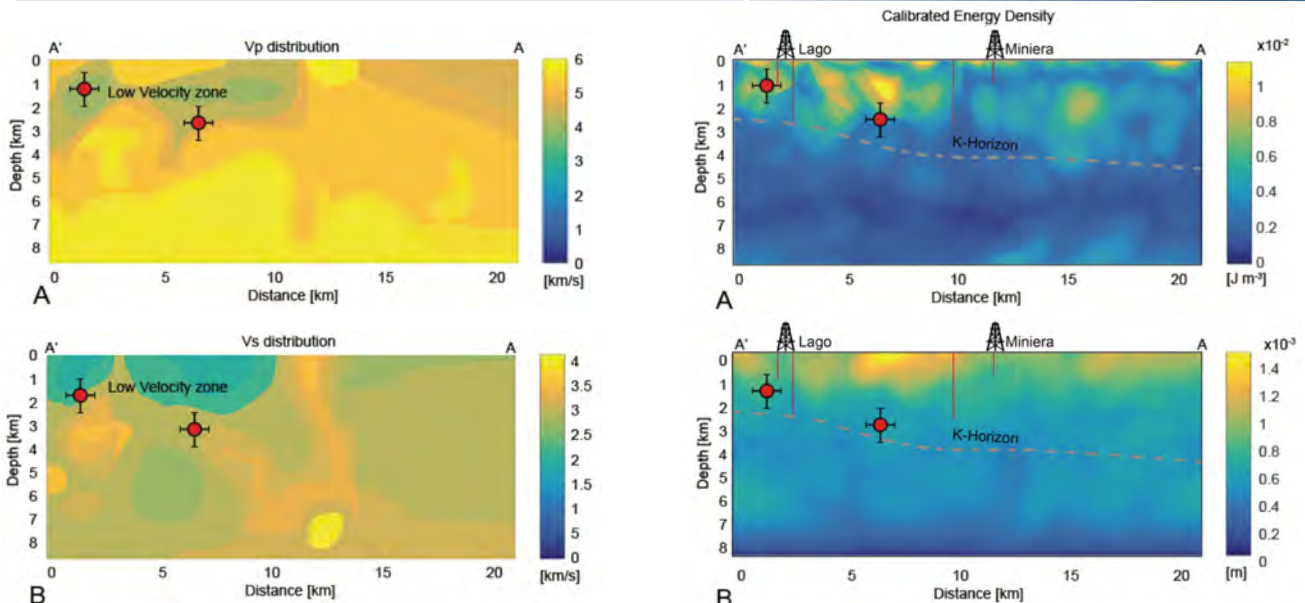
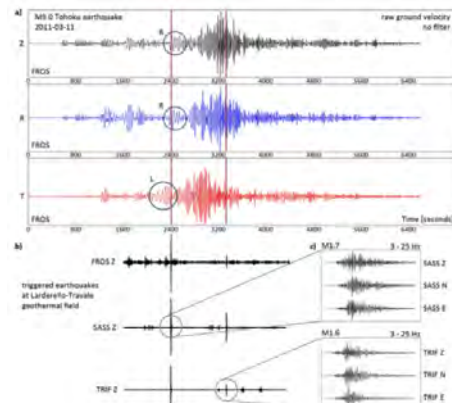
Figure 2. Triggered seismicity at the Larderello-Travale Geothermal Field by the 2012 Emilia earthquake. Image from Saccorotti et al., (2013)

Figure 3. Triggered earthquakes at Larderello-Travale geothermal field. The upper three traces show ground velocity on the vertical (Z), radial (R) and transverse (T) components of the 2011 Mw 9.0 Tohoku earthquake measured on station FROS. Circles mark the first arrivals of Rayleigh waves (Z and R) and Love waves (T). The red lines show the timing of the two possibly triggered earthquakes that are identified in the lower three

vertical traces from stations FROS, SASS and TRIF. To reveal the local earthquakes over the background Tohoku signals we applied a 5-15 Hz bandpass filter.

Figure 4. Geometry and velocity structure of the Larderello-Travale geothermal field. A) Vp distribution and B) vs. The direction of the cut A-A' is shown in Figure 1. The red circles show the location of the local earthquakes triggered by the M9.0 Tohoku earthquake and the black bars indicate the uncertainty of our localizations. Note that the events fall into regions marked by low seismic waves velocities. The Brittle ductile transition, i.e. the k-horizon [Brogi et al., 2003], is thought to occur at around 4 km depth.

Figure 5. Results of the numerical study. A) The maximum energy density is concentrated in regions marked by vp and vs anomalies, see Figure 3. The locations of the triggered earthquakes (red dots) correspond to regions of maximum concentration of energy density. Vertical red lines show geothermal boreholes.



# Structural imaging from hydrophone vertical seismic profile data at the Grimsel Borehole

Andrew Greenwood, Tobias Zahner, Ludovic Baron and Klaus Holliger

## Motivation

The development of geothermal reservoirs requires a well-developed understanding of the geological structure in general and the fracture networks enabling fluid migration in particular. In conjunction with geological mapping, core analyses, and borehole geophysics, seismic methods are a powerful means for delineating structure. Surface-based seismic reflection methods can map large domains. However, in the presence of steep dips much of the incident seismic energy is not reflected back to the surface. Conversely, the vertical seismic profile (VSP) method, which uses sources at the surface and populates a nearby borehole with receivers, is very adapt at recording this information with the additional benefit of having complementary geological and geophysical borehole measurements available for calibration.

## Principle of VSP imaging

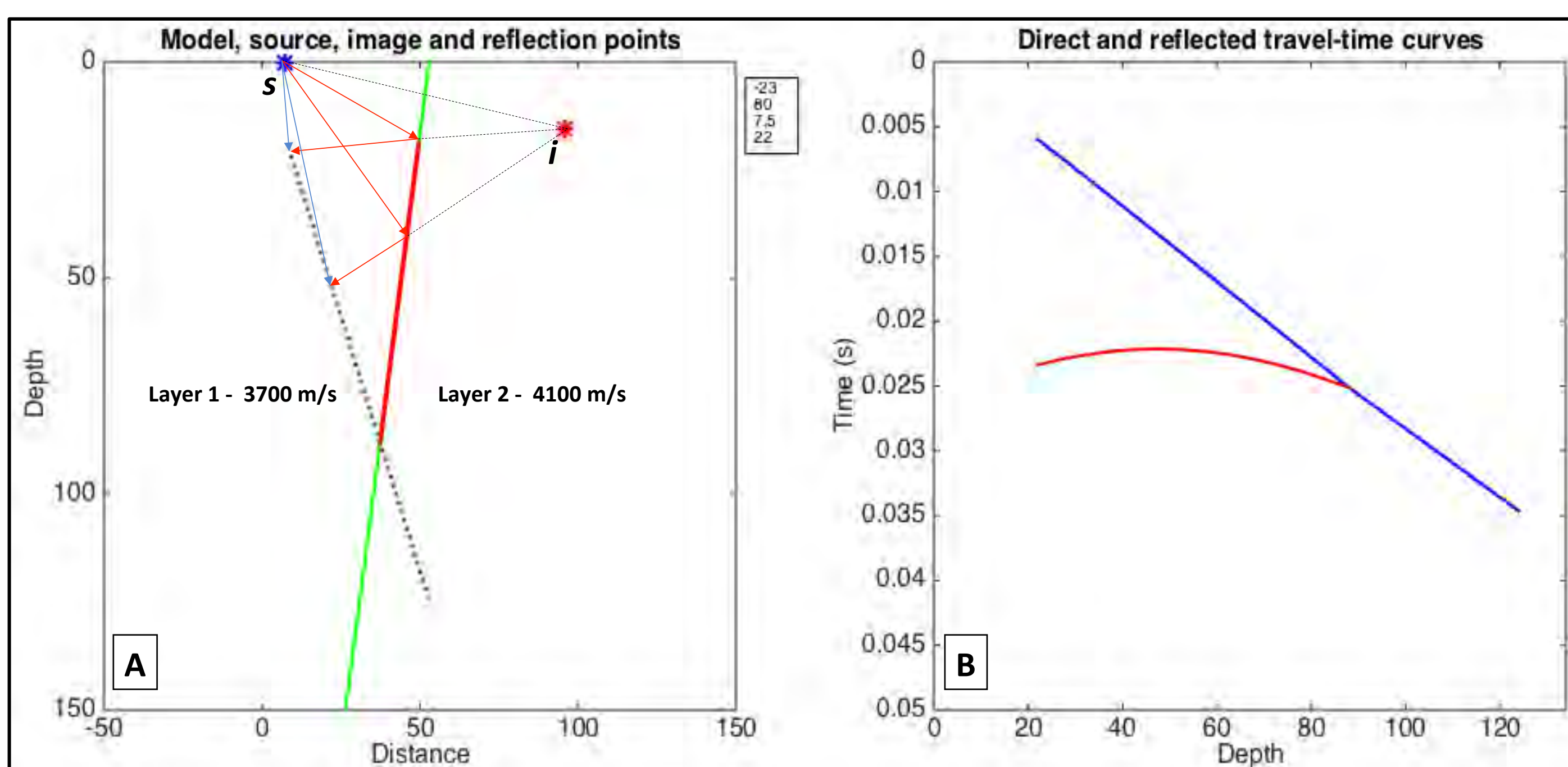


**Figure 1.** (A) Schematic illustration of the VSP imaging principle from a quasi-zero-offset single source location for a two-layer model of a steeply dipping structure (green) intersected by a borehole containing seismic receivers (black dots). *s* and *i* denote the locations of the seismic source and its image point, respectively. The portion of the structure which is seismically illuminated is marked in red. Direct (blue) and reflected (red) ray-paths are shown for two receiver locations. (B) Travel time curves for the direct (blue) and reflected (red) rays for the model depicted in (A).

## Forward modelling

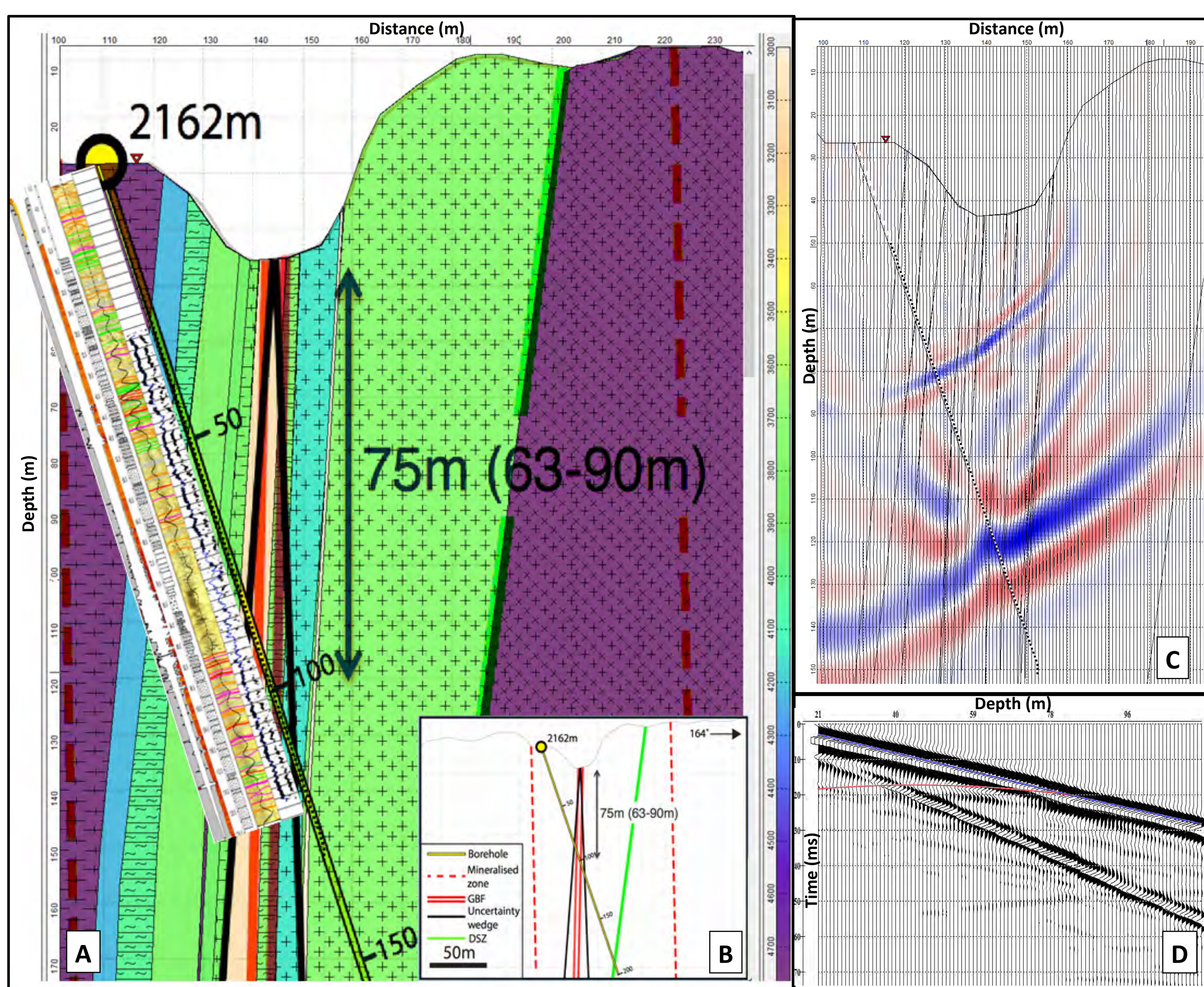


**Figure 2.** (A) Model of the Grimsel test site based on evidence from geological mapping, core analyses and borehole logging (see also posters of Caspari et al. and Zahner et al.). P-wave velocities are derived from first-arrivals and density and S-wave velocity from Gardner's equation. The main low-velocity fracture zone is cream in colour. Logs aligned with the borehole trace comprise from left to right: caliper; lithology; optical televiewer with fracture identification and reflected tube wave stack superimposed; full-wave sonic semblance. (B) Initial geological model prior to drilling and description of the various coloured lines present in A. (C) Snapshot of simulated elastic wavefield clearly showing diffraction and wavefront deformation effects related to the low-velocity zone. (D) Synthetic quasi-zero-offset VSP data. The travel time curves from Figure 1B have been superimposed to point to the main velocity contrast and the reflection from the low-velocity fractured zone.

## Quasi-zero-offset hydrophone VSP data

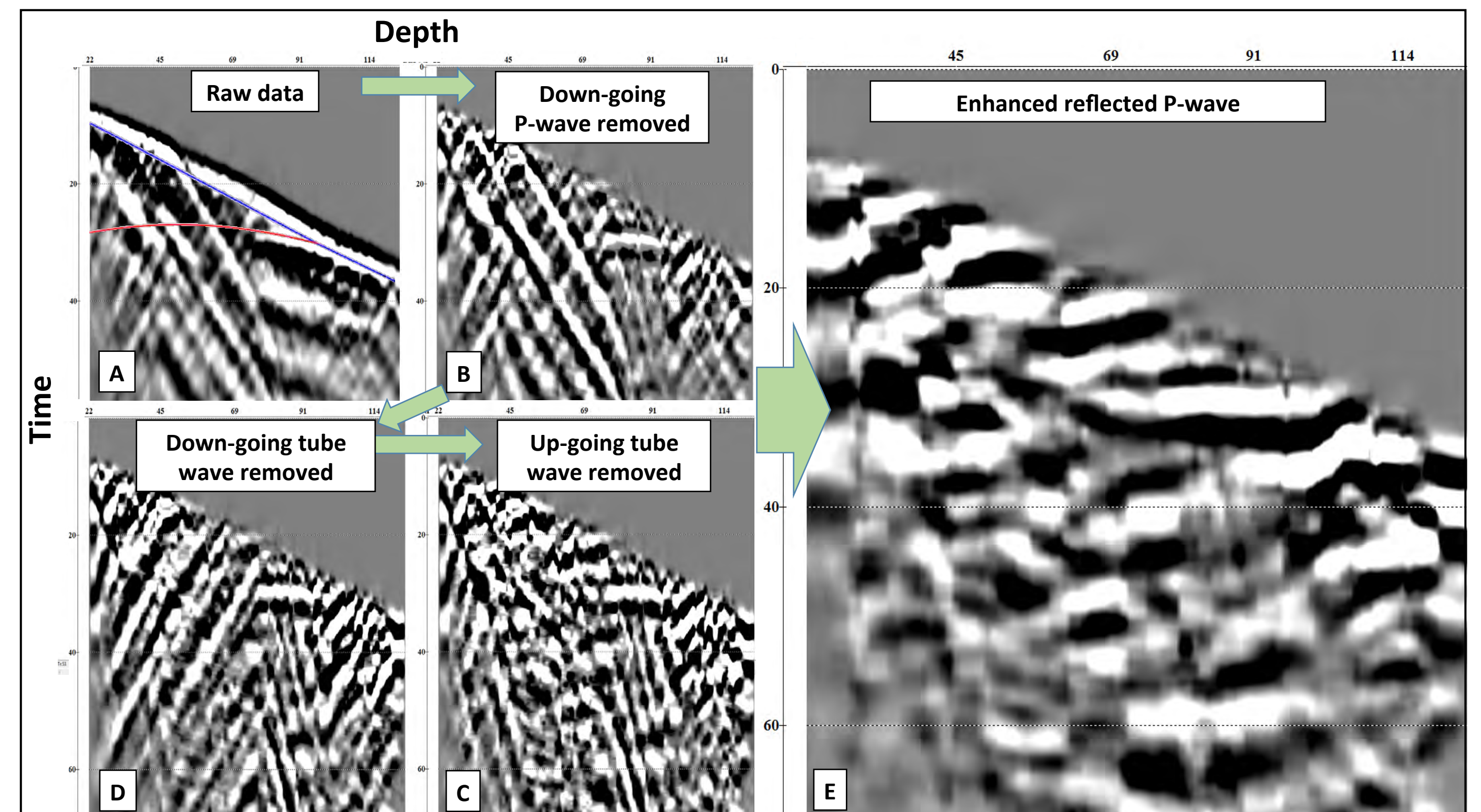


**Figure 3.** Quasi-zero-offset VSP data collected with a 24 channel, 1-m-spaced hydrophone string. (A) Raw data after amplitude balancing with reference geophone. Travel time curve from Figure 1B has been superimposed. (B) Removal of the down-going P-wave by 2D median filtering has enhanced the primary reflection from the main low-velocity fault zone as well as the tube wave events (chevron patterns) caused by fractures and borehole breakouts. (C) and (D) Removal of down- and up-going linear coherent tube wave events. (E) Enhancement of P-wave reflection events using a 3-trace 2D median filter. Data is represented in 1-way travel time and used as the input to migration imaging.

## VSP Kirchhoff migration

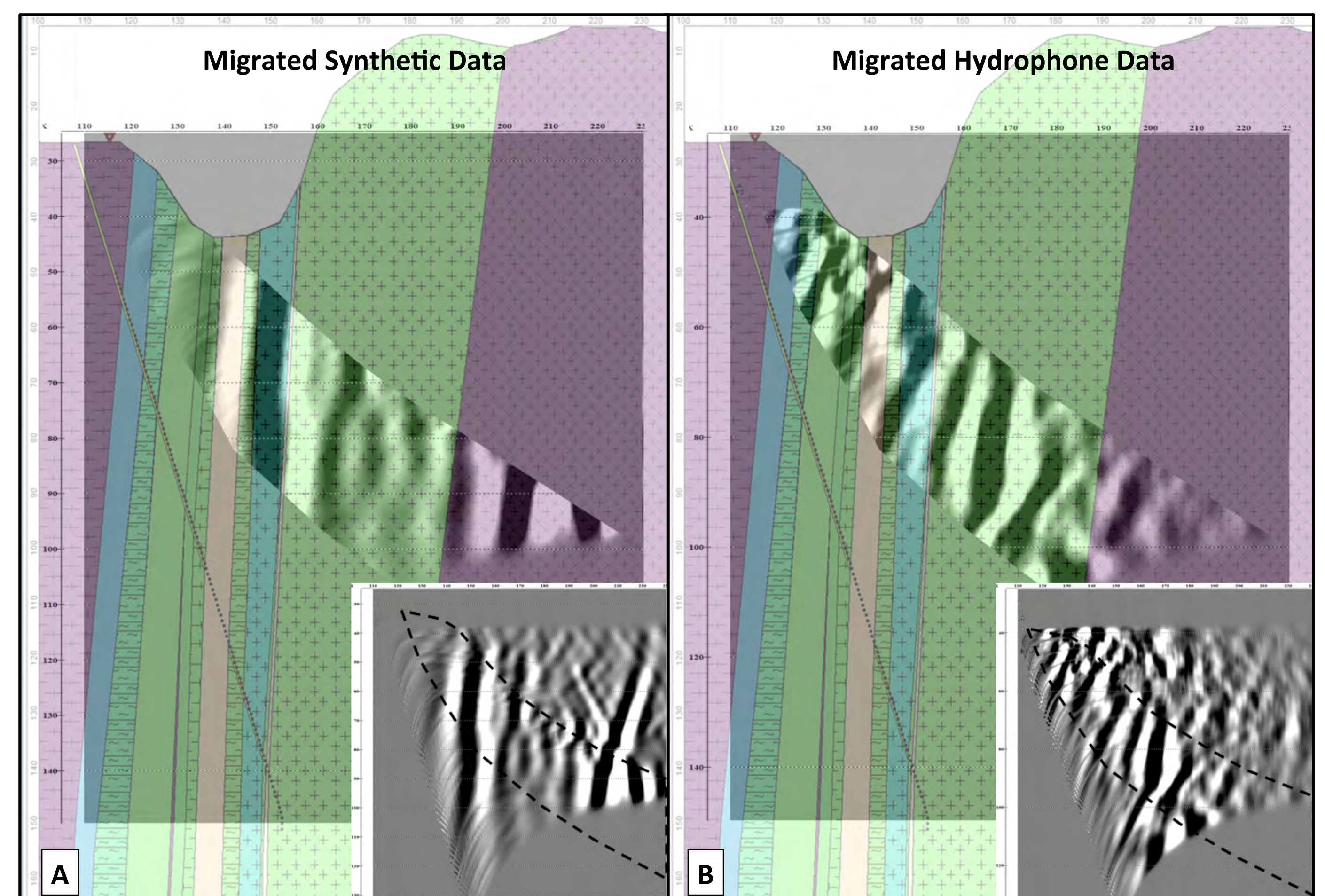


**Figure 4.** Comparison of synthetic pre-stack depth migrated (PSDM) images of synthetic and observed VSP data. (A) PSDM image generated from the synthetic seismic data of the initial Grimsel test site model. The dip and location of the main contrasting layers has been well mapped. (B) PSDM image generated from the wavefield-separated hydrophone VSP data in Figure 3E. Constant velocity models derived from the average first-arrival time were used in both cases. Inserts show the PSDM images with a dotted cropping mask. Outside of the mask, the reflection imaging is low-fold. Above the mask dramatic topography creates a reflection shadow zone and below the mask refracted arrivals are likely.

## Conclusions and outlook

Initial PSDM imaging of quasi-zero-offset hydrophone VSP data from the Grimsel test site suggests there may be some differences in structural dip with regard to the pre-survey geological model. However, there is a good overall correlation between the PSDM imaging of the numerical simulations and the VSP collected in 2015. With the implementation of a 2D velocity model and iterative forward modelling, the structural interpretation in general and the fracture characterisation in particular can be iteratively improved and extended up to several tens of meters beyond the trace of the borehole.

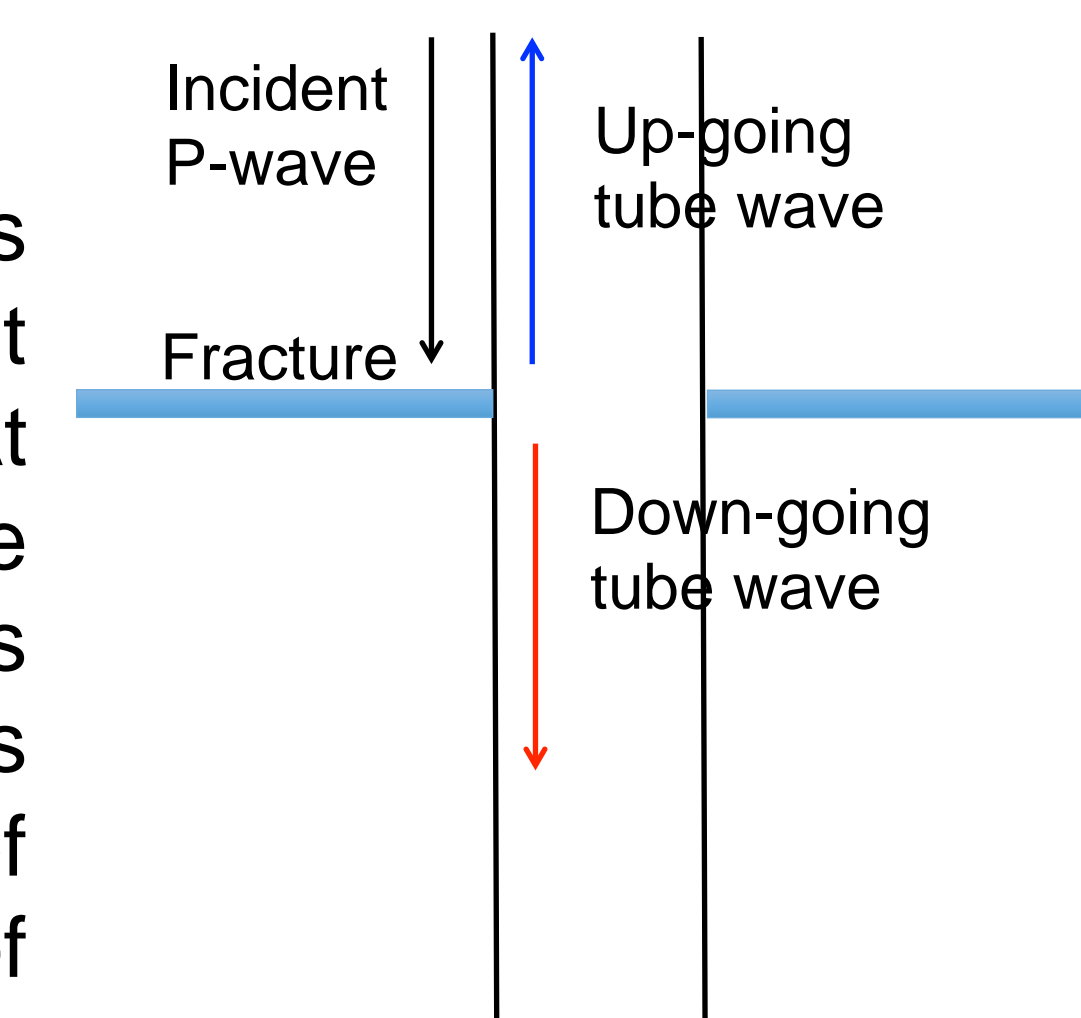
Multiple-offset VSP and surface seismic reflection and refraction data collected in July 2016 will now be added to the processing flow. This will increase the seismic fold, help to characterise the overburden, and provide an improved image by illuminating the structures of interest from a broader range of angles.

# Potential of fracture characterization from hydrophone tube wave data at the Grimsel test site

Eva Caspari, Andrew Greenwood, Tobias Zahner, Ludovic Baron, Jürg Hunziker and Klaus Holliger

## Summary

Tube waves tend to be omnipresent in hydrophone vertical seismic profiling (VSP) data and are generally considered as noise. However, some tube waves are generated by the compression of fractures crossing the borehole by the incident seismic wave field and hence contain valuable information with regard to the hydraulic transmissivity of these features. At the Grimsel test site, most tube waves correlate with fracture zones identified by optical televiewer data. However, the abundance of fractures results in complex patterns of the recorded tube wave fields, which makes a conventional analysis difficult. In this study, we show initial results of our efforts to obtain amplitude ratios of the incident P-wave and tube waves from the complex wave field patterns present in the VSP data. Such amplitude ratios can then be analysed in terms of hydraulic transmissivity of the fracture zones generating the tube waves under consideration. Another interesting aspect of tubes waves, which is also considered in this study, is their sensitivity to the shear modulus of the formation.



## Correlation of tube waves with fractures identified by optical televiewer data

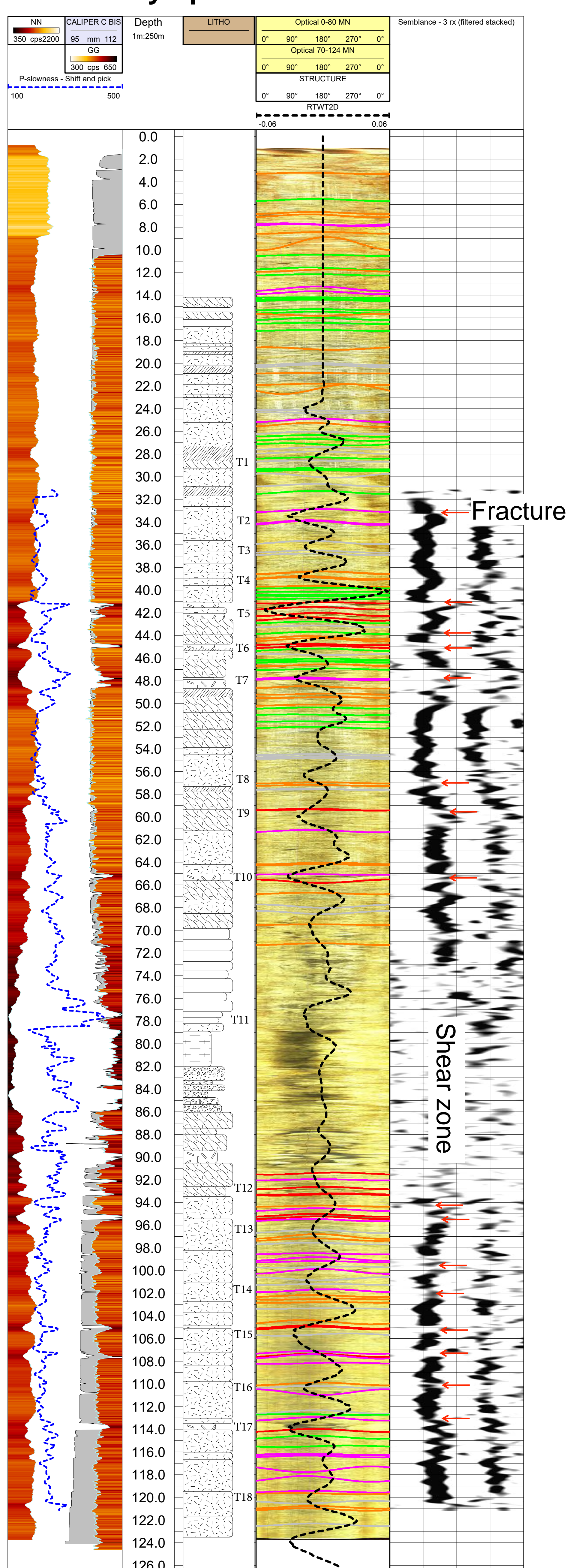


Figure 1: Middle: Optical televiewer data, identified fractures (colored lines), and reflected tube wave corridor stack. Right: Semblance of sonic logs. Left: Selected log data and litholog from core analyses. All data sets locate the fractures consistently. This confirms that most of the tube waves are generated by fractures.

## Wave field separation and reflected tube wave corridor stack

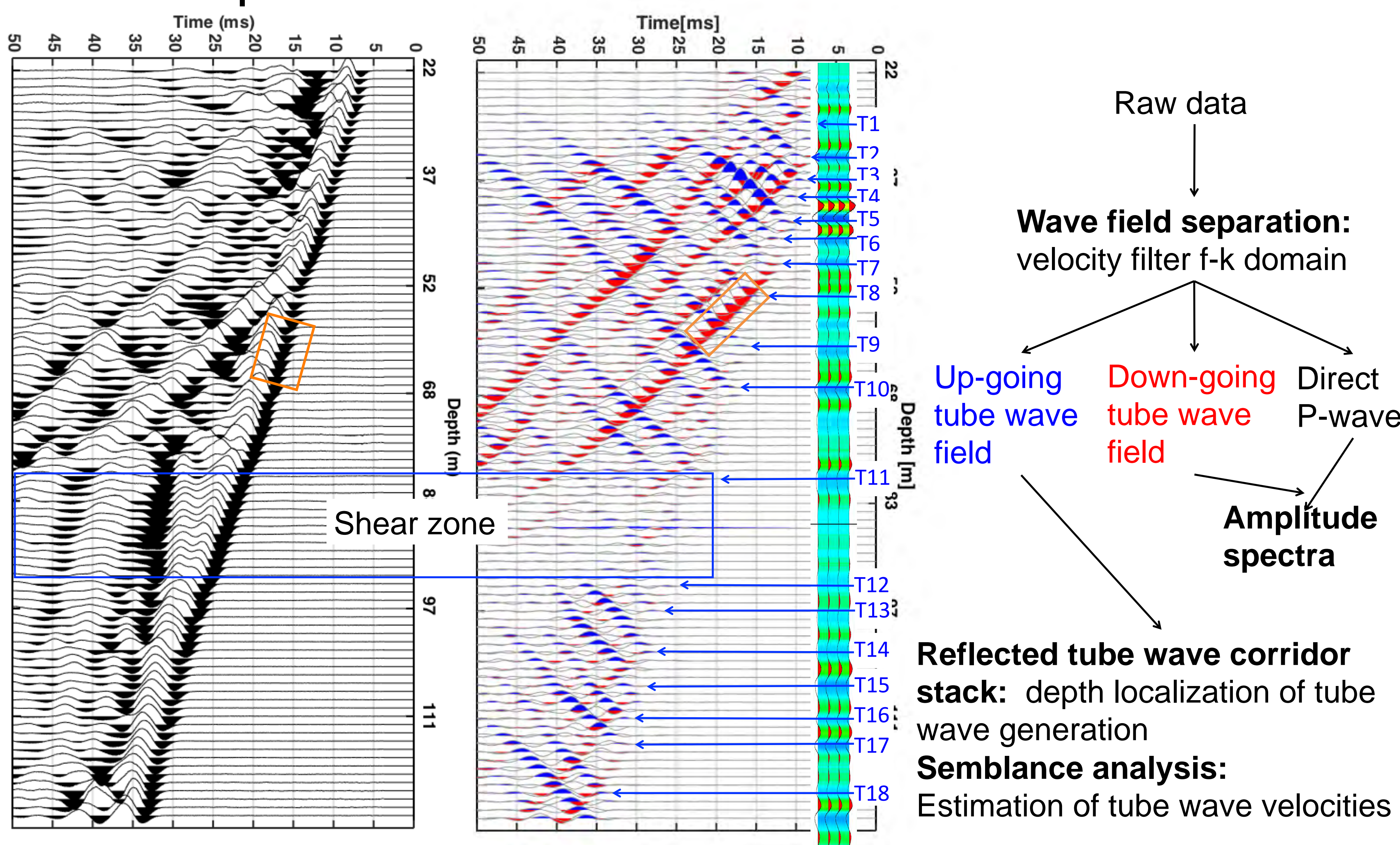


Figure 2: Left: Quasi-zero-offset VSP data. Right: Superposition of up- and down-going tube waves and reflected tube wave corridor stack. Blue arrows correspond to tube wave labels in Figure 1. The blue box denotes a major shear zone, which acts as a screen for tube waves.

## Estimation of shear wave velocity profile from tube wave velocities

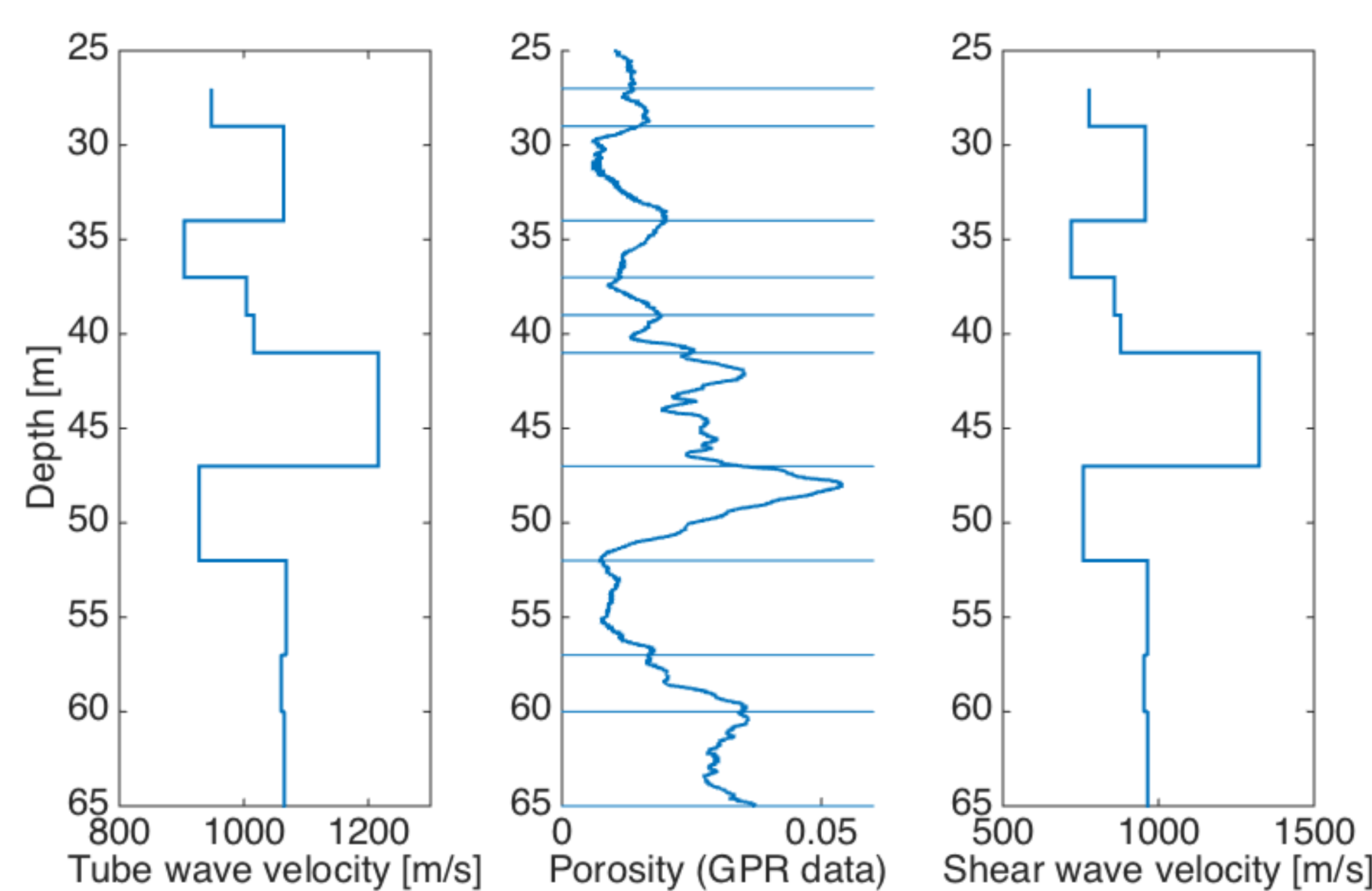


Figure 3: Left: Tube wave velocity profile; center: porosity estimated from GPR data; right: inferred shear wave velocity profile.

Tube waves are interface waves travelling along the borehole surface. In the low-frequency regime, their velocity is determined by the bulk modulus and the density of the borehole fluid and the shear modulus of the adjacent formation. Given that the fluid properties and formation density are known, tube wave velocities can be used for estimating the shear wave velocity along the borehole. The bulk density of the formation is estimated by using a mixing model constrained by the GPR porosity in conjunction with the densities of water and of a zero-porosity granitic matrix.

## Outlook: Estimation of fracture transmissivity from amplitude ratios

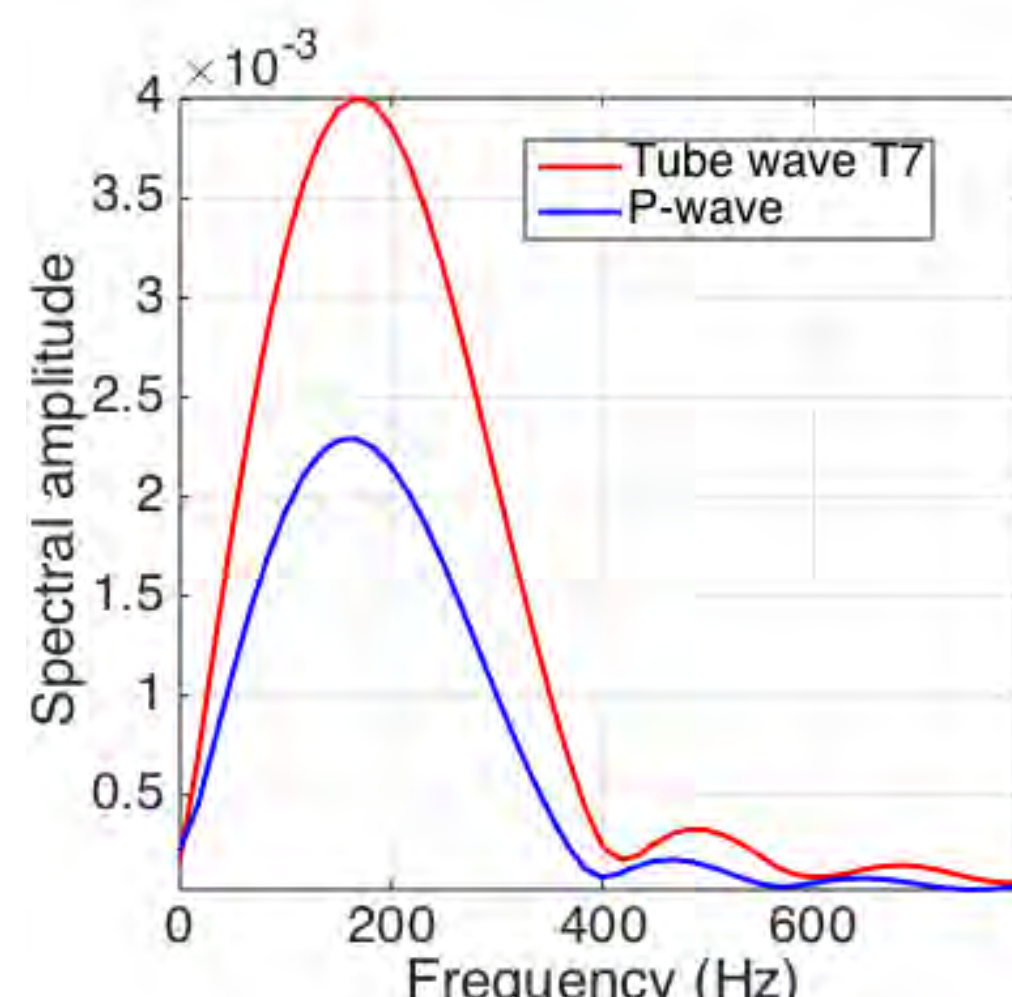


Figure 4: Amplitude spectra for the down-going tube wave T7 and the direct P-wave within the orange window in Figure 2.

A quantitative analysis of amplitude ratios in terms of the hydraulic transmissivities of the fractures generating tube waves requires:

1. Further improvements with regard to wave field separation in order to preserve original amplitudes
2. Comparison of amplitude ratios to analytical models and forward modeling of the tube wave fields

# Fracture connectivity effects on the anisotropy of acoustic waves

J. Germán Rubino<sup>1,2</sup>, Eva Caspari<sup>1</sup>, Tobias M. Müller<sup>3</sup> and Klaus Holliger<sup>1</sup>  
<sup>1</sup>University of Lausanne, <sup>2</sup>University of Western Ontario, <sup>3</sup>CSIRO Perth

## Introduction

The presence of fractures is very common in the shallower parts of the Earth's crust and they tend to dominate the mechanical and hydraulic properties of the rock. It is currently considered that fracture orientation and density may be reliably estimated from seismic data. However, the estimation of fracture parameters controlling the hydraulic properties, such as fracture aperture, connectivity, and permeability, remains rather unsuccessful. This, may be due to the fact that most corresponding analyses are based on effective medium modelling and static elasticity.

In this work, we apply a set of numerical oscillatory relaxation tests based on the theory of poroelasticity to determine the effective anisotropic seismic properties of 2D rock samples containing two orthogonal fracture sets with varying degrees of hydraulic connectivity and compare the resulting anisotropy.

## Numerical upscaling procedure

The numerical upscaling procedure is based on Biot's (1941) quasi-static poroelastic equations. By applying a set of three oscillatory relaxation tests, comprising two compressional tests and one shear test, the equivalent frequency-dependent complex-valued 2D stiffness coefficients are computed from the spatially averaged stress and strain fields by using the following relation:

$$\begin{pmatrix} \langle \sigma_{11}^k \rangle \\ \langle \sigma_{22}^k \rangle \\ \langle \sigma_{12}^k \rangle \end{pmatrix} = \begin{pmatrix} C_{11} & C_{12} & C_{16} \\ C_{12} & C_{22} & C_{26} \\ C_{16} & C_{26} & C_{66} \end{pmatrix} \begin{pmatrix} \langle \epsilon_{11}^k \rangle \\ \langle \epsilon_{22}^k \rangle \\ \langle 2\epsilon_{12}^k \rangle \end{pmatrix}$$

The components of the equivalent stiffness matrix are computed, for each frequency, following a classic least-square procedure. From this stiffness matrix, the equivalent phase velocity and attenuation of *P*- and *S*-waves as functions of incidence angle and frequency are obtained following a standard procedure for anisotropic viscoelastic solids.

## Results

We consider 2D numerical samples containing 150 vertical and 150 horizontal fractures (Fig. 1). The fractures are poroelastic objects of rectangular geometry with an aperture and a length of 0.06 cm and 4.2 cm, respectively. The properties of the background material are assumed to correspond to a homogeneous and isotropic tight sandstone. Both the fractures and the embedding material are fully saturated with water.

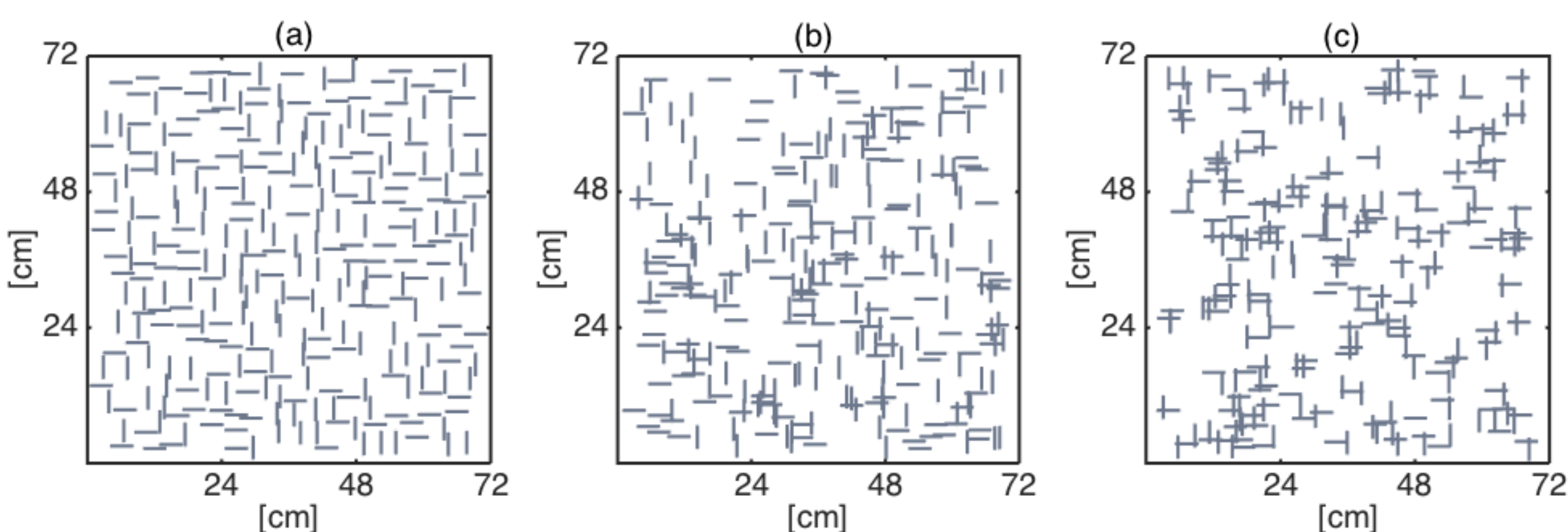


Figure 1: Synthetic rock samples employed to analyze fracture connectivity effects on velocity anisotropy. In sample (a) all fractures are unconnected, in sample (b) some fractures are connected, while in sample (c) all fractures show some connectivity.

## References

- Biot, M., 1941, General theory of three-dimensional consolidation: *Journal of Applied Physics*, 12,155–164.
- Rubino, J., E. Caspari, M. Milani, T. Müller, and K. Holliger, 2015, Seismic anisotropy in fractured low-permeability formations: The effects of hydraulic connectivity: *SEG Expanded Abstracts*,3219–3223.

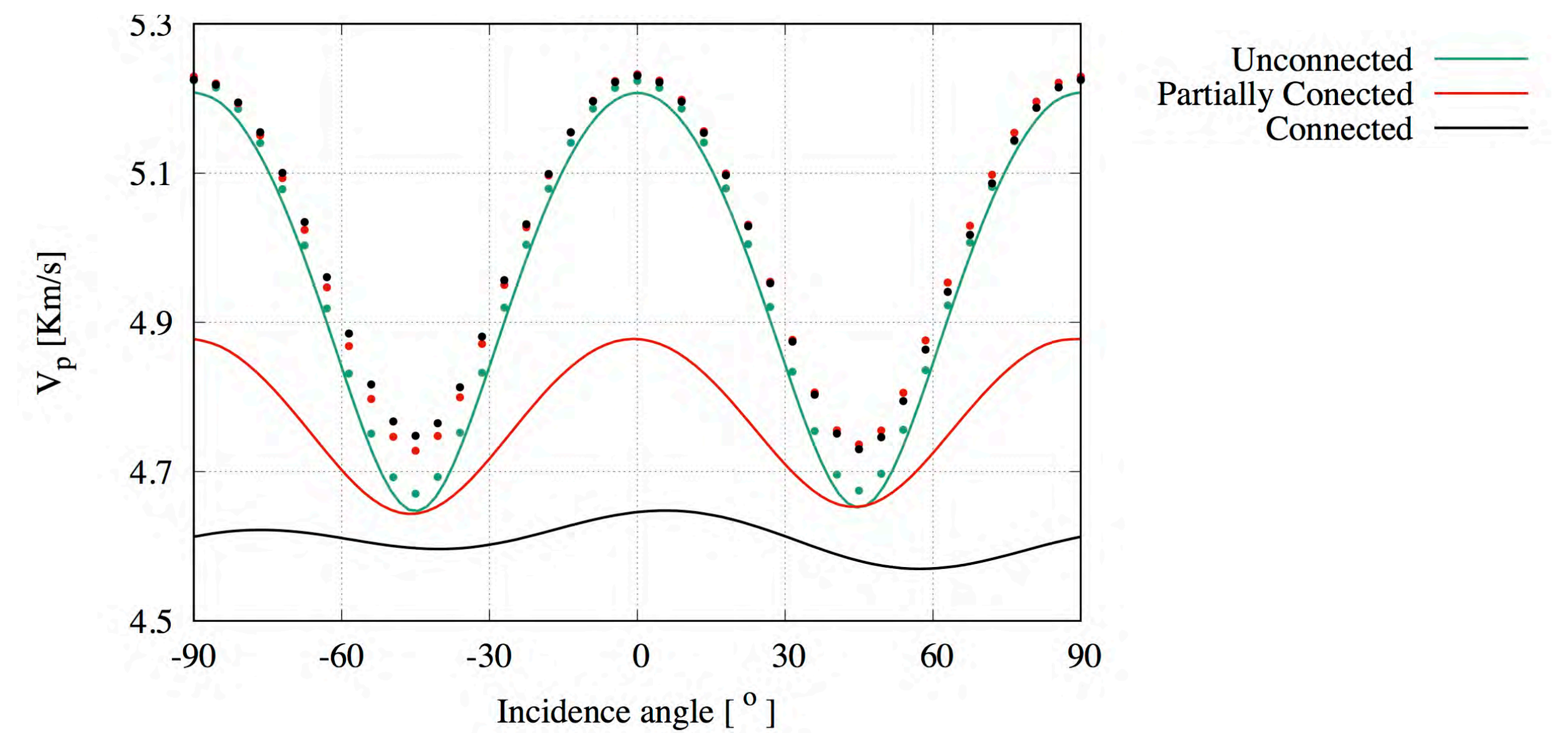


Figure 2:  $V_p$  for the samples shown in Fig. 1 (solid lines) for a frequency of 100 Hz. Dots indicate the corresponding high-frequency-limit velocities, that is, the elastic limits.

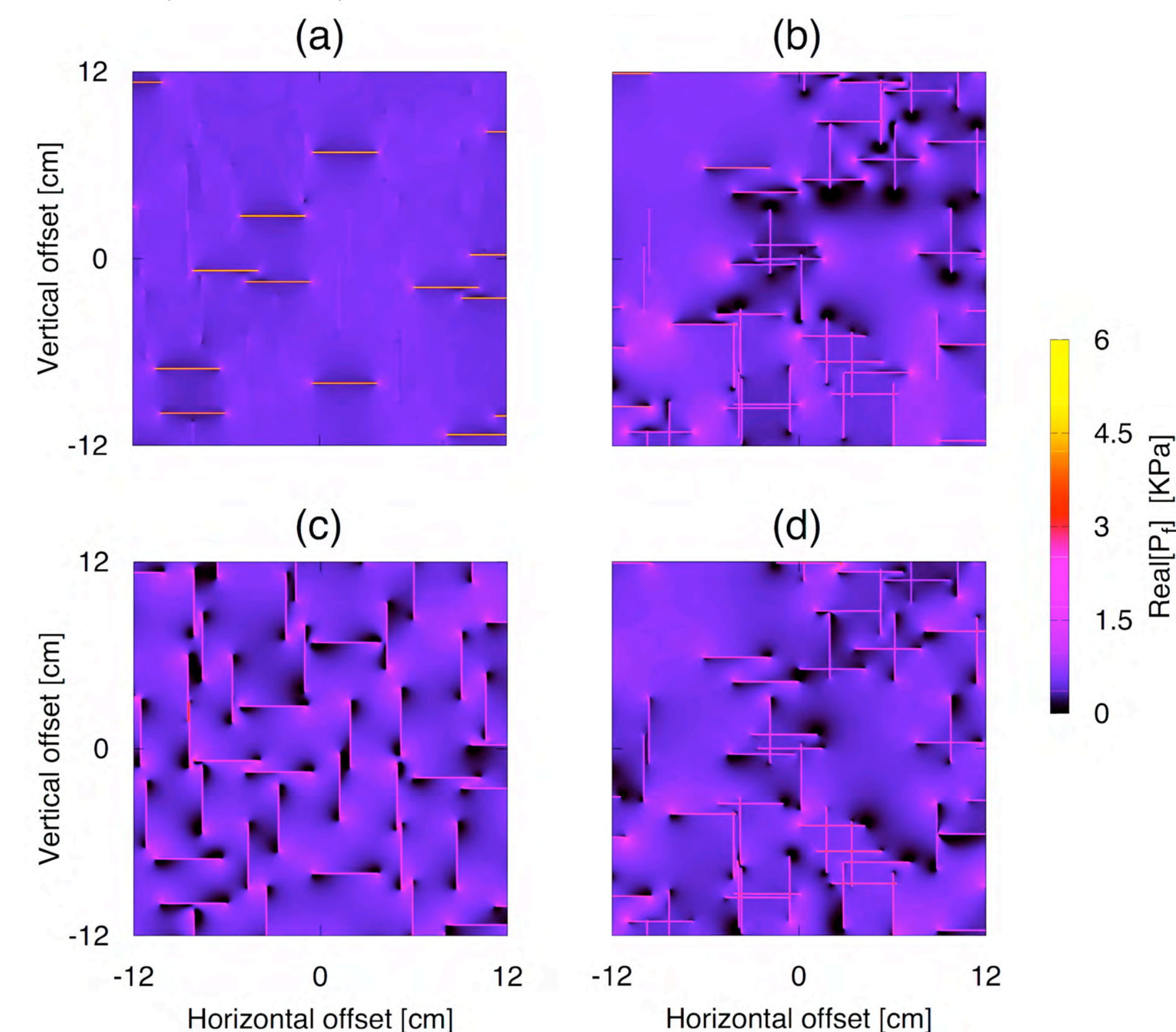


Figure 3: Blow-ups of the real part of the fluid pressure in response to a *P*-wave travelling through the central part of the (a, c) unconnected and (b, d) connected samples shown in Figure 1 at a frequency of 100 Hz. The incidence angles are (a, b) 0° and (c, d) 45°.

## Discussions and Conclusions

In the unconnected case, the level of anisotropy is very high (Fig. 2). At a frequency of 100 Hz the level of anisotropy is reduced as fracture connectivity increases. Conversely, regardless of the level of fracture connectivity, the velocity curves in the high-frequency limit are very similar. This indicates that the reduction of anisotropy when fracture connectivity is increased is not due to geometric characteristics of the fracture network but due to wave-induced fluid pressure diffusion effects.

For the unconnected sample and vertical direction of wave propagation, the compression associated with the seismic wave increases significantly the fluid pressure inside the horizontal fractures (Fig. 3a). This tends to reduce the deformability of the fractures, thus producing a stiffening effect on the rock. However, in the connected scenario, the fluid in the horizontal fractures can release its pressure into the connected vertical fractures (Figs 3b), thus reducing the stiffening effect of the fluid of the horizontal fractures and producing a lower  $V_p$  compared to the high-frequency limit. This explains the reduction of  $V_p$  for incidence angles close to 0° and 90° as the degree of connectivity is increased.

For the unconnected sample and incidence angle of 45°, all fractures experience a similar fluid pressure increase (Fig. 3c). This implies that when the fractures are connected the above mentioned fluid pressure release is negligible for this incidence angle (Fig. 3d) and hence the discrepancies between  $V_p$  for unconnected and connected situations are rather small (Fig. 2a).

While in the connected case there is a significant reduction of the discrepancies between  $V_p$  for incidence angles of 0° and 45° compared with the same discrepancies in the high-frequency-limit, this is not the case for the unconnected scenario. This, in turn, implies that the hydraulic connectivity between fractures manifests itself in a pronounced reduction of the  $V_p$  anisotropy in the seismic frequency band, which is mainly due to wave-induced fluid pressure diffusion effects.

# Geophysical characterization of an active hydrothermal shear zone in granitic rocks

## Motivation

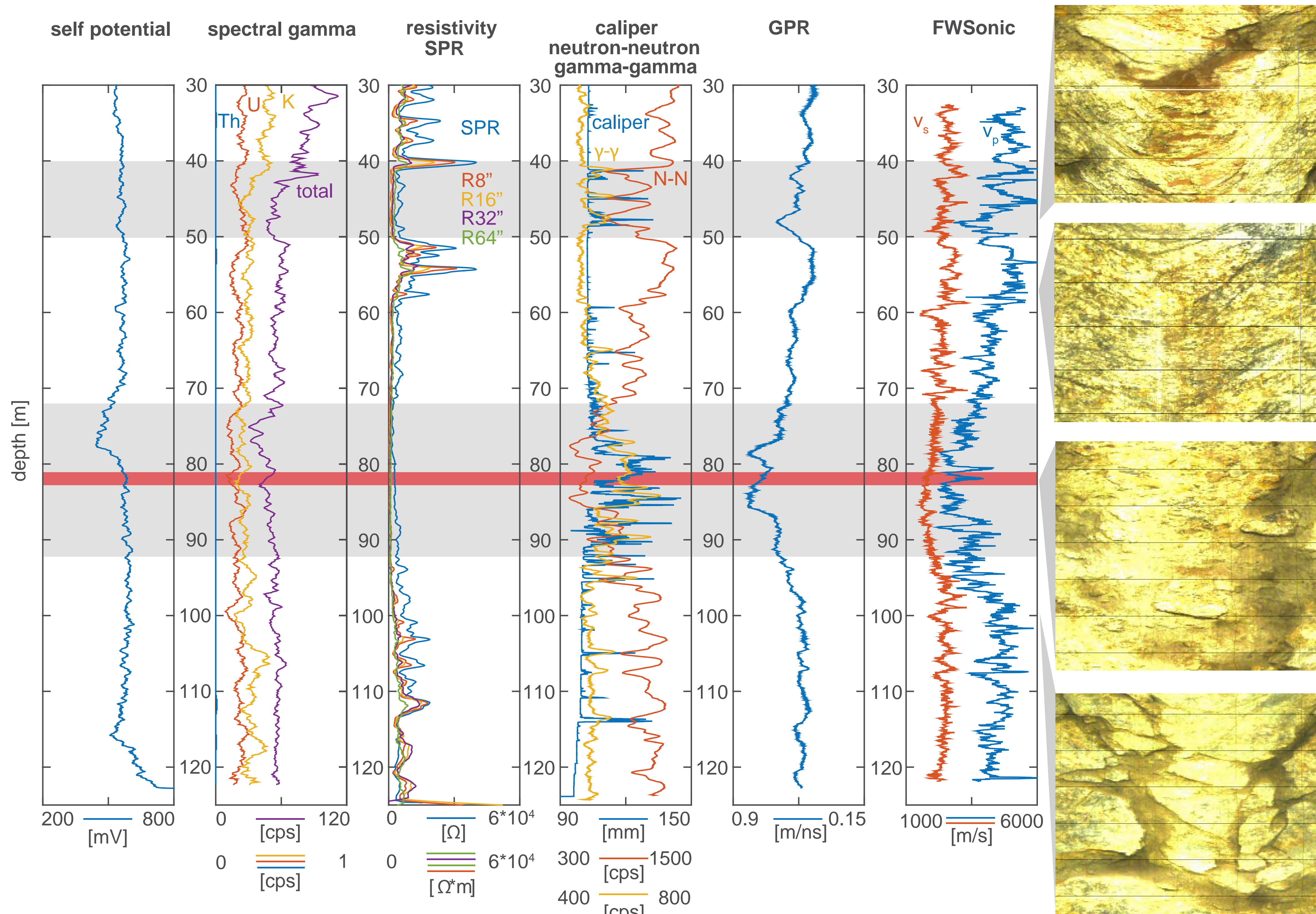
Hydrothermally active faults and shear zones in the crystalline massifs of the central Alps are currently of particular interest because of their potential similarities and analogies with planned deep petrothermal reservoirs in the Alpine foreland. In order to better understand such

hydrothermal systems, a near-vertical, hydrothermally active shear zone embedded in low-permeability granitic rocks has been drilled. This borehole is located on the Grimsel Pass in the central Swiss Alps, has an inclination of 24 degrees with regard to the vertical, and crosses the targeted shear zone between about 82 and 86 meters depth.

## Results

**Figure 1:**

A comprehensive suite of geophysical logging data has been acquired. Shown here, from left to right, are self-potential, natural gamma ray, single point resistivity, resistivity, caliper, gamma-gamma, neutron-neutron, ground-penetrating radar (GPR) and P- and S-wave of the full wave form sonic data. The red bar denotes the targeted shear zone, while the gray bars indicate areas with distinct signatures in the log data. The televiewer images to the right of the logs show that areas of higher fracture density coincide with distinct signatures in the log data. These findings are also supported by the core samples.



## Conclusions and Outlook

We have explored an active hydrothermal shear zone in granite rocks through a comprehensive suite of geophysical borehole logs and vertical seismic profiling (VSP) data. Preliminary results indicate that it should be possible to infer broadband velocity dispersion and attenuation characteristics through static multi-frequency sonic log measurements.

In conjunction the detailed GPR-based porosity estimated and the mechanical properties inferred from VSP and sonic log data, this should allow for interpreting the latter in a poroelastic context. This in turn opens the perspective of constraining the hydraulic properties in general and the permeability of fractured crystalline rocks in particular based on geophysical measurements.

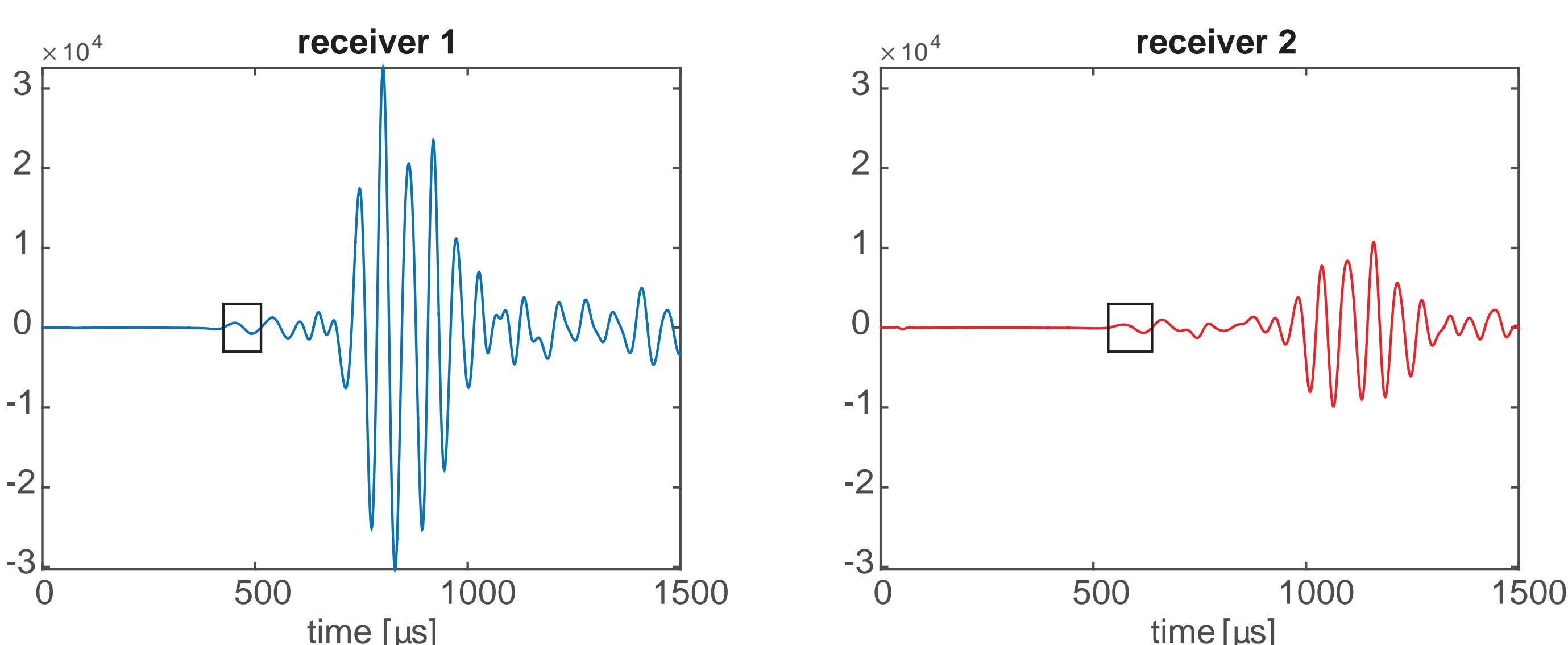


**Figure 2:** Static sonic log measurements within the hydrothermally active shear zone at ~80 m depth. The two receivers are located at distances of 3 feet (~0.9 m) and 4 feet (~1.2 m) from the source, which operated at a nominal center frequency of 25 kHz. The rectangles denote the first cycle of direct P-wave, which were used for estimating the frequency-dependent attenuation characteristics (Figure 3).

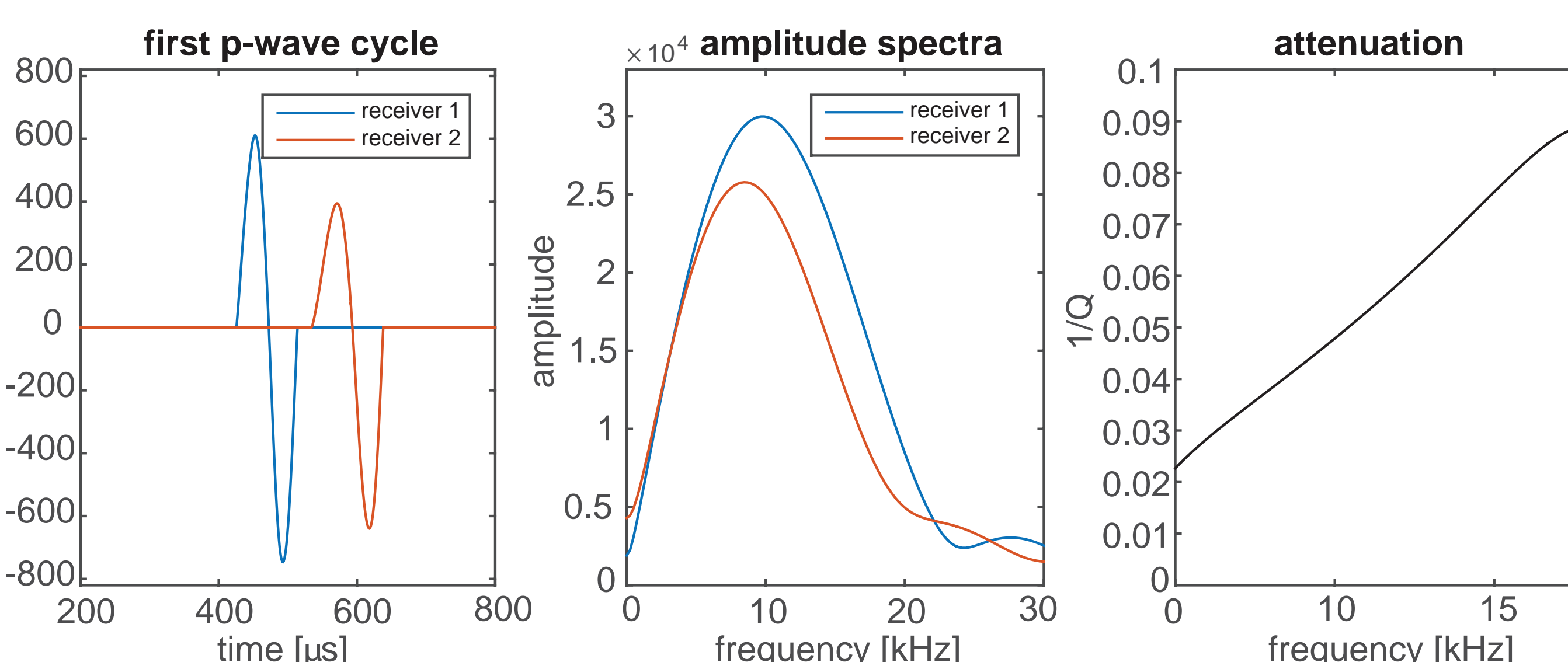


**Figure 3:** First cycle of the direct P-wave identified in Figure 2 (left), corresponding frequency spectra (center), and inverse quality factor as a function of frequency (right). The conical divergence of the direct P-wave has been compensated through an empirical correction, constrained through numerical modeling.

## Sensitivity of seismic attenuation and phase velocity to intrinsic background anisotropy in fractured formations

Nicolás D. Barbosa<sup>1</sup>, J. Germán Rubino<sup>1,2</sup>, Eva Caspari<sup>1</sup> and Klaus Holliger<sup>1</sup>.

1 University of Lausanne  
2 University of Western Ontario

### Motivation

Seismic waves propagating through fluid-saturated fractured rocks can produce significant wave-induced fluid flow (WIFF) between the fractures and the embedding background (FB-WIFF) due to the large compressibility contrasts between the two regions. In presence of hydraulically connected fractures, there is an additional manifestation of WIFF at higher frequencies related to fluid flow within connected fractures (FF-WIFF). The associated energy dissipation can result in strong attenuation and velocity dispersion. Since the level of velocity anisotropy related to the presence of fractures is highly affected by the degree of hydraulic connectivity of the fracture network, it may provide information on the level of fracture connectivity. So far, research has been limited to isotropic backgrounds containing fractures. This is a reasonable assumption in many scenarios. In the practically important case of fractured shales considered in this study, we do, however, have to account for the pronounced intrinsic transverse anisotropy. Modelling both the background and the fractures as poroelastic media, we use numerical oscillatory relaxation tests to determine the effective anisotropic seismic properties of the probed fractured rock. We perform a sensitivity analysis to explore the role played by the intrinsic anisotropy of the background on the FB-WIFF and FF-WIFF attenuation peaks as well as on the phase velocity curves. For comparison, we apply the same methodology to the case of a sample characterized by an isotropic background.

### Methodology

1) We consider a square rock sample representative of a fractured shale (Fig. 1) and model its seismic response in a poroelastic framework.

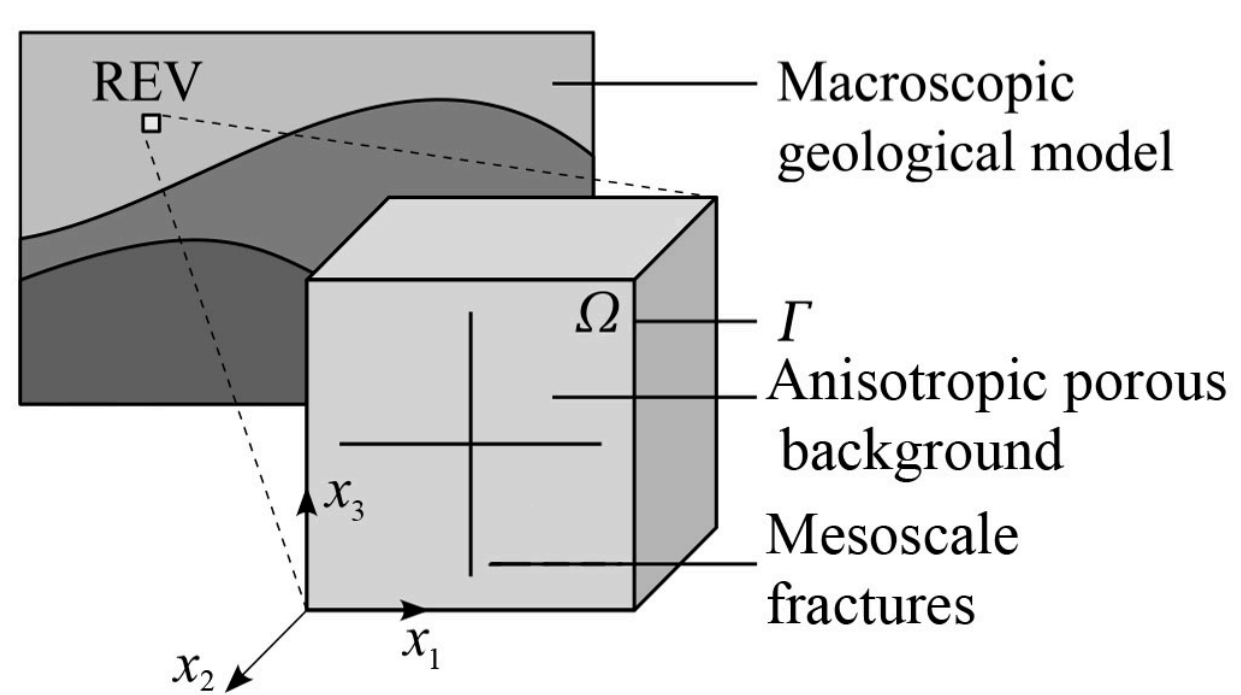


Fig. 1: Elementary volume of a fractured rock. The background has vertical transverse isotropy (VTI) and very low permeability. The fractures are isotropic highly compliant porous features characterized by very high permeability. The sample is fully fluid-saturated.

3) The solid and relative fluid displacement fields resulting from each oscillatory relaxation test are obtained by solving the quasi-static poroelastic equations (Biot, 1941) in the space-frequency domain under the boundary conditions in (2):

$$\nabla \cdot \sigma = 0$$

$$i\omega \mathbf{w} = -\frac{\kappa}{\eta} \nabla p_f$$

$$\begin{bmatrix} \sigma_{11} \\ \sigma_{33} \\ \sigma_{13} \\ p_f \end{bmatrix} = \begin{bmatrix} C_{11} & C_{13} & 0 & -\alpha_1 M \\ C_{13} & C_{33} & 0 & -\alpha_3 M \\ 0 & 0 & C_{55} & 0 \\ -\alpha_1 M & -\alpha_3 M & 0 & M \end{bmatrix} \begin{bmatrix} \varepsilon_{11} \\ \varepsilon_{33} \\ 2\varepsilon_{13} \\ \zeta \end{bmatrix}$$

4) We represent the response of the probed formation by an equivalent homogeneous anisotropic viscoelastic solid at the sample's scale:

$$\begin{bmatrix} \langle \sigma_{11}^k \rangle \\ \langle \sigma_{33}^k \rangle \\ \langle \sigma_{13}^k \rangle \\ \langle \sigma_{13}^k \rangle \end{bmatrix} = \begin{bmatrix} D_{11} & D_{13} & D_{15} \\ D_{13} & D_{33} & D_{35} \\ D_{15} & D_{35} & D_{55} \end{bmatrix} \begin{bmatrix} \langle \varepsilon_{11}^k \rangle \\ \langle \varepsilon_{33}^k \rangle \\ \langle 2\varepsilon_{13}^k \rangle \end{bmatrix}$$

The average stress and strain components over the sample's volume for each test ( $k=1, 2, 3$ ) are used to compute the components of the equivalent stiffness matrix following a classic least-square procedure (Rubino et al., 2015).

2) We estimate the effective anisotropic seismic properties of the sample by following a numerical upscaling procedure (Fig. 2).

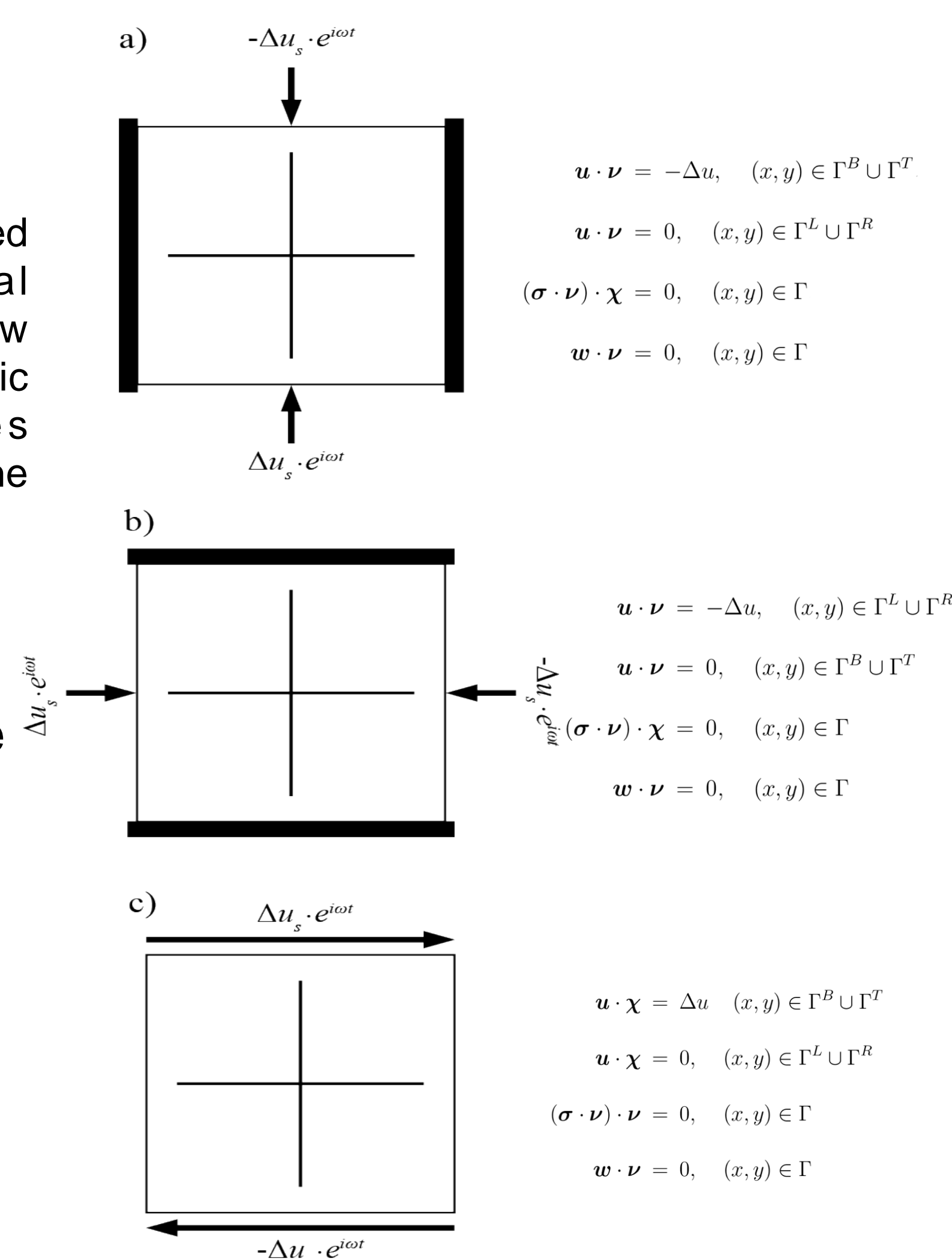


Fig. 2: Schematic illustration of the numerical oscillatory relaxation tests.

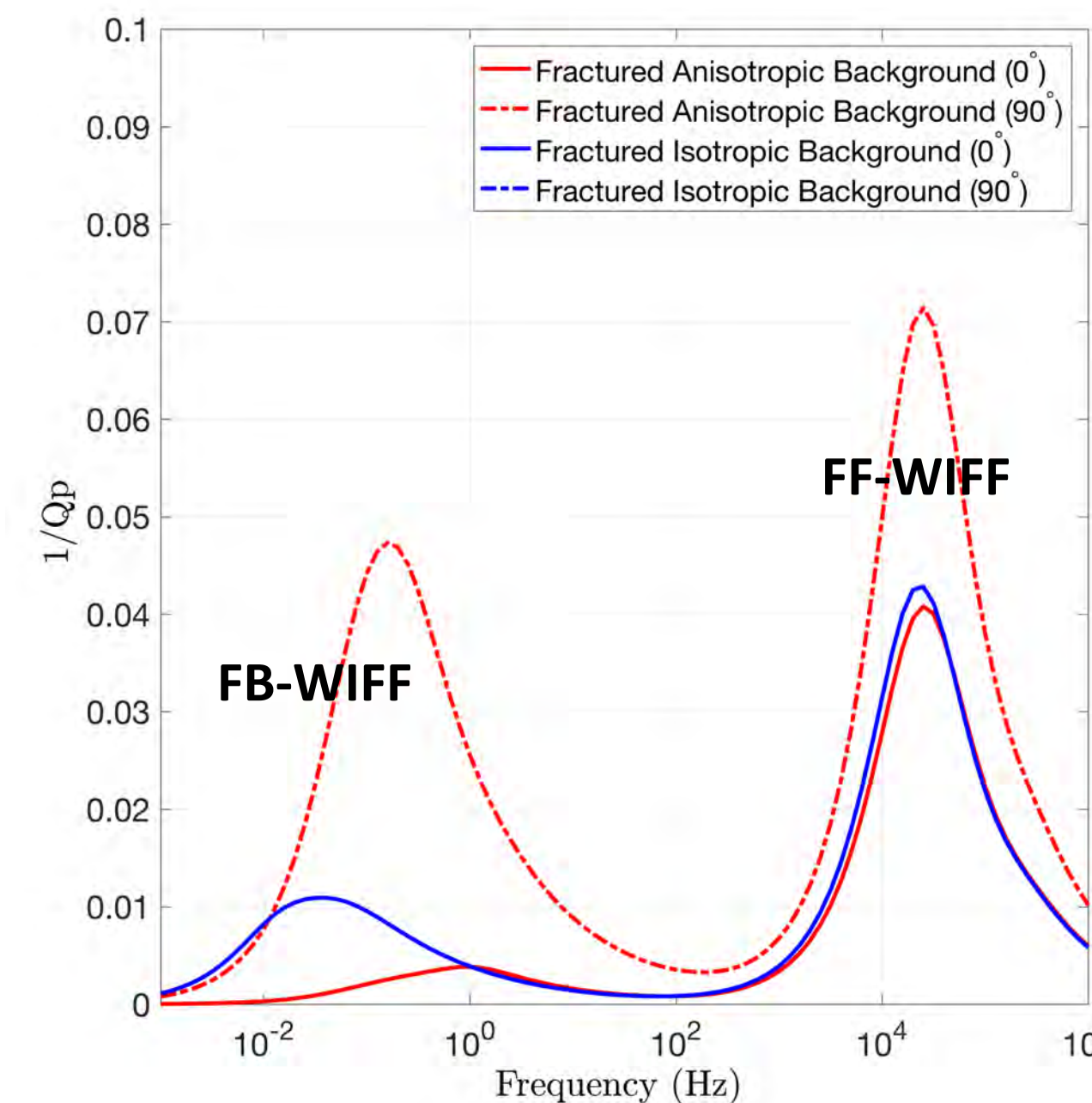


Fig. 3: P-wave attenuation as a function of frequency for vertical and horizontal directions of wave propagation.

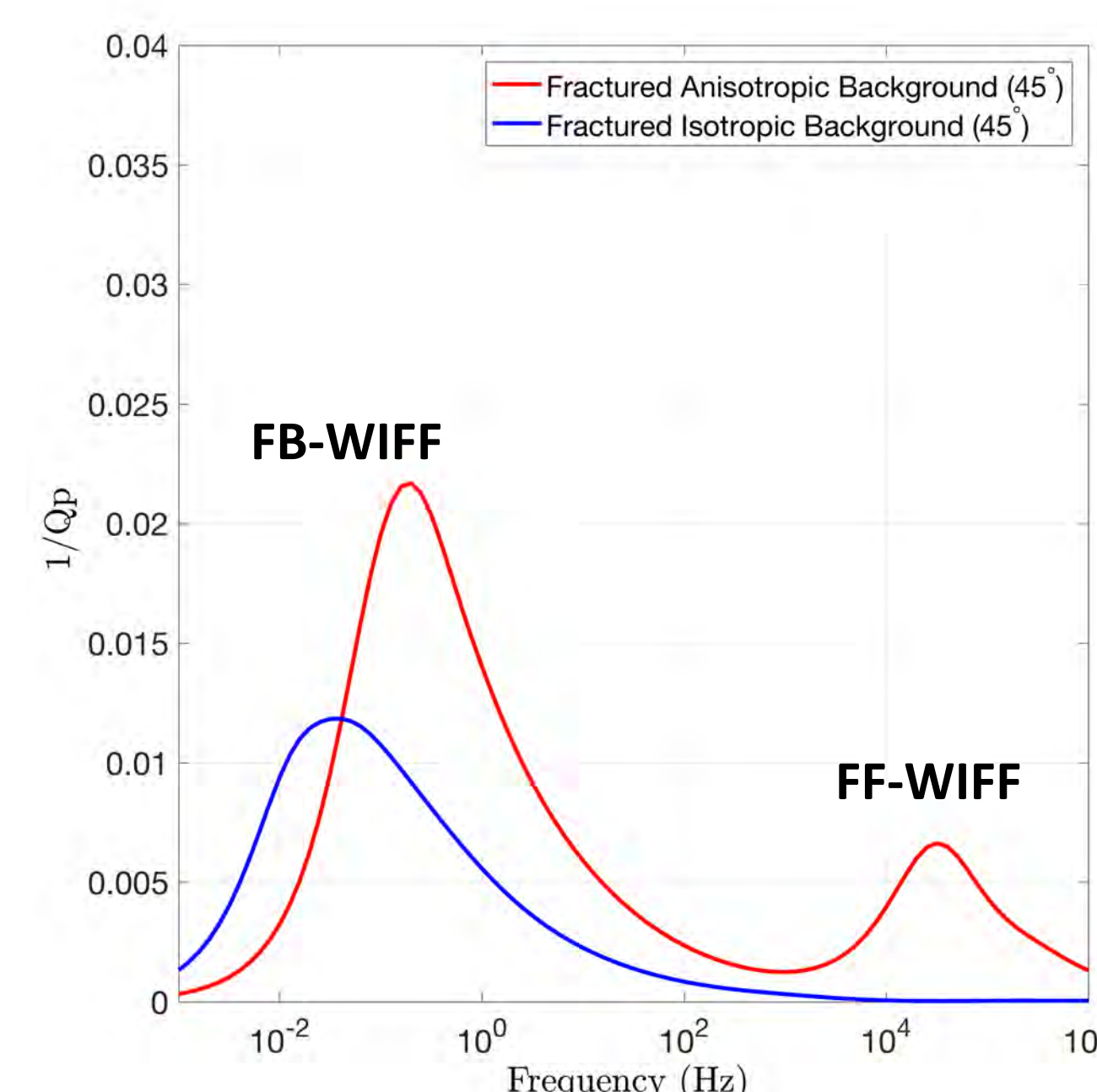


Fig. 4: P-wave seismic attenuation as a function of frequency for P-wave incident at 45°.

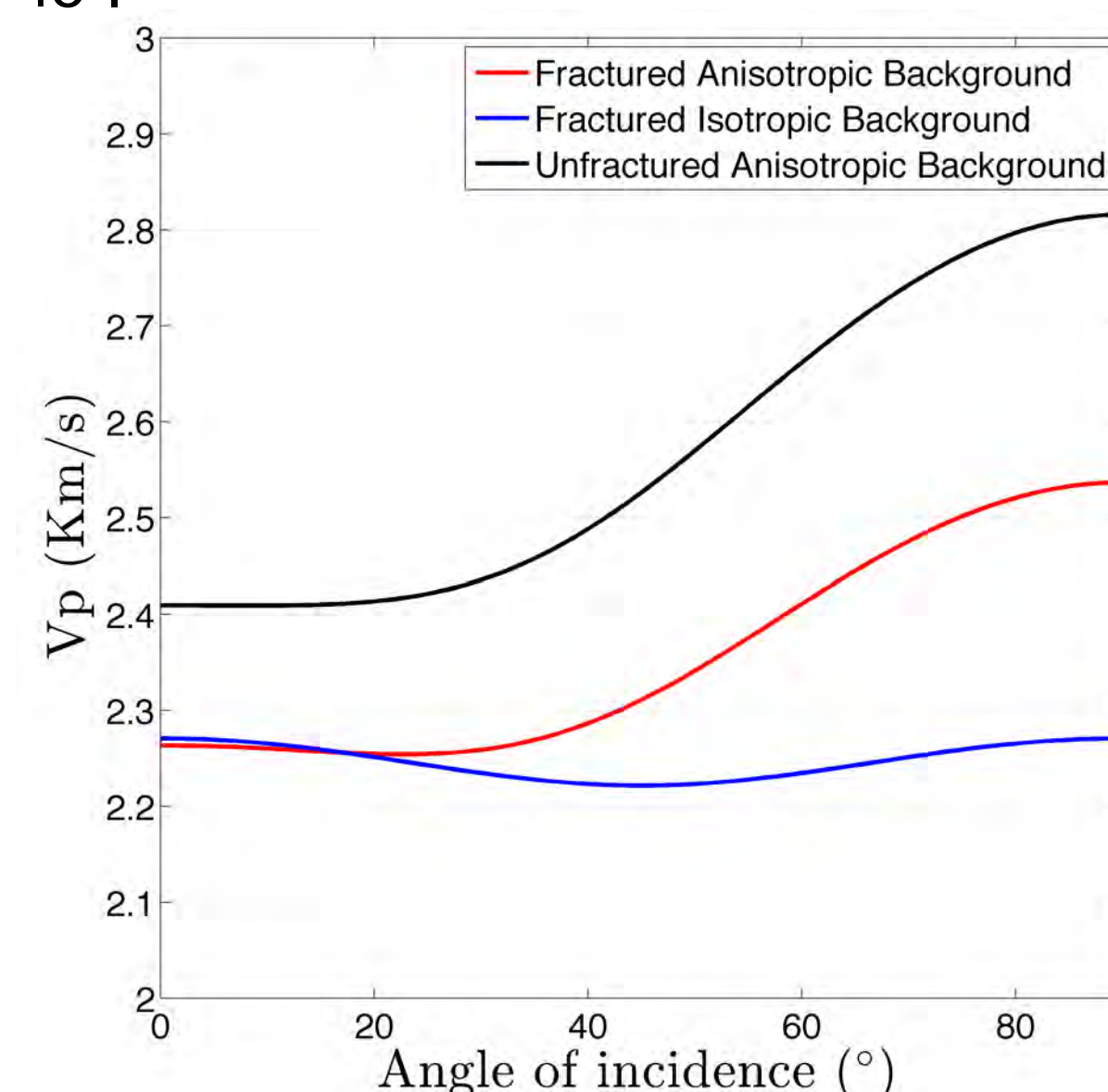


Fig. 5: P-wave phase velocity as a function of angle of incidence for  $f=100$  Hz.

FB-WIFF (Iso.)  $\approx 40$  mHz  
FB-WIFF (Aniso.)  $\approx 1$  Hz ( $0^\circ$ ) /  $0.1$  Hz ( $90^\circ$ )  
FF-WIFF (Iso/Aniso.)  $\approx 25$  kHz.

The FB-WIFF characteristic frequency is primarily controlled by the permeability and elastic moduli of the background. For very low background permeabilities, it is located below the seismic frequency band. However, since we assume an anisotropic background permeability tensor,  $\kappa$ , such that  $\kappa_x > \kappa_z = \kappa_{iso}$ , the effective permeability of the background is increased in the anisotropic case with respect to the isotropic one, and the attenuation peak is shifted towards higher frequencies.

For 45° incidence and isotropic background, both fractures experience similar fluid pressure increases (Fig. 4). Consequently, the fluid pressure gradient between the fractures and, correspondingly, the attenuation peak due to FF-WIFF, become negligible. For anisotropic background, the fluid pressure gradient between the fractures is also reduced, but we still observe some attenuation at high frequencies due to FF-WIFF, as the compressibility contrast between fracture and background changes for different directions due to the stiffness anisotropy of the background.

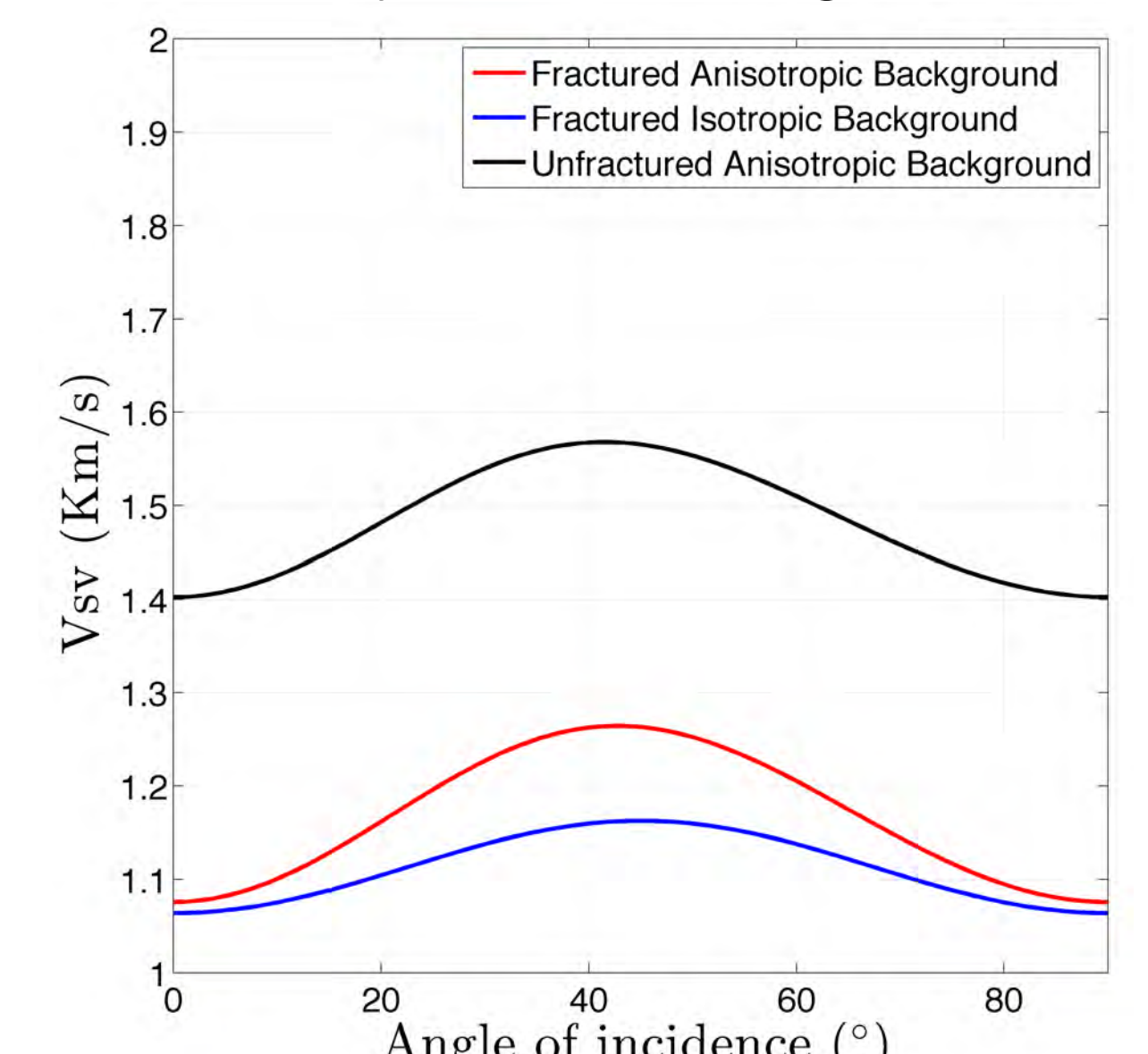


Fig. 6: S-wave phase velocity as a function of angle of incidence for  $f=100$  Hz.

Figs. 5 and 6 show that the angle dependence of the phase velocity is mainly controlled by the anisotropy of the background.

### Conclusions

We observe that the attenuation peaks due to FF-WIFF and FB-WIFF are affected by the anisotropy of the background, as it changes the compressibility contrast with respect to the fractures. Our results suggest that permeability anisotropy of the background does not affect the attenuation peak due to FF-WIFF, as in this limit, there is no fluid flow from fractures to background. Conversely, the frequency at which the FB-WIFF attenuation peak occurs is influenced by background anisotropy. We found that the angle dependence of P- and S-wave velocities in rocks containing orthogonal fractures aligned with the axes of symmetry of the embedding anisotropic background is mainly defined by the anisotropy of the latter. These results encourage us to extend this analysis to fracture networks and anisotropic backgrounds of higher complexity, as well as to consider the influence on S-wave splitting for 3D samples.

### References

- Biot, M. A., 1941, General theory of three-dimensional consolidation: J. Appl. Phys., 12, 155–164.
- Rubino, J., E. Caspari, M. Milani, T. M. Müller, and K. Holliger, 2015, Seismic anisotropy in fractured low-permeability formations: the effects of hydraulic connectivity: Exp. Abstr. Ann. Meet. Soc. Expl. Geophys.

### Results

We compute the velocity and attenuation of P- and S-waves as functions of incidence angle and frequency following a standard procedure for anisotropic viscoelastic solids. For an isotropic background (Fig.3, blue lines), the responses are the same for horizontal and vertical incidence, due to the symmetry of the fractures in the sample. Regardless of the anisotropy of the background, we observe two characteristic frequencies where attenuation is maximal (FB-WIFF and FF-WIFF).